THÈSE

Présentée au Département D'électrotechnique

Pour l'obtention du diplôme de

DOCTORAT

Domaine : Sciences et Technologie

Filière : Electrotechnique   **Option : Electrotechnique**

Par

BOULANOUAR Hasna

THÈME

Contribution to the study and analysis of silicone insulating materials performance under DC and AC voltages.

Soutenue le 09/01/2020 devant le Jury :

Ahmed GHERBI	**Professeur**	**Univ. Ferhat Abbas Sétif 1**	**Président**
Abdelhafid BAYADI	**Professeur**	**Univ. Ferhat Abbas Sétif 1**	**Directeur de thèse**
Hocine MOULAI	**Professeur**	**Univ. Houari Boumediene Alger**	**Examinateur**
Leila Mokhnache	**Professeur**	**Univ. Mostefa Benboulaid Batna 2**	**Examinatrice**
Hamou NOURI	**Professeur**	**Univ. Ferhat Abbas Sétif 1**	**Examinateur**

DECLARATION

This work has not previously been accepted in substance for any degree and is not concurrently submitted in candidature for any degree.

Signed ....(Boulanouar Hasna)

Date ....

STATEMENT 1

This thesis is being submitted to obtain the diploma of the Ph.D. 3rd cycle (LMD).

Signed ....(Boulanouar Hasna)

Date ....

STATEMENT 2

This thesis is the result of my own work/investigation, except where otherwise stated. Other sources are acknowledged by explicit references. A bibliography is appended

Signed ....(Boulanouar Hasna)

Date ....

STATEMENT 2

I give consent for my thesis, if accepted, to be available for photocopying only at the university, and for the title and summary to be made available to outside organisations.

Signed ....(Boulanouar Hasna)

Date ....

PUBICATIONS

Journal:

1. **Hasna Boulanouar**, Abdelhafid Bayadi, Abderrahmane Haddad,. "Analysis of textured silicone rubber performance under contaminated conditions",. *IET Science, Measurement & Technology*, Vol.13, n°.3, pp. 461-468, May 2019.

2. Hocine Terrab, **Hasna Boulanouar**, Abdelhafid Bayadi,. "Flashover process analysis of non-uniformly polluted insulation surface using experimental design methodology and finite element method",. *Electric Power Systems Research*, Vol. 163, Part B, pp. 581-589, October 2018.

Conference:

1. Samia satta, **Hasna Boulanouar**, Abdelhafid Bayadi,. "Distribution de la tension et du champ électrique des plaques isolants sous condition de pollution",. 8th International conference on electrical engineering (CEE 2014), Batna, Algeria, 16-17 November 2014.

2. **Hasna Boulanouar**, Abdelhafid Bayadi, Samia satta,. "L'effet des gouttes d'eau et la couche de pollution sur la distribution de tension et du champ électrique",. The 9th International conference on electrical engineering and first workshop on robotics and controls (CEE 2016), Batna, Algeria, 02-04 Octobre 2016.

3. **Hasna Boulanouar**, Abdelhafid Bayadi, Abderrahmane Haddad,. "Three Dimensional analysis of textured silicone rubber surface effect on the potential and the electrical field distribution",. 1ére Ecole d'Automne sur les Matériaux Emergents, (EAME 2017), Setif, Algeria, 28 November 2017.

PhD days:

1. Boulanouar H, Bayadi A, "PhD student's day", University Setif, April 2013.
2. Boulanouar H, Bayadi A, "PhD student's day", University Setif, May 2014.
3. Boulanouar H, Bayadi A, "PhD student's day", University Setif, May 2015.

ملـخص

بالنسبة لأنظمة نقل وتوزيع الطاقة الكهربائية لمسافات طويلة، يُنظر إلى تقنية التيار المباشر العالي الجهد (**HVDC**) على أنها الخيار الأكثر انتشارًا وجاذبية من الناحية الاقتصادية. لضمان موثوقية الشبكات الكهربائية الحالية المباشرة، من الضروري معرفة سلوك المعدات الكهربائية مثل العوازل. على الرغم من أن عوازل مطاط السيليكون تقدم أداءً كهربائيًا فائقًا مقارنة بالعوازل الزجاجية والخزفية التقليدية. و مع ذلك، في الظروف البيئية شديدة التلوث، تكون معرضة لآثار التدهور بسبب طبيعتها العضوية. قد ينتج عن ذلك عطل العازل ويشكل تحديًا أكبر في الحفاظ على موثوقية نظام الطاقة. لهذا السبب، ينبغي إجراء البحوث لتطوير تصميم مناسب للحد من الأضرار الناجمة عن التلوث الشديد.

في هذا العمل تم إجراء تحقيقات تجريبية على العوازل من مطاط السليكون باستخدام اختبار المستوى المائل تحت التوتر المستمر الموجب و المتناوب. تمت مقارنة أداء عينات تقليدية مستطيلة مع عينات جديدة مزخرفة لتقييم الأداء ضد التآكل و التتبع. تم تقييم أداء كل عازل من خلال مراقبة نشاط التفريغ لفهم جيد لعملية التدهور، كذلك تم قياس تيار التسرب و فقدان الوزن.

تمت دراسة المجال الكهربائي على طول العينات المزخرفة و التقليدية في ظروف الجافة و نظيفة و كذلك في الظروف الملوثة الرطبة بإستخدام طريقة العناصر المتناهية COMSOL Multiphysics. تم تصميم نماذج ثلاثية الأبعاد (3D) بالإستعانة ببرنامج التصميم اوتوكاد (AutoCAD). في حالة توزيع التلوث الغير المنتظم تم استخدام منهجية التصميم التجريبي مع طريقة العناصر المتناهية لاستقصاء سلوك العوازل المزخرفة. تم تحديد مناطق الحقول العالية على أسطح عوازل السيلكون المطاط. أظهرت هذه الدراسة معلومات مفيدة حول سلوك الأسطح المزخرفة.

كلمات مفتاحية : مطاط السيلكون، العينات المزخرفة، الشيخوخة، التدهور ، اختبار مستوى مائل، الحقل الكهربائي، طريقة الحدود المتناهية، منهجية التصميم التجريبي**.**

Résumé

Pour les réseaux de transport et de distribution d'électricité à longue distance, la technologie de courant continu haute tension (CCHT) est considérée comme la solution la plus répandue et économiquement la plus intéressante. Pour assurer la fiabilité des réseaux électriques en courant continu, il est nécessaire de connaître le comportement des équipements électriques tels que les isolateurs. Bien que les isolateurs en caoutchouc de silicone offrent des performances électriques supérieures à celles des isolateurs traditionnels en verre et en porcelaine. Cependant, dans des conditions environnementales extrêmement polluées, ils sont sensibles aux effets de dégradation en raison de leur nature organique. Cela peut entraîner une défaillance de l'isolation et poser un plus grand problème pour maintenir la fiabilité du système électrique. Pour cette raison, les matériaux utilisés dans les systèmes d'isolation haute tension devraient être testés afin de déterminer s'ils résistent à l'érosion et au cheminement. Pour cette raison, des recherches devraient être menées afin de développer une conception appropriée pour réduire les dégradations causées par la pollution sévère.

Dans ce travail, des essais expérimentaux ont été effectués sur les isolateurs en caoutchouc de silicone en utilisant le test plan incliné sous le courant continu (CC) positive et courant alternatif CA. Des échantillons rectangulaires en caoutchouc de silicone avec une surface plane ont été testés et comparés aux échantillons texturés pour évaluer la performance contre l'érosion et le cheminement. La performance de chaque isolateur a été évaluée en surveillant les activités des décharges pour bien comprendre le processus de dégradation, ont été également mesurés le courant de fuite et la perte de poids.

Le champ électrique le long des surfaces texturées en caoutchouc silicone dans des conditions propres, ainsi que dans des conditions de pollution humide, a été étudié par la méthode des éléments finis COMSOL Multiphysics. Les modèles tridimensionnels (3D) des différentes surfaces texturées ont été dessinés par le progiciel de conception assistée par ordinateur (AutoCAD). Dans le cas d'une répartition non uniforme de la pollution, la méthode du plan d'expérience a été utilisée avec la méthode des éléments finis pour identifier le champ électrique maximal sur la surface texturée. Cette étude a montré des informations utiles sur le comportement de la surface texturée dans différentes conditions de fonctionnement.

Mots clés : Caoutchouc de silicone, Echantillons texturés, Vieillissement, Dégradation, Essai en plan incliné, Champ électrique, Méthode des éléments finis, Méthode des plans d'expériences.

Abstract

For long-distance electric power transmission and distribution systems, the high-voltage direct current (HVDC) technology is viewed as the most widespread and economically appealing option. To ensure the reliability of direct current electrical networks, it is necessary to know the behaviour of electrical equipment such as insulators. Although silicone rubber insulators offer superior electrical performance compared to traditional glass and porcelain insulators. However, in highly polluted environmental conditions, they are susceptible to degradation effects due to their organic nature. This may result in insulation failure and poses a greater challenge in maintaining the reliability of the power system. For this reason, research should be carried out to develop an appropriate design to reduce the damage caused by severe pollution.

In this work, experimental tests on silicone rubber insulators were performed using an inclined plane test under positive DC and AC voltages. Rectangular samples with a plane surface were compared to textured design to evaluate the performance against erosion and tracking. The performance of each insulator was assessed by monitoring the discharge activity to clearly understand the degradation process, leakage current and weight loss were also measured.

The electric field along the textured silicone rubber surfaces under dry and clean conditions, as well as under wet pollution conditions, was studied using finite element method COMSOL Multiphysics. Three-dimensional (3D) models of the different textured surface were designed by Computer Aided Design (AutoCAD) software package. In the case of non-uniform pollution distribution, the design of experiment method was used with the finite element method to identify the maximum electric field on the textured surface. This study showed useful information's about the behaviour of the textured surface in different operating conditions.

Key words: Silicone rubber material, Textured samples, Aging, Degradation, Inclined plane test, Electric field, Finite elements method, Design of experiment method.

Dedication

****

To the most precious, warm-hearted and the candle of my life that was always looking forward to seeing me in such a day, my mother who's passed the way before she realizes her wish. Here I am, I now have achieved one of your hopes. I dedicate my graduation and success to you. You who deserve to celebrate it...Allah's blessing be on you, may the paradise be your house.

*To my father, my sister **Karima** and my brother **Fares**, for their continued love, support and encouragement.*

****

ACKNOWLEDGEMENTS

TABLE OF CONTENT

Chapter 01

INTRODUCTION

Chapter 02

HIGH VOLTAGE COMPOSITE INSULATORS

Chapter 03

LITERATURE REVIEW

Chapter 04

COMPARATIVE PERFORMANCE OF SILICONE RUBBER POLYMERIC INSULATORS UNDER HVDC AND HVAC VOLTAGES USING THE INCLINED PLANE TEST

Chapter 05

INVESTIGATIONS OF ELECTRIC FIELD AND POTENTIAL DISTRIBUTION OVER THE SURFACE OF TEXTURED SILICONE RUBBER INSULATORS

Chapter 06

GENERAL CONCLUSIONS AND FUTURE WORKS

REFERENCES

LIST OF FIGURES

LIST OF TABLES

LIST OF ABBREVIATIONS AND SYMBOLS

List of Abbreviations

2-D /3-D	Two / Three dimensions
AC	Alternating Current
ANOVA	Analyse of variance
ASTM	American Society for Testing Materials
ATH	Alumina Trihydrate
BEM	Boundary Element Method
CTV	Constant Tracking Voltage
DB	Dry-Bands
DOE	Design of Experiment Method
EPDM	Ethylene-Propylene-Diene Monomer
EPM	Ethylene Propylene Monomer
EPR	Ethylene-Propylene Rubber
EPRI	Electric Power Research Institute
FEM	Finite Element Method
FRP	Fibre Reinforced Plastic
HC	Hydrophobicity Classification
HTV	High-Temperature Vulcanizing
HV	High Voltage
HVDC	High-Voltage Direct Current
IEC	International Electrotechnical Commission
IPT	Inclined-Plane Test
IRT	Infrared thermography
ITV	Initial Tracking Voltage
LC	Leakage current
LMW	Low Molecular Weight
LSR	Liquid Silicone Rubber
PDMS	Polydimethylsiloxane
RMS	Root Mean Square
RTV	Room-Temperature Vulcanizing
RWDT	Rotating Wheel Dip Test
SiR	Silicone Rubber
STRI	Swedish Transmission Research Institute
USA	United States of America
UV	Ultra-Violet Radiation

Symbols

kV	Kilovolt
CH_3	Methyl Group
Si-O	Siloxane bond
Si	Silicon
O	Oxygen
°C	Degrees Centigrade
$Al\ (OH)_3$	Alumina trihydrate
SiO_2	Silica
%	Percent
θ_c	Static contact angle
SiO_2	Silica
NaCl	Salt (Sodium chloride).
mA	Milli-ampere
µA	Microampere
°	Degree (angle)
θ	Inclination angle
θ_a	Advancing contact angle
θ_r	Receding contact angle
E	Electric field
J	Leakage current density
P	Power dissipation
a	Radius of the circle
b	Radius of the sphere
c	Height of the sphere
A_p	Surface area of the protuberance
A_t	Area of the triangular plane surface
σ	Conductivity
I	Current
α	Area factor
β	Creepage factor
$\alpha\beta$	Power density factor
Hz	Hertz
mm	Millimetre
V	Volt
S	Seconds
ml	Micro litres
min	Minute
NH_4CL	Ammonium chloride
g	Gram

m	Sample mass
v	Sample volume
ρ'	Density of the material
ε	Permittivity
σ	Conductivity
ε_r	Relative permittivity
ρ	Space charge density
T	Thickness of the pollution layer
W	Width of the pollution layer
L	Location of the pollution layer
P-value	Probability of testing the significance of the null hypothesis
F	Standard statistical Coefficient "F"

Chapter 01

INTRODUCTION

1.1. Background

Developments of the modern world depend significantly upon a continuous electric power supply. With growing demand, utilities must provide secure and reliable power delivery while maximising the performance of the power distribution system from both technical and economic standpoints. High voltage power lines have been widely used to transmit the electric energy from the power stations to the end users. Outdoor insulators are among the key components in the electric power transmission network, essentially required for two primary purposes: 1) to isolate the transmission tower from the high-voltage source, and 2) to provide a load-bearing platform capable of supporting heavy overhead conductors well above the ground [1].

Two main categories of insulators have been employed for overhead lines depending on the material used: Ceramic and polymeric insulators. Decades of in-service performance have demonstrated that ceramic insulators, made of porcelain and glass, show good performance, they provide excellent resistance to material degradation caused by ultraviolet (UV) radiation and discharge activities [2]. However, they suffer from having hydrophilic surface properties, which means that water can easily form a continuous conductive film along the creepage path, thus allowing high surface leakage currents to flow on their wetted surfaces. Also, they have disadvantages related to their mass, the costs of their installation, their fragility under mechanical and vandalism constraints.

During recent decades polymer insulators have been introduced and widely used due to their better pollution performance. Insulators made of polymer materials are often called composite or non-ceramic insulators. Non-ceramic insulators offer several advantages over porcelain insulators. The most important advantage of polymeric insulators is their better performance in the polluted environment due to

their good hydrophobic surface property under wet conditions such as rain, fog and dew [3]. This water repellent property forces water to be deposited in a form of discrete beads. The reduction of surface wetting, therefore, leads to a reduction in the discharge activity and dry band arcing on the polymeric surface and ultimately improves the anti-pollution performance. Moreover, they have high mechanical strength to weight ratio, less prone to damage due to vandalism because of it elasticity surface, and reduced maintenance costs [4, 5].

A polymeric insulator consists of a core fiberglass rod, two metal end fittings, and polymer weather sheds, which are shaped and spaced over the fiberglass rod to protect the rod and to provide the required leakage distance. Silicone rubber is a polymer widely adopted for outdoor insulation. Unlike other polymers, like EPDM (ethylene propylene diene monomer), it retains its hydrophobic status throughout service life and, in addition, has the ability to transfer this hydrophobicity to the adhering pollutants.

1.2. Problem Statement

The hydrophobic surface of polymeric insulators offers a significant advantage compared with glass or porcelain. However, under severe ambient conditions, dry band formation is not totally eliminated, especially before hydrophobic recovery can occur in the overlaying pollution layer. The outside service environment consists of wetting in the form of rain, fog, dew and direct spray; pollutants from the sea and roads that are salted during winter months in cold climates; and also chemicals from industry. In addition, insulator housings are subjected to ultra-violet (UV), temperature extremes, over voltages due to switching and lightning surges, and mechanical loads due to wind and ice.

Unlike porcelain and glass, polymeric materials have weak chemical bonds that can substantially degrade over time and they are more susceptible to chemical degradation under the multiple stresses likely to be encountered in service. In addition, they suffer from cracking, crazing, erosion and tracking. Moreover, their life expectancy is difficult to evaluate [4].

Changes in surface properties influenced by service and climatic conditions may eventually lead to a loss of surface hydrophobicity, thereby promoting the formation of a continuous conductive film on its surface. The resulting leakage current under system voltage generates resistive heating that evaporates water from the wet surfaces, risking the formation of dry bands [6].

One of the main factors contributing to the development of discharges on insulator surfaces is the electric field distribution on the insulator surface, which in turn controls the current density. The usually non-uniform field profile along the surface has peak regions in which dry bands are formed. High electric fields trigger corona and discharge activities that contribute considerably to premature degradation through surface tracking and erosion. Under extreme conditions, intense electric arcs could puncture the polymeric housing and, more seriously, cause insulation failure from severe deterioration [7, 8]

1.3. Textured Insulators

Pollution flashover constitutes the predominant parameter for the design and dimensioning of high voltage insulators [9]. The effect of the design on the performance of outdoor ceramic insulators has been widely investigated [10, 11]. It has been proved that the open profiles or aerodynamic designs are more preferred for desertic conditions. However, insulators with more corrugated ribs are preferred for foggy conditions [12-14]. In fact, increasing the creepage length of ceramic insulators through complex shapes have been as a good solution for anti-fog insulator design. However, this complex shape cannot be adopted for polymeric insulators. For this reason, a new polymeric insulator design has been patented recently [15], where the smooth insulating surface is replaced by a textured silicone rubber surface. This texture has been designed to improve the anti-dry band as well as the anti-fog properties of the insulators in polluted areas. This design presents the advantage of increasing the surface area and then can reduce the leakage current density. Moreover, this solution is able to increase the longitudinal creepage distance and to reduce the stress applied in specific areas [15-18].

Textured patterns consist of intersecting or contiguous hemispherical protuberances. This raised geometry does not impede the removal of the insulator from the mould during casting. The main aim of textured surface is to lower power dissipation on the insulator surface by reducing both leakage current density and the electric field gradient. This design concept aspires to reduce tracking and erosion on the insulator surface and to improve the flashover strength under conditions of heavy pollution.

1.4. Objectives of the present work

During the last 40 years, extensive efforts have been made to achieve a better understanding of the aging in polymeric outdoor insulation materials, by employing different techniques to investigate the material characteristics and the changes in properties due to degradation. Several experimental and simulation techniques have been conducted to assess the surface degradation due to discharge activities, dry band arcing and high electric field. Simulations of the electric field over the surface of the insulators are intended to determine the high-stress regions on the surface of the insulator. The research programme of this thesis is divided into two parts (experimental and simulation) to investigate and describe the behaviour of textured silicone rubber insulators.

The objective of experimental research is to compare and contrast the accelerated ageing characteristics of textured SiR insulation materials using the inclined plane test under AC and DC applications.

The general objective of simulation research is to study the electric field and potential distributions along textured insulators, first, under dry and clean conditions and then, under various wet conditions. A commercially available software (COMSOL Multiphysics) based on the FEM is employed for the modelling and the calculation for the textured SiR insulators under different surface conditions.

The specific objectives of this research work can be summarized as follows:

- To investigate the long-term aging performance of SiR polymeric insulators with different profiles, with textured and non-textured designs using an inclined plane test (IPT) and to compare the surface degradation under AC and positive

DC excitations.

- To prove the effectiveness of textured surfaces in reducing the thermal damage on silicone rubber insulation due to surface heating induced by surface discharges.

- To identify and demonstrate the optimum textured designs that show the maximum reduction of surface erosion.

- To evaluate the localised surface conductance on conventional and textured insulators by identifying and understanding the variation trends of the conductance and its distribution across the surface of each insulator.

- To investigate the potential and electric field distributions along silicone textured surfaces with different diameters of hemispherical protuberances at DC, under clean and dry conditions.

- To examine the effectiveness of textured material for electric field stress control around the polymeric insulator.

- To investigate the effect of uniform pollution layer on the electric field and potential distribution along the textured silicone rubber patterns.

- To study the impact of non-uniform pollution layer on the electric field. The mathematical and statistical analyses have been used to evaluate the contribution of the studied factors and their interaction on the total variation of the electric field.

1.5. Methods

In order to achieve the objectives of this research work, numerical and experimental studies were performed. Each of them follows a methodology whose different steps are described below.

For experimental methods, a series of laboratory experiments were performed in the Power Systems Laboratory at American University of Sharjah, (UAE). These experiments were carried out using the DC-AC high voltage tracking testing machine, which is specially designed to perform the inclined-plane test (IPT).

The IPT is one of the most successful experiments to test the resistance to tracking and erosion for polymeric insulator and is described in the IEC 60587

international standard [19]. Rectangular standard size samples are mounted at a 45° angle and subjected to high voltage stress. A salt contaminant solution is fed from the top of the sample and traverses the test surface. The test is designed to encourage the formation of dry-bands and surface discharges in order to monitor surface erosion and tracking. A series of tests at AC and positive DC were performed on two different rectangular SiR designs (smooth and textured) to study their aging performance and the degradation levels on each insulator surface. A visual video camera was used in order to record any indications of aging on the surface of the tested insulators.

For numerical analysis, they can be used to calculate the electric field and voltage distribution along textured silicone rubber surface under clean and different polluted conditions. Three-dimensional (3D) models of different textured surfaces were designed by Computer Aided Design (AutoCAD) software package. These samples were imported into COMSOL Multiphysics 4.3b for computation purposes. In the case of non-uniform pollution distribution, we have combined the finite element (FEM) with the design of experiment method to investigate and describe the behaviour of textured SiR Insulators.

1.6. Contribution of the present work

1) The standardised test methods for outdoor polymeric insulators are (a) salt-fog tests (b) clean-fog tests (c) rotating-wheel tests and (d) inclined plane tests (IPT). Of these tests, the IPT has been widely utilized in the industry and even at the research scale. Recently, many tests were carried out for evaluating resistance to track the erosion of silicone rubber textured patterns used under AC voltage according to the inclined plane test methods indicated in the IEC 60587 standard [16-18, 20, 21]. However, no research has been carried out to investigate the behaviour of textured insulators under DC voltage according to the IPT. Therefore, the originality of the experimental study is to evaluate and compare the performance of textured insulators and conventional insulators at DC voltage by using the IPT. Also, the textured and conventional surface insulators degradation under AC and positive DC voltage were investigated.

2) Electric field analysis around high-voltage insulators is with extreme importance during the development of new polymeric insulators design. The numerical method can be used to estimate the electric field strength because it is considered an economical and efficient way. Recently, the finite-element method (FEM) has been widely employed in HV engineering and numerous models have been developed for clean and polluted insulators [22-25]. However, to the best of our knowledge, no numerical models regarding textured insulator based on the FEM method were developed.

The originality of numerical study lies in aspects that can be described as follows:

- The maximum electric field is calculated taking into account various available patterns of hemispherical protuberance having different diameters under clean condition.

- A statistical model based on the design of experiment methodology is developed to study the maximum electric field in a textured insulator polluted in a non-uniform way. This work takes into account three factors characterizing the distribution of the pollution layer. The plan used provides much information for a better interpretation of the electric field under different pollution conditions.

1.7. Thesis Organization

This thesis is divided into six (6) chapters. In this chapter, a general introduction of this thesis is given. Also, the research objectives, used methods, and the main contributions of this work are briefly described.

Chapter 2 provides a literature review of high voltage polymeric insulators, particularly SiR Insulators. General insights into polymeric insulators including key advantages, chemical composition structure of SiR Surfaces, structural design, loss and recovery of SiR surface hydrophobicity, and factors contributing to the ageing or degradation process are presented. In addition, a review of the proposed methods for laboratory testing of polymeric insulators and the different diagnostic techniques currently available are presented.

Chapter 3 describes the design principles of textured patterns used in this study. The IPT setup and methods are described. In this chapter, the literature review of the research work pertained to the erosion mechanism in the IPT is presented. Also, the literature review of tests carried out for evaluating resistance to the erosion of silicone rubber textured patterns in standard AC IPT are presented.

Chapter 4 presents the silicone rubber samples (conventional plain-surface and textured) used in experimental study, in addition to the equipment and procedures used for the experiments to investigating the performance of silicone rubber insulators. The tests were performed according to IEC60587 to compare the aging performance, especially the resistance to erosion, of SiR polymeric insulators under AC and positive DC. Analyses and interpretations of the whole results obtained in the experiment are presented in this chapter.

Chapter 5 presents the investigation of electric stress on textured and non-textured polymeric insulators by means of computer simulations. These simulations are intended to identify regions of the high electric field stress over the insulator surface. A commercial finite element package is employed for insulator modelling to determine electric potential and field distribution along the distance between electrodes under dry-clean and wet-polluted surface conditions, with uniform and non-uniform pollution models. The simulation results are discussed in this chapter.

Chapter 6 presents general conclusions based on the findings in this study, and proposed some suggestions for future research.

Chapter 02

HIGH VOLTAGE COMPOSITE INSULATORS

2.1. Introduction

Polymeric insulators for outdoor applications have been commercially produced for more than four decades, and the demand is increasing rapidly due to their encouraging performance under diverse conditions. Massive deployment of polymeric insulators throughout the power industries has resulted in large-scale research investigations aimed at enhancing in-service operation that could last for at least thirty to forty years, just as was the case of their ceramic counterparts.

This chapter describes composite insulators and then discuss the degradation and failure modes of these insulators with a particular emphasis on the origin of defects and their consequences. Also, a review of the methods proposed for the laboratory testing of polymeric insulators is presented. Finally, the different diagnostic and monitoring techniques of composite insulators currently available are presented.

2.2. Composite insulators for high voltage

The selection and acceptance of outdoor insulators in high voltage equipment's rely on the assurance of good and long- term stable properties of these products. Life time's ranging for a few decades and very low failure rates are desired.

In 1950's United State of American (USA) started the use of polymeric insulators, the practical performance of these insulators was far less than satisfactory, with a number of problems and failures made the insulators unpopular in the market [26].

However, in 1970's, polymeric insulators came into spotlight with the development of Fibre Reinforced Plastic (FRP) technology with improved housing material; the reliability of polymers has improved significantly [27]. Power utilities started using composite insulators and have become popular in high voltage

applications due to their better pollution performance, lightweight, resistance against vandalism etc, steadily increasing their share on the market when compared to the traditional insulators made of porcelain or glass.

2.2.1. Composite insulation materials

Several types of polymeric materials have been developed by manufacturers, each with specific properties. In the field of outdoor insulators, three classes are particularly used: epoxy resins, Ethylene-Propylene Rubber (EPR) and Silicone Rubber (SiR) [28-30].

Epoxy resin materials are suitable for distribution insulation with a voltage up to 69 kV, and their long-term performance in clean environments is relatively successful. However, in polluted environments, their performance is unsatisfactory [28].

There are three types of Ethylene Propylene Rubber (EPR) in common use in overhead outdoor insulations: Ethylene-Propylene-Diene monomer (EPDM), Ethylene Propylene Monomer (EPM), and a co-polymer of ethylene-propylene and silicone [28, 29]. These materials are suitable for distribution and transmission systems with up to 765 kV [28]. Their long-term performance in clean environments has been successful. In polluted environments, their performance has been mixed, with some good experience, but generally, their long-term performance has been unsatisfactory.

Currently, the third generation of polymeric insulators is used extensively in service, where several experimental studies were conducted and appropriate modifications were made and adopted. The housing material of these insulators is mostly SiR. These materials have proven to be the most reliable for outdoor electrical insulation systems [31].

2.2.2. Silicone rubber used in outdoor insulation

The backbone structure of SiR is composed of alternating inorganic siloxane bond (Si-O) with methyl groups (CH_3) added, forming polydimethylsiloxane (PDMS) as shown in Figure 2.1. The silicon-oxygen (Si-O) linkage in the silicone polymer chain is the same as that in sand, quartz, and glass. This bond is responsible for the

good high-temperature stability of the silicones and their resistance to weathering, corona discharge, and oxidation by ozone, and ultra- violet (UV) radiation, thereby, ensuring a long-term stable performance over an extensive range of in-service conditions [5].

Silicone-based insulation housing can be classified with respect to the curing temperature to High-Temperature Vulcanizing (HTV), Room-Temperature Vulcanizing (RTV) and Liquid SiR (LSR). The HTV SiR is cured at high temperature, at 180°C, and pressure, and is commonly used in outdoor transmission and distribution as well as station post insulators. The RTV SiR can be supplied either in one- or two-component compounds. The first is cured at room temperature and commonly used in coating of ceramic insulators; whereas, the two-part RTV SiR cures at a lower temperature as compared to the HTV SiR, and is widely used for insulation housing of large equipment, such as transformer bushings in power stations. Unfilled LSR is supplied in two parts including the base polymer and curing agent, and can be cured at 200 °C within a few minutes [32].

Fillers are added to the SiR insulations to control different properties, such as mechanical stability and improve the resistance to tracking and erosion, which are added relatively in small amounts. The most common fillers used for SiR are Alumina trihydrate filler (ATH) (Al (OH)$_3$) this provides better resistance to tracking and erosion [33] and Silica filler (SiO2) improves the mechanical strength of silicone compounds [34].
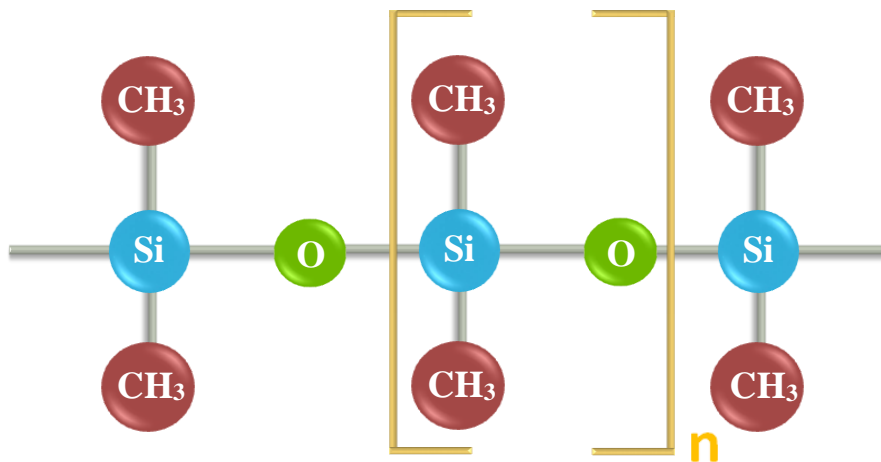
Figure 2.1 Chemical structure of silicone rubber [32]

2.2.3. Benefits and limitation of polymeric insulators

The material used for this work is SiR that has a number of advantages compared to the conventional glass and porcelain insulators; the main advantage of SiR Insulators is that their light weight. This makes it attractive in many ways, especially regarding installation and maintenance costs reduction [35]. Polymeric insulators have numerous other advantages including the following:

- Light weight: Polymeric insulators offer significant weight reduction compared to the corresponding ceramic insulation systems (much as 90%) [36]. There is less need for strong heavy support and cranes for installation, which results in easier handling and substantial savings in overall installation, operation and maintenance costs.

- Resistance to damage: Polymeric insulators with elastic properties help to prevent the risk of breakage during transportation or vandalism from gunshots that could lead to cascading failure as was experienced with ceramic insulators, this significantly reduces the loss [37].

- High mechanical strength: Polymeric insulators have a high mechanical strength to weight ratio that allows for longer spans and less expensive tower structures. They provide improved mechanical strength under bending, deflection and compression stress. It has been reported [38] that polymeric insulators passed mechanical tests under extreme conditions without any permanent damage.

- Hydrophobicity: Hydrophobic properties of silicone rubber significantly reduces the leakage current and the probability of dry band formation, which consequently results in reduced flashover voltages [28, 39- 41].

- Recovery of hydrophobicity: Even though silicone housing can temporarily lose its hydrophobicity under severe conditions, these materials are able to regain hydrophobicity after a sufficient resting period with the absence of discharge activity [42].

- Improved contamination performance: Polymeric insulators have low surface energy resulting in a water repellent or hydrophobic surface. This property can also be transferred to an overlying pollution layer [43] enabling improved pollution performance for insulation systems in highly contaminated regions such as coastal and

industrial areas.

Despite the abovementioned advantages, polymeric outdoor insulators, however, suffer from a problem of material deterioration, known as ageing. This is primarily due to concurrent stresses; environmental, electrical and mechanical stresses encountered in a diverse range of service conditions.

- Polymeric materials which are organic in nature have weaker bonds, and hence susceptible to chemical change and compound degradations.

- Degradation can lead to changes in the surface properties of polymeric insulator, which can reduce electrical performance and increase the amount of surface discharge activity occurring in wet and polluted conditions, causing ablation of the material surface.

- Polymeric insulators can lose hydrophobicity due to a combination of exposure to UV, moisture, heat, and electric discharge activities that may occur on the insulator surface.

Due to utilities' increased experience with these insulators through extensive research conducted in laboratory and field test stations, several problems have almost been eliminated by the use of new manufacturing techniques and excellent materials [44,45], the failure rate of polymer insulators has decreased to 26% of its initial value [46].

The new technology of polymeric insulators has possibilities for use in many applications of high voltage systems. However, their expected lifetime is still an issue of concern to some power utilities. Therefore, further researches are required regarding choosing an appropriate insulator design and manufacturing, investigating the composition of polymeric materials and the understanding of electrical, chemical, and mechanical deterioration mechanisms.

2.2.4. Hydrophobicity of silicon rubber

A hydrophobic surface is defined as a surface which is not readily wettable. Water on the surface does not form a continuous film, but forms individual droplets. The hydrophobic property of an insulating material is very important when speaking about the operating performance of the electrical equipment. On a hydrophobic surface

no water film will be formed which will result in low leakage current between the high voltage and ground electrode. The silicone rubber surfaces are more hydrophobic than conventional insulators. This property contributes to the longevity of insulation materials.

The simplest way of quantifying hydrophobicity is by measuring the static contact angle (θ_c) of a water droplet. Figure 2.2 illustrates the behaviour of a water droplet on a hydrophilic and hydrophobic surface. A contact angle $\theta_c \leq 90°$ indicates that the surface is hydrophilic; while contact angles $\theta_c > 90°$ indicate that the surface is hydrophobic [47]. For new SiR it is approximately 100° while for glass and porcelain it is 44° and 47° respectively [48].

(a)   (b)
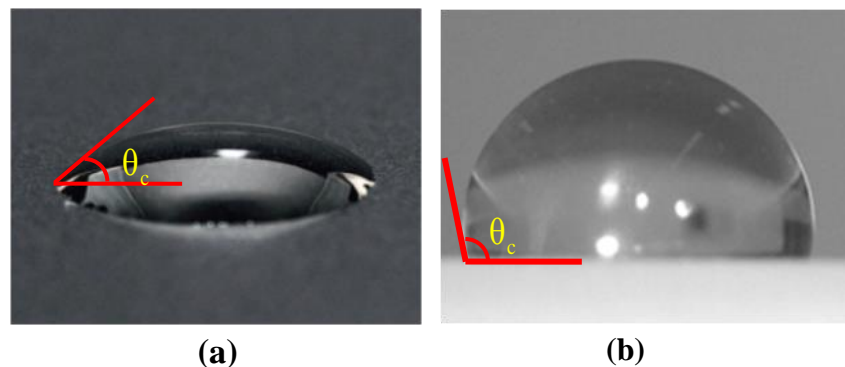
Figure 2.2 Behaviour of water droplet on an insulating surface
(a) Hydrophilic surface (Porcelain) and (b) Hydrophobic surface (Silicone) [49]

2.2.5. Silicone rubber insulators construction

Long-rod SiR insulators, which are used for different overhead lines and distribution systems, have the same design structure, but the size of these insulators and the end fitting shapes are variously based on the application for which they are used [50].

The SiR polymeric insulators are composed of three (3) main components (Figure 2.3) [4]:

1) *The fiberglass core*

The core is the central part of the polymer insulator made of fiberglass reinforced epoxy resin to provide the appropriate mechanical strength. Epoxy resins offer better electrical properties than polyester resins which are applied in some cases to reduce costs [4].

2) *The metal end fittings*

The end fittings are generally made of metal (cast iron, aluminium alloy and forged steel [32]). Their shape is very important to limit the corona discharges that cause premature degradation of the polymeric material. The Figure 2.4 shows typical end fittings shapes. The dimensions comply with the IEC 60120 and IEC 61466 standards [51, 52].
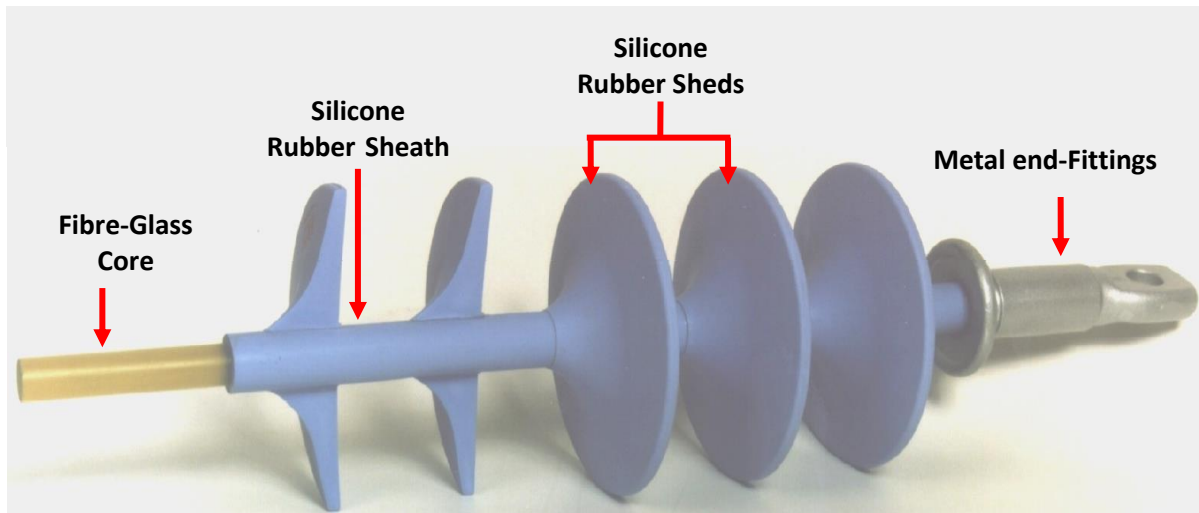
Figure 2.3 Construction details of a composite insulator

Figure 2.4 Typical end fittings for composite long rod insulators

3) *The SiR Housing (The sheds and sheath)*

The core is encapsulated in a protective housing consisting of the sheds, and the sheath. The sheath protects the fiberglass core from damages due to electrical discharges and environmental stresses, and the sheds provide the required leakage distance.

The housing is manufactured from a variety of materials. EPDM and SiR are the two most common polymeric compounds used for outdoor high voltage insulation

system. SiR compound is generally preferred because of its excellent electrical performance in various polluted environments. This is attributed to the strong hydrophobic surface properties, contrasted with EPDM which starts to show hydrophilic effects on exposure to prolonged wetting and electrical activity [53]. Numerous studies have shown that silicone rubber surfaces recover their hydrophobicity more quickly than EPDM surfaces [54, 55], and maintains its hydrophobic surface for a much longer time than the EPDM samples [33], this is the main reason for which SiR material is preferred to be used in heavily-polluted environments.

2.3. Degradation of polymeric insulator

Composite insulators are subjected, during their lifetime, to various combined stresses that cause more or less irreversible damage. These stresses can be grouped into three main categories, namely, environmental (temperature, moisture, UV sunlight, and humidity), electrical (discharge activities in the form of surface arcing or corona activity), and mechanical stress [56].

The polymeric materials, due to their weak organic bonds, are vulnerable to chemical change on exposure to these stresses, which consequently lead to degradation and ageing of the polymeric insulator [57]. The main factors leading to degradation of polymer insulators are illustrated in Figure 2.5.

For the pollution performance, the damage induced by surface discharges is of critical importance. The temperature produced by surface discharges can decompose the organic polymer, leaving traces of carbon forming resistive paths, a procedure called tracking [58, 59]. Erosion is the thermal damage associated with the loss of material from the polymer surface, especially in regions of localised discharge activity. Both tracking and erosion effectively reduce the performance of the insulator, and polymeric materials used on outdoor insulators should be assessed for their ability to resist such degradation.

Mechanical stress develops when strong winds move the line, causing oscillation. The consequent vibrations can cause the formation of fissures at the joint interface between the core and the metal flanges. In some cold-climate countries, ice

accretion on both the conductor and weather sheds housing could generate additional loading stress on the polymeric insulator. In hot desert regions, the average temperature can easily reach 40°C during the day and drop below 10°C at night. This considerable change in ambient temperature results in a cyclic process of thermal expansion and shrinkage that can loosen the connection at the core-end fitting interface, affecting the mechanical strength of the polymeric insulators.

The aging processes in composite insulators are complex due to a large number of ageing factors and due to the effect of one stress over another [60, 61]. Spellman et al. [56] reviewed the main ageing factors leading to polymeric insulators degradation.
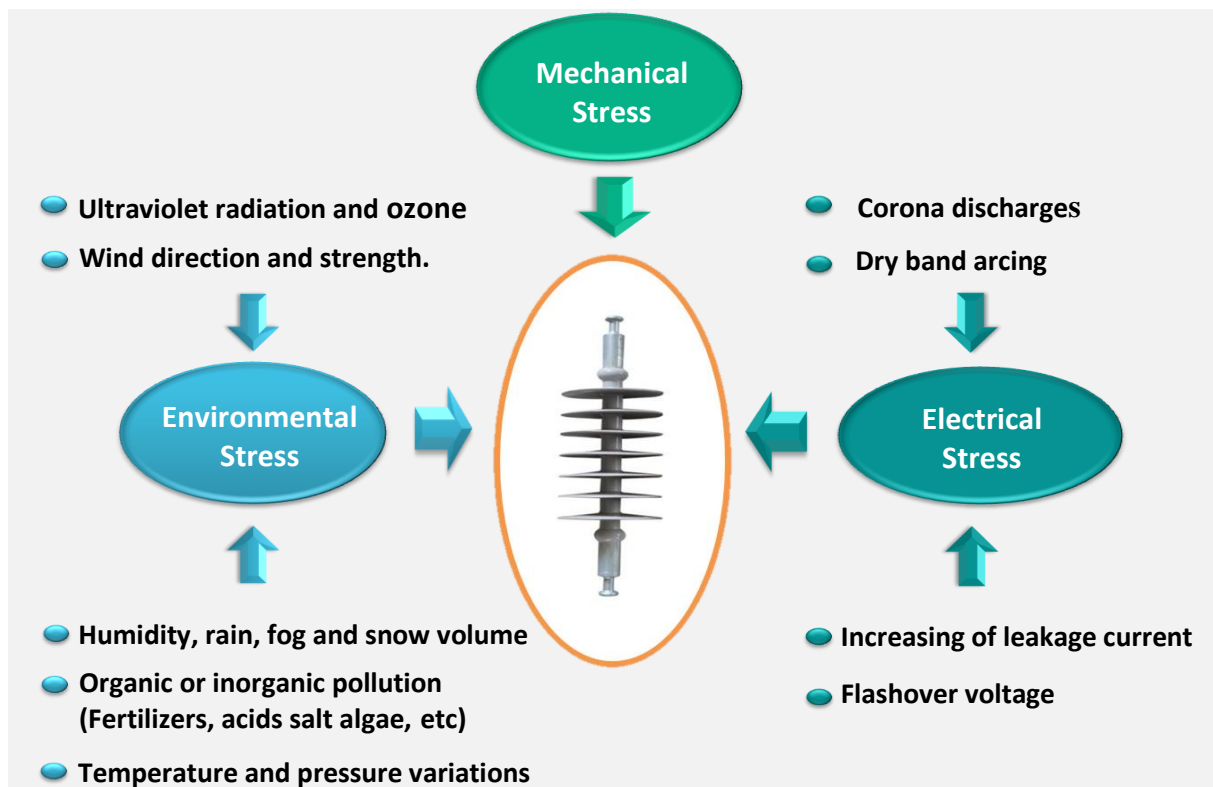
Figure 2.5 Factors affecting the ageing rate of composite insulators

2.3.1. Ageing mechanisms of silicone rubber insulators

The ageing mechanisms and flashover processes are different for traditional ceramic systems and composite insulators. This is mainly due to the higher hydrophobicity of the polymeric surfaces of composite systems and the different ageing characteristics [4, 62]. This is particularly true for silicone rubber. The insulator surface degrades in the great majority of cases under electric stress arcing

synergistically with organic and inorganic pollution and humidity. Electrical discharges are the main cause of damage, resulting in an increase in the leakage current, loss of hydrophobicity, erosion, and tracking on the insulation surface [63].

The ageing mechanisms and flashover processes is a multi-step process for a SiR insulator. The main steps are explained as follows [64]:

⇒ **Contamination builds up**: The insulator surface gradually gets polluted during service. For both marine and inland pollution, the surface tends to accumulate a uniform pollution layer.

⇒ **Diffusion of low molecular weight Chains**: Diffusion would drive the low molecular weight chains to be out of the bulk of the polymer. The LMW will form a thin layer on the insulator surface and covering the pollution.

⇒ **Wetting of the Surface**: Dew, early morning fog, light rain or high humidity produces water droplets on the hydrophobic surface of the polymer insulator, as shown in Figure 2.6a. Salt from pollutant dissolves in the water drops, which become conductive. At this stage, the diffusion will drive water from the droplet to travel through the thin polymer layer and later, into the dry pollution. This condition will generate a high resistive layer around each droplet, as shown in Figure 2.6 (b).

⇒ **Ohmic heating**: The small leakage current passes through a highly resistive layer of the insulator surface. As the electrolyte has a negative thermal coefficient, the surface resistance will decrease gradually, and the leakage current will increase due to heating. At the same time, drying and loss of moisture increase the surface resistance. The two contrasting phenomena attain equilibrium at a lower level value of leakage current.

⇒ **Effect of electric field on water droplet**: The development of the wetting process increases the water droplets' density and reduces the distance between them. The applied electric field results in a force, which flattens and lengthens the droplets. If the distance between the drops is small, the adjacent droplets gather together, and filaments are created, as shown in Figure 2.6 (c).

⇒ **Spot discharge**: Filaments that have been formed would reduce the distance between the electrodes, which leads to an increment in the electric field between the adjacent filaments. This field intensification would produce spot

discharges between the filaments as demonstrated by Figure 2.6 (d). It can be seen that the spot discharge is randomly distributed along the insulator surface.

⇒ **Loss of hydrophobicity**: Spot discharges age the polymeric layer around the droplets and reduce the hydrophobicity. This reduction of hydrophobicity joins the filaments together and increases the field strength. High electric field around the electrode would create corona and surface discharges which then destroy the hydrophobicity property. Reduction of hydrophobicity eventually joins the filaments together. Combination of filaments would also form the wet region, as shown in Figure 2.6 (e).

⇒ **Dry band formation**: Due to the non-uniform heating effect, areas of high resistance, known as dry-bands (DB) are formed and interrupt the flow of leakage current. If, however, the resistance of the unabridged portion of the pollution is not high enough, more DB may follow and the subsequent increase in local field gradients across them causes localised arcing. Consequently, temperature increases and ionized plasma is formed. The temperature generated due to repeated DB arcing can reach beyond the safe limit of organic material, namely 400 °C. If the temperature exceeds beyond this limit, it can lead to tracking and erosion [65, 66].

⇒ **Flashover:** The growth of wet areas along with the further elongation of water filaments finally creates a conductive path capable of leading to a flashover when the arc voltage gradient is lower than that of the filament $E_{arc} < E_{filament}$ (Figure 2.6 (f)). The flashover and degradation are the main influence on the overall electrical performance. However, these two aspects are not necessarily dependent on each other. Service experience [67] has indicated that polymeric insulator flashovers can occur without any substantial degradation (erosion and/or tracking), and in some situations, surface erosion has occurred without leading to a flashover.

2.3.2. Loss and recovery of hydrophobicity on SiR

Hydrophobicity is a dynamic characteristic that could be lost due to different environmental and electrical stress, but can also be repeatedly recovered [68].

The hydrophobic surface property of silicone rubber is temporarily lost when continuously exposed to several factors such as the accumulation of pollution layers,

electrical stresses (partial discharge, arc and corona) and UV radiation, which leads to the oxidation of the surface. Oxidation leads to the formation of inorganic structures of silica (SiO_2). Kim et al [69] have shown that exposure to the salt fog of silicone under high electrical stress results in the formation of a surface layer of SiO_2. Zhu et al. [70] have shown the loss of hydrophobic properties after the application of discharges to a silicone surface.
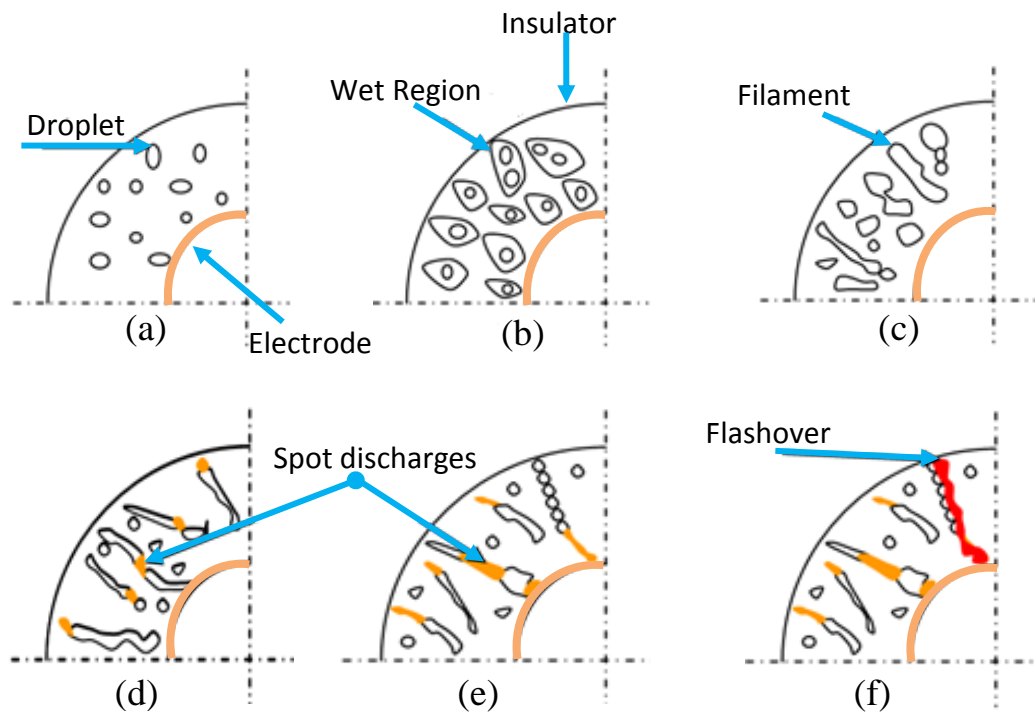
Figure 2.6 Ageing mechanisms of silicone rubber insulators [64]

The recovery of surface hydrophobicity is happened due to the diffusion of low molecular weight (LMW) silicone chains from the bulk material to the surface, forming a lattice type thin layer consisting of methyl groups (CH_3), this phenomenon has been defined by Gorur et al [71]. It has been observed that the surface regains hydrophobicity after sufficient resting period with the absence of discharge activity [42, 72].

Interestingly, this phenomenon can also be transferred to the pollution layer [73- 75]. With time, pollution becomes completely hydrophobic and this happens for all pollution except for the case of a solid homogeneous salt layer, which is very rare for natural pollution [68]. This means that the hydrophobic character of the surface is maintained at all times, enabling improved pollution performance for insulation

systems in highly contaminated regions such as coastal and industrial areas. It has been observed [76] that the insulators with 20 years old in service still have the ability to transfer hydrophobicity as fast as the new ones.

Investigations by Vlastos and Sherif [77] showed that SiR could remain hydrophobic after nine years of exposure to a contaminated coastal environment.

2.3.3. Polymeric insulators failure modes
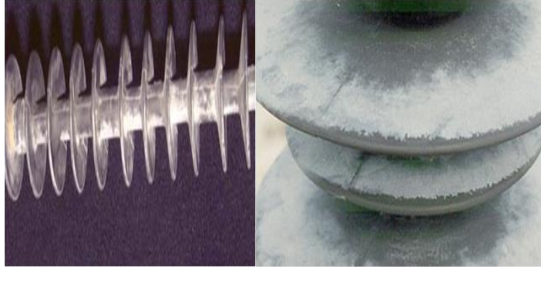
There are different types and forms of deterioration, damage, and modes of failure. Knowledge on the possible failure modes and their causes is required, will greatly facilitate informed decisions on the choice of insulators for given service conditions, as well as devising appropriate maintenance and inspection procedures.

Two different institutes have presented specific definitions and images for the identification of different degradation and damaging process that can be visually identified on polymeric insulators: The Electric Power Research Institute (EPRI, USA) [78] and the Swedish Transmission Research Institute (STRI, Sweden) [79]. A third visual guide [80] from the Transmission Department of Florida Power & Light Co (USA) to help the activities of its own maintenance personnel which include two options: replace or keep in service.

2.3.3.1. Deterioration

Deterioration is defined as superficial ageing that occurs on the composite insulator as a direct result of exposure to the service environment, electrical stress, mechanical loading and/or careless handling. This ageing is not expected to cause a significant reduction in the insulator's performance and/or lifetime, and does not represent reliability risk. These conditions do not normally require the replacement of these insulators. As specific limits, deterioration does not significantly reduce the thickness of the polymer housing (i.e. by more than 1mm at the sheath) that prevents moisture ingress to the core rod [79-81]. The most significant deterioration processes occurring in polymeric insulators are presented in Table 2.1.

Table 2.1 Classification and description of composite insulator deterioration

Chalking- appearance of a rough and whitish powdery surface, due to some filler particles of the housing material caused by UV radiation and electrical activity.	
Colour changes - change in base colour of the housing material of the polymer caused by oxidation, UV attack, weathering, and/or corona discharge activity.	
Cracking - any surface fracture to depths greater than 0.1 mm. Stress cracking breaks weak linkages between polymers (does not break internal polymer strong bonds) when mechanical stresses cause minute cracks in the polymer and they propagate rapidly under harsh environmental conditions.	
Crazing - surface micro-fractures of depths approximately 0.01 mm to 0.1 mm. Crazing is a network of very fine cracks on the surface of a material.	
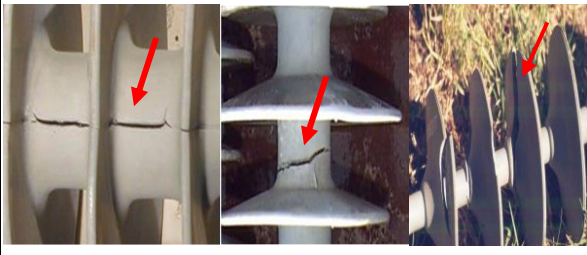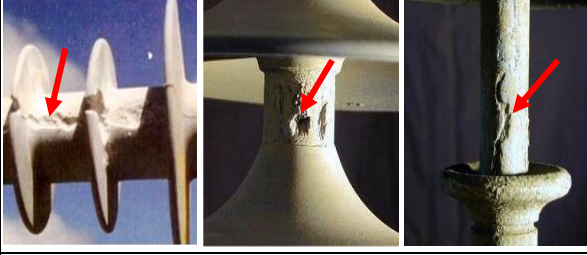
2.3.3.2. Damage

Damage is defined as irreversible changes to the composite insulator that occur as a consequence or progression of pre-existing surface deterioration and/or external influences (careless handling, vandalism, misapplication, lightning, pollution, etc). Damage may be expected to have a negative impact on the insulator's performance and/or the lifetime. Sometimes an insulator is damaged in such a way, or to such a degree, that leaving it in service presents an unacceptable risk and it must be removed [45, 79 - 81].

Table 2.2 summarizes the most common damages that can be detected during visual inspection processes of composites insulators. A highly illustrative photographic exhibition of deterioration, damage, and failures on different insulators aged in service is presented in [78-85] and constitute very complete and graphical support for the

personnel in charge of the inspection, diagnosis, maintenance activities.

Table 2.2 Classification and description of composite insulator damage.

Fracture - This leads to mechanical degradation of the fiberglass core rod and is characterised by some smooth fracture surfaces. This failure mode is attributed to an attack by nitric acid generated by corona discharge activity in a moist environment. The exact source of the acid has been a topic of much debate. However, it is now thought that the brittle fracture may be due to a combination of factors and is not always described by a single mechanism.	
Splitting/cutting - Irreversible break, tear, crack or material loss in polymer housing (e.g. shed, sheath) which reduces the creepage distance (i.e. by more than 10%) or the thickness of the polymer sheath (i.e. by more than 1mm).	
Erosion - Irreversible and non-conducting degradation of the surface of the insulator that occurs by major loss of material, which significantly reduces the thickness of the polymer sheath that prevents moisture ingress to the core rod (i.e. by more than 1mm). This can be uniform or localized.	
Corona cutting - Scissoring of the polymer material resulting from exposure to localized high levels of ultra-violet energy associated with the presence of corona discharges.	
Tracking/Carbonising - Irreversible degradation by formation of conductive paths (tracks) starting and developing on the polymer material (hydrocarbon polymers), with appearance of carbon paths that cannot be easily removed and are conductive even in the dry state.	
Puncture: Holes in the insulator sheath/shank or shed.	

2.4. Artificial pollution testing methods of polymeric insulators

Laboratory tests are performed in order to provide a comparison of different insulator types and materials, a view of the performance of insulators under different conditions and to investigate the behaviour of materials under certain types of stresses. Further, they can also be conducted in order to test the insulators withstand on severe stressing or to a worst-case scenario which can be decided according to the pollution severity of the installation site [86]. Different facilities and types of tests have been developed which predict the ageing effects in advance and thus are called accelerated ageing methods.

The four basic standardized tests that researchers usually follow are the salt-fog test [87], the clean- fog or solid-layer test [87], the inclined-plane test [19 - 88] and the rotating wheel dip test (tracking wheel test) [89], and other approaches for evaluating tracking and erosion have been developed [90].

2.4.1. Clean-fog and Salt-fog test

In the clean-fog test (solid layer test), the insulators or specimens are artificially contaminated (contaminants are usually made of Kaolin, NaCl, and water) and left to dry before entering the clean-fog chamber. And then, the dry contaminated insulators are energized and subjected to a fog generated from tap water to wet the contaminating layer gradually. This test method simulates the condition in which a contaminant that has accumulated on the insulator surface is gradually wetted by natural sources of moisture leading to an increase in the possibility of the flashover phenomenon.

The salt-fog tests are conducted in specially designed salt-fog chambers. The tested insulator or specimen is put in the chamber and salt-fog is used as an artificial pollutant. This procedure simulates coastal pollution where a thin conductive layer (formed by salt) covers the insulator surface. The fog is produced by rows of sprayers arranged on either side of the insulator. The spray consists of two nozzles, one delivering the salt solution and the other arranged perpendicular to the other provides a stream of compressed air to atomize the solution [87].

The leakage current amplitude, the cumulative charge, the weight loss and the failure time are the main parameters measured from this type of test. The parameters

of the salt-fog (conductivity of the water, flow rate) have different effects on the results of flashover voltage and leakage current [91]. A factor that must be considered when testing silicone rubber is the ability of this material to recover hydrophobicity after damage by surface discharges. In a continuous the fog test, silicone rubber samples quickly lose their hydrophobicity and are then susceptible to erosion damage from increased discharge activity. It has been found that providing rest periods without fog of between 8 and 24 hours can allow recovery of hydrophobicity, dramatically improving the performance of SiR [33]. A schematic diagram of the test setup is shown in Figure 2.7.
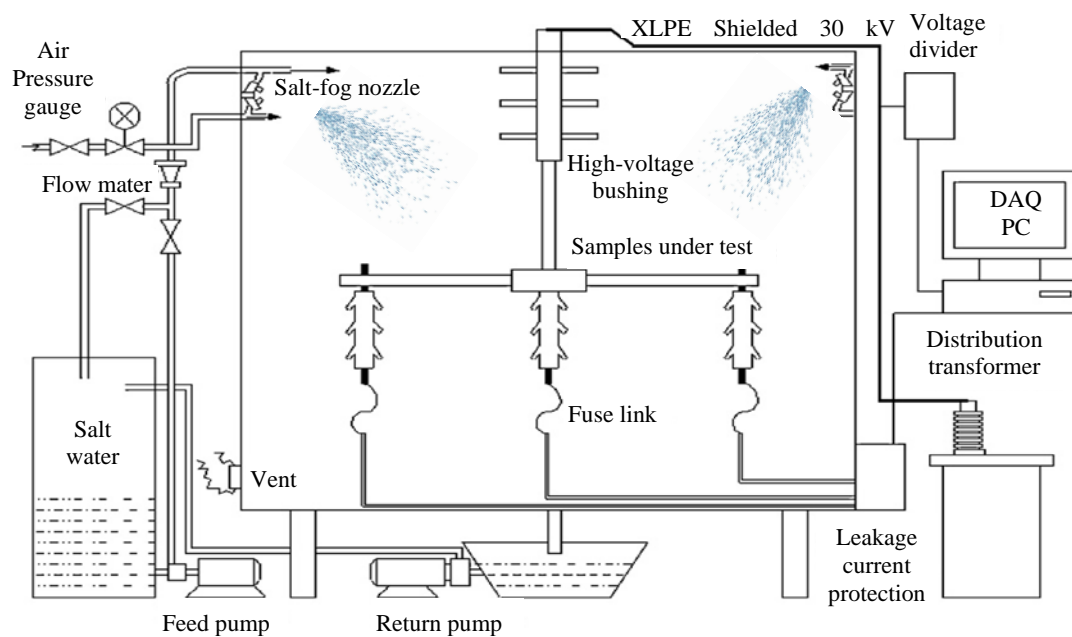
Figure 2.7 Schematic diagram of the salt fog chamber test [92]

2.4.2. Rotating wheel dip test (RWDT)

The rotating wheel dip test (RWDT) is one of the most commonly used methods of investigating the performance of high voltage insulators. Based on the standard IEC 62217 [89], RWDT has been considered as a screening test in order to identify any material or design unsuitable for use in overhead transmission lines.

In this method, the tested insulators are fixed on a rotating wheel and are turned around continuously, dipped to salted water and then exposed to high voltage. A schematic of the RWDT setup is illustrated in Figure 2.8.

The insulators under test have to go through four positions in one cycle; the positions are at 0°, 90°, 180° and 270°. The different positions of the cycle may be described as:

1) The insulator is dipped into a saline solution. 2) The insulator is left to standing of in a horizontal position to reduce the saline solution from its surface. 3) The insulator is in the vertical, it touch the copper tape so it is under the voltage supply. 4) The surface of the insulator that had been heated by the dry band sparking is allowed to cool. The test is stopped when the breakdown occurs, or when the leakage current value exceeds 300 mA.
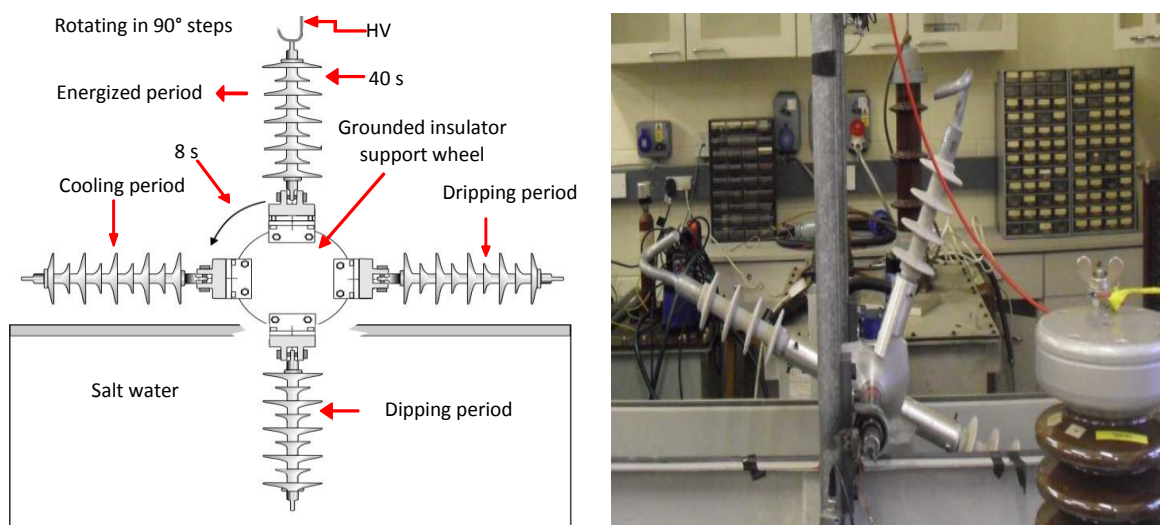
Figure 2.8 Schematic diagram of rotating wheel dip test [89, 93]

2.4.3. Inclined-plane test (IPT)

The inclined-plane test (IPT) is a well-established material test for the assessment of the resistance of insulating materials against erosion and tracking and is described in the IEC 60587 international standard and ASTM D2303 [19,88]. The test set-up of the IPT is illustrated in Figure 2.9.

Rectangular standard size samples are mounted at a 45° angle and subjected to high voltage stress. A salt contaminant solution is fed from the top of the sample and traverses the test surface. During this test, the leakage current flows through the conductive path may cause partial evaporation of the contaminated and lead to the

formation of dry bands and arcing. The concept of this test is described in Chapter 3.

Figure 2.9 Test set-up for the inclined plane test according to the IEC 60587 standard [94].

2.5. Diagnostic methods

The aim of diagnostics is, in general, to get relevant information about the state of technical systems [95]. In insulator applications, this means that diagnostics should be a way to help electricity supply companies in making decisions about maintenance or replacement. It is basically associated with reducing costs and minimizing the risk of damage. There are several tools available to monitor the aging of materials under test. These tools can be classified into several categories: electrical and physical tools. At present, the most realistic condition assessment techniques are visual inspections, hydrophobicity evaluations, leakage current and electric field distribution measurements.

2.5.1. Visual Inspections

Visual inspection is the most common technique used by utilities to identify defected composite insulators in service [35, 96, 97]. Visual inspection can help to detect main ageing processes such as tracking, erosion, splitting, puncture, or any other obvious damage.

Imaging techniques, such as infrared thermography (IRT), ultraviolet (UV), and light amplification equipment, were able to detect the presence of discharge activities on the insulator surface. IRT imaging equipment was found useful for providing indications of internal faults, like tracking, that may potentially lead to failure of the insulator [45].

2.5.2. Leakage current measurements

The degradation process such as tracking, erosion and loss of hydrophobicity can develop significantly on the surfaces of the insulation, due to the appearance of leakage current. For this reason, leakage current measurement is one of the most suitable parameters to evaluate the performance of the material surface [98].

The leakage current activity is very rapidly affected by any change in weather or any other parameter. Even slight humidity changes show an effect in the change of the value of leakage current. For this reason, it is used frequently as a parameter for analysis.

Gorur et al. [33] found that both the magnitude of the peak current and the number of current pulses have presented good indicators of the surface condition and tracking damage of the polymeric insulators. It has also been shown that the transition of the silicone rubber surface from a hydrophobic to a hydrophilic surface due to dry band discharges. Loss of hydrophobicity was accompanied by an increase in average leakage current. The contact or the wetting angle was high (about 90°) initially when the surface was non-wettable and was low (about 30°) when the surface was wettable.

Figure 2.10 illustrates some examples of leakage current patterns. Full analysis of the leakage current signals along specific extension of time offers good information about the degradation processes that are occurring on the insulators surface and its relation with the environmental conditions and pollution [99-101].

Results from literature [102-106] showed that leakage current parameters (e.g. peak and rms values) provide valuable information that can be used to evaluate the polymeric insulator performance.

2.5.3. Measurement of hydrophobicity

Traditionally, the state of hydrophobicity on material surfaces is established through measuring contact angles (θ_c). The most commonly used method is the so-called sessile drop technique [107], since measurement of the contact angle technique is applicable only in the laboratory environment and is difficult to perform for the whole insulator surface, or on complex surfaces such as on textured insulators. To overcome this, a simple test method for hydrophobicity classification (HC) has been

introduced by the Swedish Transmission Research Institute (STRI) [108], which has been now adopted by the IEC [109].
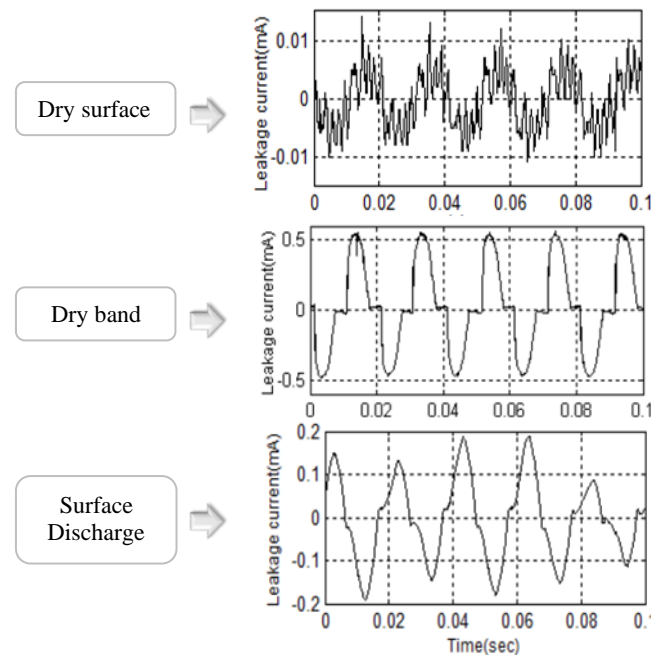
Figure 2.10 Leakage current patterns [100]

2.5.3.1. Contact angle method

The contact angle method is a measurement that involves the evaluation of the contact angle formed between the edge of a single droplet of water and the surface of a solid material.

In this technique, a water drop is placed on the horizontal surface using a syringe. The static contact angle is then measured manually using a goniometer. The angle on the inside of the drop is measured (Figure 2.11). An idealized surface with perfect hydrophobicity will have an angle of 180°. A sample that is completely hydrophilic will have a contact angle equal to 0°. To be considered hydrophobic, the contact angle must be at least 90°; to be considered super hydrophobic; the contact angle must be more than 150°.

2.5.3.2. STRI hydrophobicity classification

It is a simple procedure that allows to manually obtaining a measurement of the hydrophobic properties of the insulating surfaces in the outdoor environment. The degree of the wettability of a surface of an insulator surface is divided into seven hydrophobicity classes (HC-1 to HC-7) [108]. HC-1 is the most water-repellent

(completely hydrophobic) class whereas HC-7 refers to completely hydrophilic surfaces.

First, the surface is sprayed with water. One thing to consider while spraying for hydrophobicity test is to keep samples at inclinations of 10° to 35° from the horizontal. These inclinations should be chosen as they represent well typical inclinations of insulator surfaces in actual service. Then, the hydrophobicity of the insulator surface is identified by comparing the surface with one of the standard photographs of the hydrophobicity classes (HC). Table 2.3 shows the STRI criteria for determination of HC.

$\theta = 0°$ (Completely hydrophilic surface) $\theta_c = 30°$ (Hydrophilic surface) $\theta_c = 90°$ (Minimum hydrophobic surface)

Water drop

θ_c θ_c θ_c

$\theta_c = 110°$ (Hydrophobicity typical of silicone rubber) $\theta_c = 180°$ (Super-hydrophobic surface)

θ_c
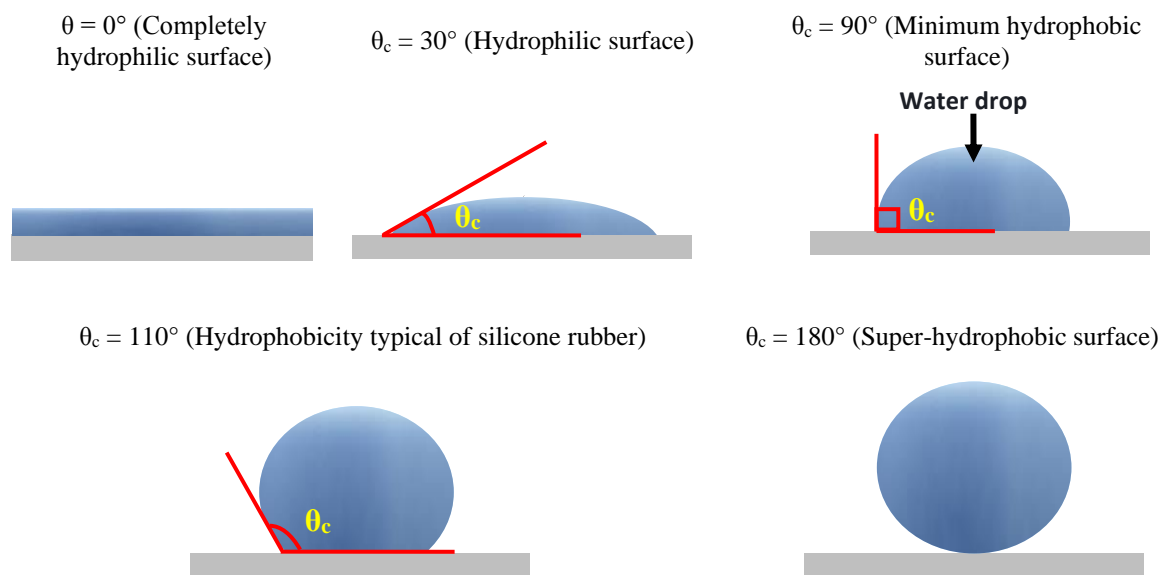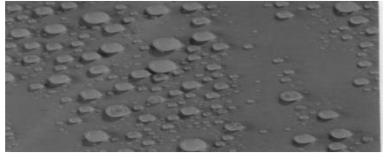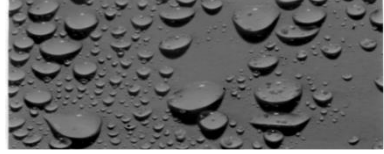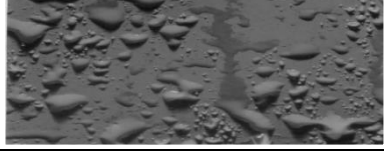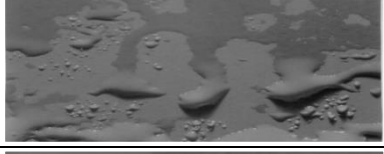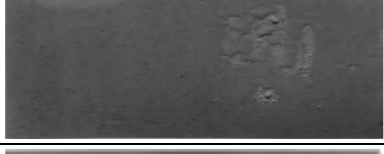
Figure 2.11 Possible contact angle values

A water drop deposited on an inclined surface is defined in Figure 2.12. There exist two different contact angles, the advancing contact angle (θ_a) and the receding contact angle (θ_r).

The disadvantage of this technique is that the measurement is dependent on operator's judgment. To deal with this problem, Berg et al [110] proposed use of digital image analysis for estimating the average hydrophobic properties of surfaces. Application of such procedure, where computer software interprets the image, makes the examination more objective and increases its accuracy. Tokoro et al [111] also applied image analysis to study hydrophobic properties of SIR.

Table 2.3 Criteria for estimation of the hydrophobicity classification (HC) [108]

HC	Description	Pictures
1	Only discrete droplets are formed. This corresponds to $\theta_r \approx 80°$ or larger for the droplets.	
2	The major part of the surface is covered by droplets with a shape, still regular but deviates from circular form. This corresponds to $50° < \theta_r < 80°$ for the majority of droplets.	
3	Only discrete droplets are formed. The major part of the surface is covered by droplets with an irregular shape. This corresponds to $20° < \theta_r < 50°$ for the majority of droplets.	
4	Both discrete droplets and wetted traces from the water runnels or water film are observed ($\theta_r = 0°$). Less than 10% of the observed area is covered by water runnels or film.	
5	Both discrete droplets and wetted traces from the water film are observed. More than 10% but less than 90% of the observed area is covered by water runnels or film.	
6	More than 90% but less than 100% of the observed area is covered by water runnels or film (i.e. small non-watted areas (spots/ traces) are still observed.	
7	Continuous water film is observed over the whole tested area.	
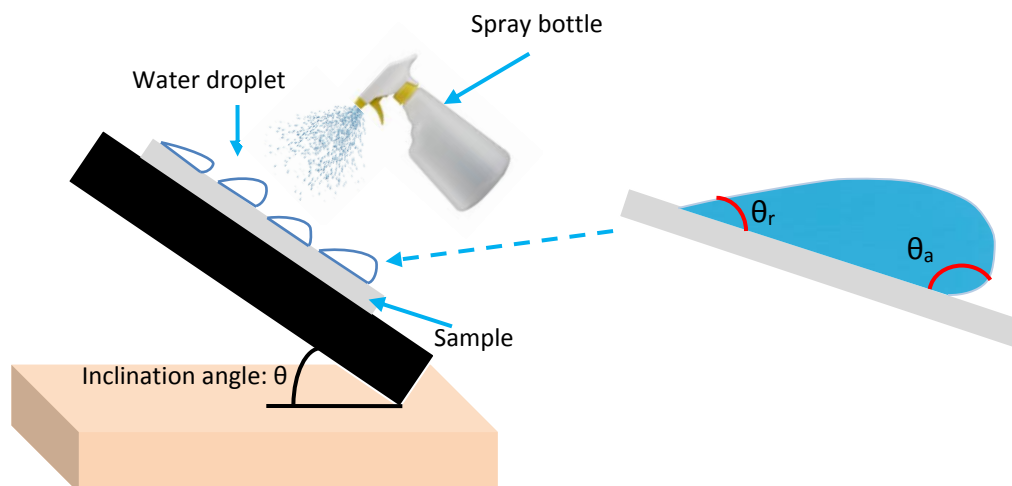
Figure 2.12 water droplet on an inclined paln surface

2.5.4. Measurements of electric field distribution

Results from many accelerated ageing tests have indicated that electrical stress plays a significant role in material degradation and ageing of polymeric insulators. Non-uniform and high electric field, combined with other stresses, triggers damaging discharge activities on the insulator surface. Determination of the electric field provides a better understanding of the phenomena associated with surface discharges, and is particularly important for insulator design and optimisation in order to avoid such undesirable consequences. The electric field around the polymeric insulator can be obtained through two approaches: experimental measurements, and numerical computations.

2.5.4.1. Experimental methods

In order to obtain measurements of the electric field strength distribution along an insulator, several kinds of devices were designed and used in laboratory and field tests. Initially, capacitive probes, flux meters and dipole antennas were used as the electric field strength measuring devices. With increasing demand for an accurate measurement tool, researchers have developed a more advanced and reliable probe using optical sensors to obtain voltage and field distribution at higher precision [112, 113]. Hidaka [112,114] published comprehensive reviews related to the Pockels sensor for electric field strength measurement. In his papers, he described the structure of the Pockels sensor in detail. Passive measurement based on Pockels effect offers many advantages which include 1) direct electric field measurement, 2) wide range in frequency up to GHz, and 3) less distortion [114]. In a recent investigation, Zeng et. al. [115] has successfully developed an integrated electro-optic sensor featuring a small and compact portable design which makes on-site measurements more feasible.

2.5.4.2. Numerical Computation

Numerical approaches have always been a useful technique for solving many high voltage insulation problems. These approaches become more important when practical measurements are difficult or impossible to implement, highly risky and expensive with sophisticated laboratory setup and equipment [116, 117]. Numerical computations through analytical expression [118-120] or circuit representations [121]

can be a good alternative, but these methods are rather complex and not applicable for diverse practical problems. For these reasons, numerical techniques using computer modelling and simulation are preferred among researchers. Field simulation packages offer faster and cost-effective methods to obtain desirable results with substantial accuracy. This method is particularly useful in the design optimisation and development of many high voltage and power systems. There are several commercial software packages available for the computation of the electric field. COMSOL Multiphysics, Coulomb, ANSYS/Emag and Maxwell 3D are the most popular ones. Most of the available software is based on two numerical methods, namely, Finite Element Method (FEM) and Boundary Element Method (BEM). A comprehensive reference book related to numerical electric field analysis methods is authored by Zhou [122].

2.6. Conclusion

This chapter provides an overview of the main properties of polymer insulators in high voltage systems. The use of polymeric materials is currently the state-of-the-art technology for the improvement of the anti-pollution performance of insulators, mainly due to the water repellent properties of these materials. However, polymeric materials in service suffer from ageing degradation that could permanently or temporarily reduce their performance.

The textured insulator is a novel design for polymeric insulators invented recently, which designed to reduce the surface damage caused by discharge activities and dry band arcing. The present work describes the design principles of texture patterns and the literature review of experimental investigations using standard tests.

Chapter 03

LITERATURE REVIEW

3.1. Introduction

The widespread use of SiR insulators for overhead lines and distribution systems has not led to the complete elimination of discharge activities and dry bands even with the use of superior hydrophobic materials. Harsh environmental conditions would still result in discharge activities on the insulator surface, and the surface degradation due to these discharges is still a subject of concern. While 'cap and pin' ceramic insulators employ special anti-fog designs of increased leakage path introduced by the presence of corrugated ribs, such this complex shape cannot be used for polymeric insulators due to the moulding limitations.

Textured insulators are a novel approach for the improvement of polymeric insulators using a surface design consisting of an array of hemispherical protuberances of various configurations and range of diameters. The aim of this design is to reduce the power dissipation by reducing both the electric field strength and the current density.

In this chapter, the design principles of texture patterns and the inclined plane test setups used in this study were described. Also, a literature review for the studies pertained to the inclined plane tests performed to evaluate the erosion resistance of non-textured and textured silicone rubber insulators was presented. Finally, research studies related to the determination of the electric field distribution along the polymeric insulators by using the FEM were also reviewed.

3.2. Texturing of polymeric insulators

The hydrophobic surface of polymeric insulators offers a significant advantage like silicone rubber. These types of insulators are gaining acceptance for use with overhead lines at distribution voltages up to 132 kV. However, under severe ambient conditions, dry band formation is not totally eliminated and would still result in partial

discharging on the insulator surface.

The surface leakage current on a polluted polymeric insulator has the highest density in the regions of the smallest contour perimeter which are the shank sections, where washing is least effective and deposits may accumulate. As a consequence, the surface electric field strength is also at a maximum in this region, and there is a heightened risk of surface heating, which may cause dry-bands, partial arcs on the surface and consequential thermal damage.

With the aim of improving the pollution performance of silicone rubber insulators, a new design has been invented recently [15] by employing a textured surface (Figure 3.1).
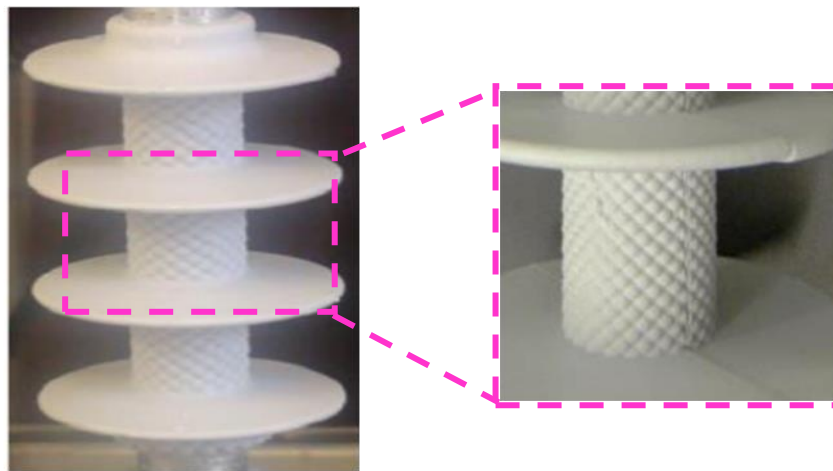
Figure 3.1 Insulator with small hemisphere [123]

Textured patterns consist of an array of intersecting or contiguous protuberances [124, 17]. The main aim of this design is to lower power dissipation on the insulator surface by reducing both leakage current density and the electric field gradient, as shown in Equation 3.1.

$$P = E.J \qquad\qquad (3.1)$$

Where E is the electric field, J is the surface current density and P is power dissipation. An increase of surface area can reduce the leakage current density in the susceptible shank region, and a substantial increase in the longitudinal creepage distance without increasing the overall longitudinal length of the insulator could

reduce the electric field stress. Moreover, the texture pattern can have multiple paths for current conduction, as soon as one current path starts to dry as a result of Joule heating, its resistance will increase. However, the current flow will switch to an alternative path of lower resistance before severe thermal damage occurs. Therefore, textured patterns were expected to alleviate the damage induced on polymeric materials due to surface discharges, compared with non-textured samples of the same material [18, 21].

3.2.1. Textured design principles

3.2.1.1. Surface patterns

The geometry of such protuberances could be spherical, ellipsoidal, paraboloidal, hyperboloidal, conical and pyramidal or other symmetrical form. The textured arrays offer a controlled variation of surface area [15].

Figure 3.2 (a) represent a side view of protuberance of height that is formed as part of a sphere and has a height "c" and a base as a circle of radius "a". The radius of the sphere is "b". The top view of an array of contiguous part-spherical protuberances is shown (Figure 3.2.b).

(a)   (b)
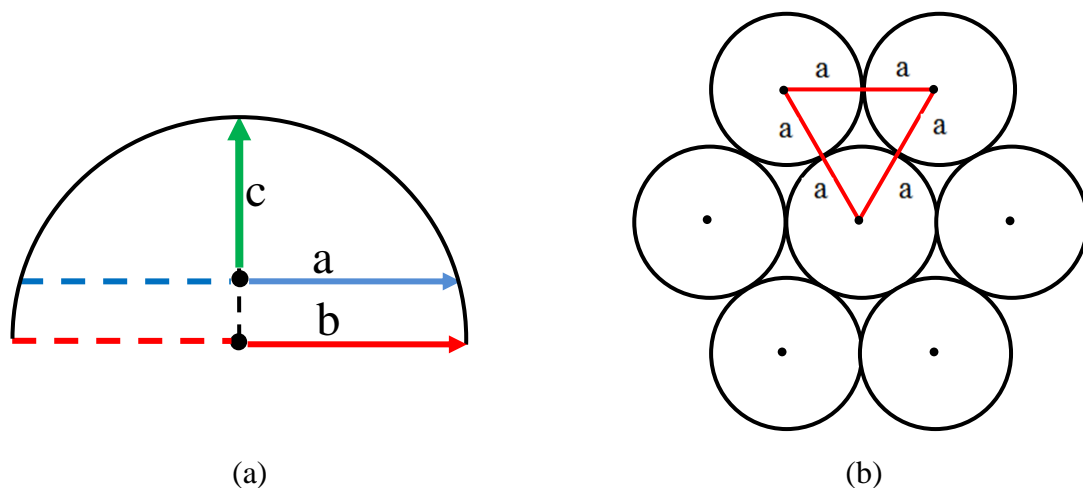
Figure 3.2 (a) Side view of part-spherical protuberance (b) Top view of an array of contiguous part-spherical protuberances [15]

In this case,

$$a^2 = c\ 2b - c \tag{3.2}$$

and the surface area of the protuberance is

$$A_p = 2\pi bc \tag{3.3}$$

From Figure 3.2 (b), the area of the triangular plane surface is

$$A_t = \sqrt{3}\, a^2 \tag{3.4}$$

The three adjacent protuberances will increase this surface area to

$$A_{pt} = \frac{A_P}{2} + A_t - \frac{\pi a^2}{2} \tag{3.5}$$

$$A_{pt} = a^2 \left[\frac{\pi b}{2b\text{-}c} + \sqrt{3}\frac{\pi}{2} \right] \tag{3.6}$$

Therefore, the spherical protuberances will increase the surface area by a ratio

$$\frac{A_{pt}}{A_t} = 1 + \frac{\pi c}{2\sqrt{3}} \frac{1}{2b - c} \tag{3.7}$$

The increase is dependent on the choice of the ratio of protuberance height "c", to spherical radius "b". Hemispherical protuberances (b=c) will have the limiting value of the area ratio.

$$\frac{A_{pt}}{A_t}\Big|_{\substack{hemisphere \\ b\,=\,c}} = 1 + \frac{\pi}{2\sqrt{3}} = 1.907 \tag{3.8}$$

For a tightly arranged array of adjacent hemispherical protuberances, the surface will increase close to a limiting value of 2, which is the ratio of the hemisphere surface to the surface of the circular base. Ratios greater than 2 can be achieved by utilising other geometrical arrangements [18].

The patent [15] describes the use of several patterned textures of hemispherical protuberances. This will give an increase in both surface area and creepage length. Figure 3.3 shows four patterns representing plan views of either contiguous or intersecting protuberances. Figure 3.3 (a) illustrates the geometric configuration of the contiguous hexagonal pattern. Pattern "B" follows a hexagonal intersection of overlapping hemispherical protuberances while the intersections of patterns "C" and "D" have a square and triangular shape respectively [124, 18, 125].

3.2.1.2. Creepage distance

The typical approach for the design of outdoor insulators for polluted

environments is the increase of the creepage distance per unit of axial length. The textured patterns aim to achieve longer creepage without then necessarily increasing the overall length of the structure.

The arrowed paths shown in Figure 3.3 indicate the surface creepage lengths for textured patterns. These are circular arc paths, although appearing linear in the plan view in Figures 3.3 (b), 3.3 (c) and 3.3 (d).

For example, the longitudinal creepage distance per row, in the direction of the electric field strength along the contiguous hemispherical protuberances pattern of Figure 3.3 (a), is 2.093a compared with $\sqrt{3}\,a$ on a plane surface. This is a per-unit creepage distance increase of 1.209. As a result, the value of the electric field (E) is significantly reduced.
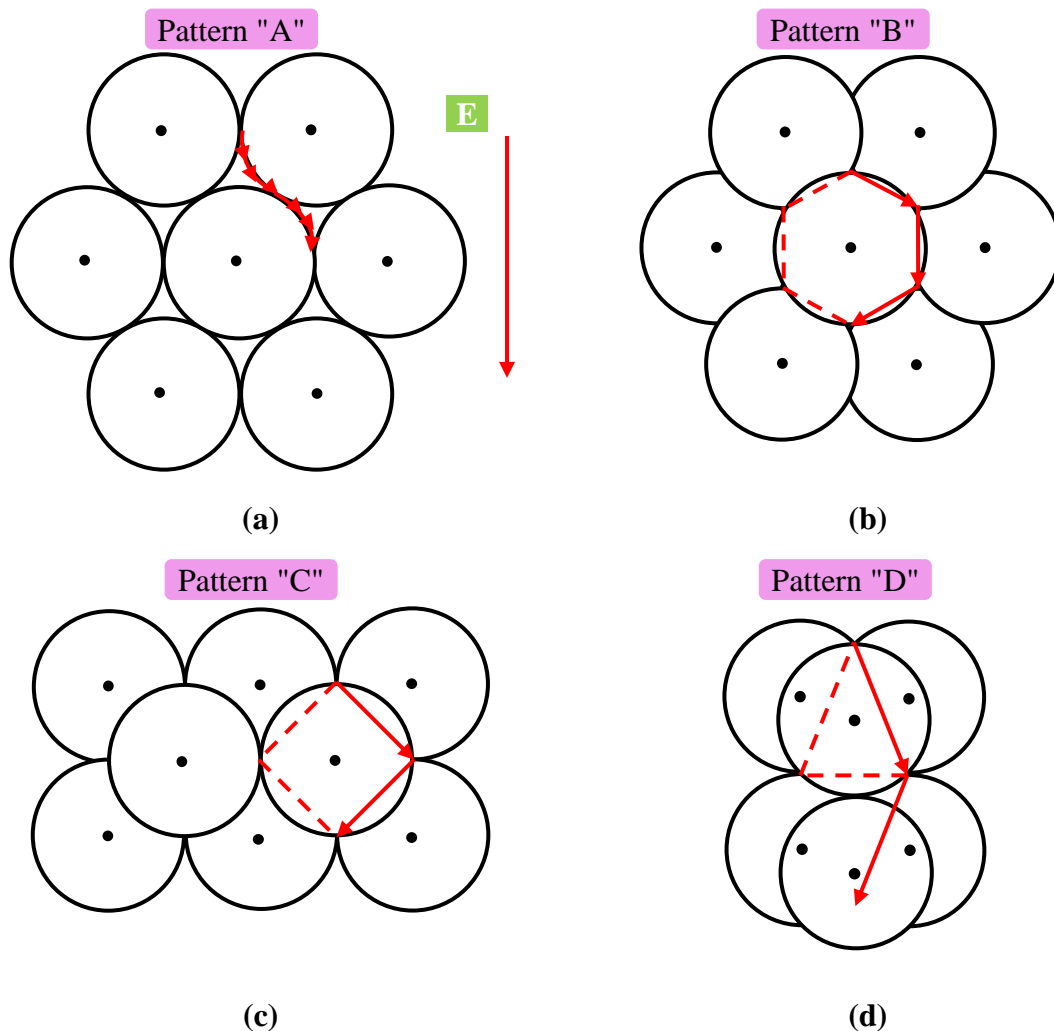
Figure 3.3 Textured patterns: (a) Contiguous hexagonal, (b) Intersecting hexagonal, (c) Intersecting square and (d) Intersecting triangular [18]

3.2.1.3. Power dissipation factor

For outdoor insulation under severe environmental conditions, a uniform pollution layer with conductivity σ (S/m) and thickness t (m) are assumed to coat both surface designs of textured and non-textured insulators. The layer conductance for both surfaces is specified by:

$$k = t \cdot \sigma \qquad (S) \tag{3.9}$$

This layer can result in a significant conduction current *(I)* with non-uniform current density *(J)*. The leakage current density inside the pollution layer at position *(x)* is given by:

$$J_{layer} = \frac{I}{x.t} \qquad (A/m^2) \tag{3.10}$$

Assuming the layer thickness *(t)* to be constant, the surface leakage current density becomes:

$$J = J_{layer} \cdot t \qquad (A/m) \tag{3.11}$$

The surface regions of the greatest *(J)* and *(E)* can cause a considerable heating of the pollution layer, which may ultimately lead to dry bad formation on the insulator surface. The power dissipation *(P)* per unit area of the surface layer heating is given by Equation (3.1).

The use of insulator surface texturing increases the surface area of an insulator by a factor α, consequently the current density '*J*' will be reduced by the same factor (*J* non-textured /*J* textured = α). The texture at the same time also increases the creepage distance in the field direction by a factor '*β*', and will therefore reduce the surface electric field strength by the same factor (*E* non-textured /*E* textured = *β*).

The local power dissipation *P* (W/m²) per unit area will, consequently, be reduced by the combined power density factor (*α . β*):

$$\alpha.\beta = \frac{P_{non-textured}}{P_{textured}} = \frac{E_{non-textured}}{E_{textured}} \cdot \frac{J_{non-textured}}{J_{textured}} \tag{3.12}$$

While the anti-fog designs increase only the creepage distance, thus affecting

only factor β, textured patterns could control both the surface area (factor α) and the creepage distance (factor β) independently, thus achieving different combined power density factors ($\alpha.\beta$).

This common factor can be an effective feature for the ability of the textured design to inhibit the drying of the pollution layer by reducing the dissipation of surface power dissipation.

3.2.1.4. Theoretical classification of candidate textures

It is instructive to compare the power density factors ($\alpha.\beta$) associated with a variety of textures that result from an increase in both area and creepage factors. Table 3.1 shows the calculated area and creepage factors for the texture types shown in Figure 3.3. Thus, on the basis of the results shown in Table 3.1, Textures 2 (Intersecting hexagonal) and 3 (Intersecting square) appear to be the most promising for an anti-fog insulator [17, 18, 125].

Table 3.1 Theoretical classification of textured patterns (Table adopted from [18])

Texture	Area factor α	Creepage factor β	Power density factor $\alpha.\beta$
Contiguous hexagonal	1.907	1.209	2.306
Intersecting hexagonal	1.446	2.356	3.407
Intersecting square	1.301	2.222	2.891
Intersecting triangular	1.209	1.814	2.193

Recently, many tests were carried out for evaluating resistance to track the erosion of silicone rubber textured patterns used under severe ambient conditions according to the IPT methods indicated in the IEC 60587 standard under AC voltage [17, 18, 20, 21, 125-127]. We will discuss in detail this works and the most important results obtained in the following section.

3.3. The inclined plane test (IPT)

The inclined plane test method, described in the IEC-60587 [19] standard, is used to evaluate the resistance of polymeric housing insulators to tracking and erosion under severe ambient conditions and AC voltages at 50 Hz frequency. A rectangular

test sample with dimensions of 120 mm x 50 mm and a thickness of approximately 6 mm is mounted on a support stand, which is inclined at 45° to the horizontal with the test surface facing downwards. The insulation surface is then contaminated with a liquid contaminant, which flows (drips) from the HV electrode at the top of the sample to the ground electrode at the bottom of the sample. The application of a test voltage causes leakage current to flow along the contaminant path, which causes electrical discharges and subsequent tracking and erosion of the material (Figure 3.4).

1) Arrival of the contaminant   2) Filter-paper pad   3) Top electrode (HV)
4) Test insulating specimen   5) Contaminant   6) Bottom electrode (Ground)
7) Insulating specimen support
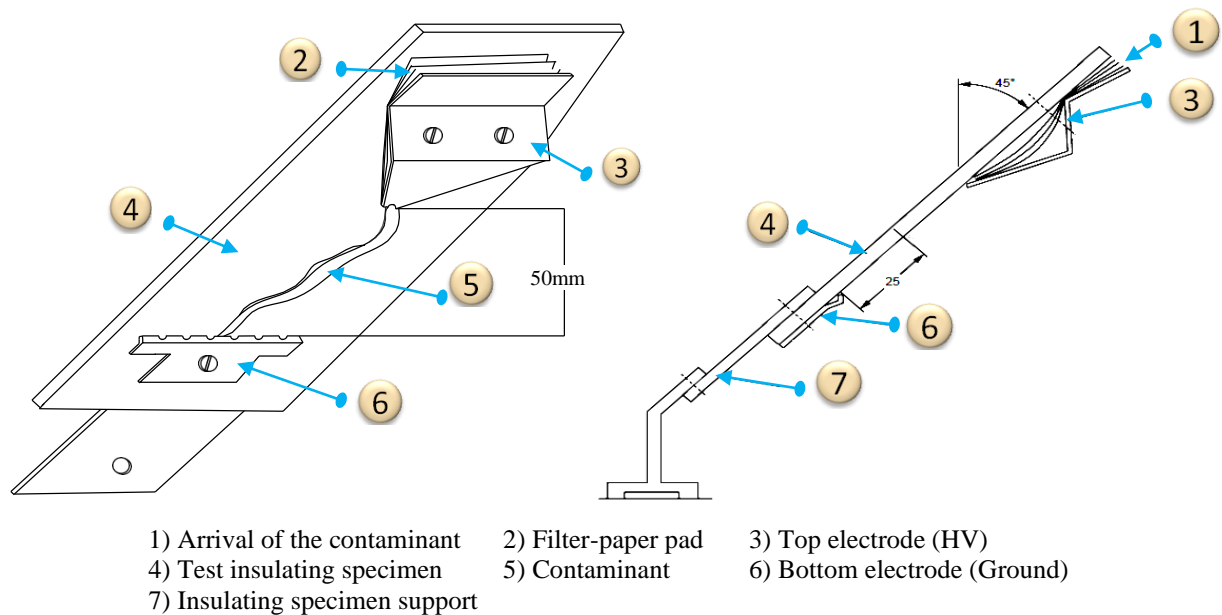
Figure 3.4 The IEC-60587 inclined-plane test sample with fitted stainless steel electrodes. Figure taken from [19]

The contaminant should be composed by:

- 0,1 % ± 0,002 % by mass of NH_4Cl (ammonium chloride) analytical quality;

- 0, 02 % ± 0,002 % by mass of isooctylphenoxypolyethoxyethanol (a non-ionic wetting agent) in distilled or de-ionized water.

Eight layers of filter-paper are clamped between the top electrode and the specimen. Their shape is indicated in Figure 3.5. The contaminant shall be fed into this filter-paper pad so that a uniform flow between the top and the bottom electrodes shall occur before voltage application.

The electrical electrodes shall be made of stainless steel. Figure 3.6 shows the dimensions of the HV and ground electrode.

Dimensions in millimetres
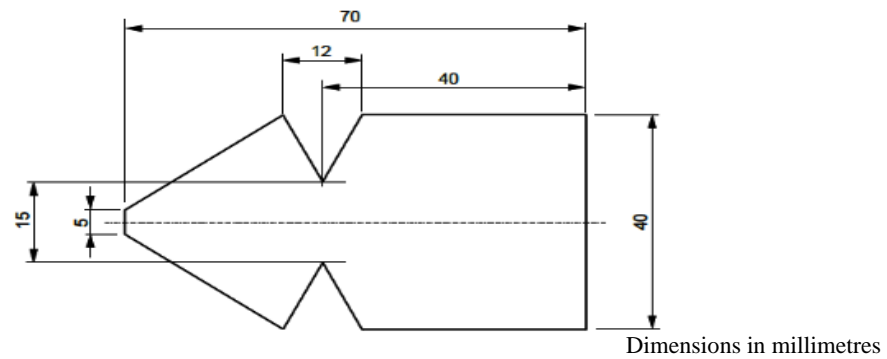
Figure 3.5 Filter paper dimensions [19]

Six semi-circulars
Cut-outs: ⌀ 2.5mm

Dimensions in millimetres

(a)   (b)
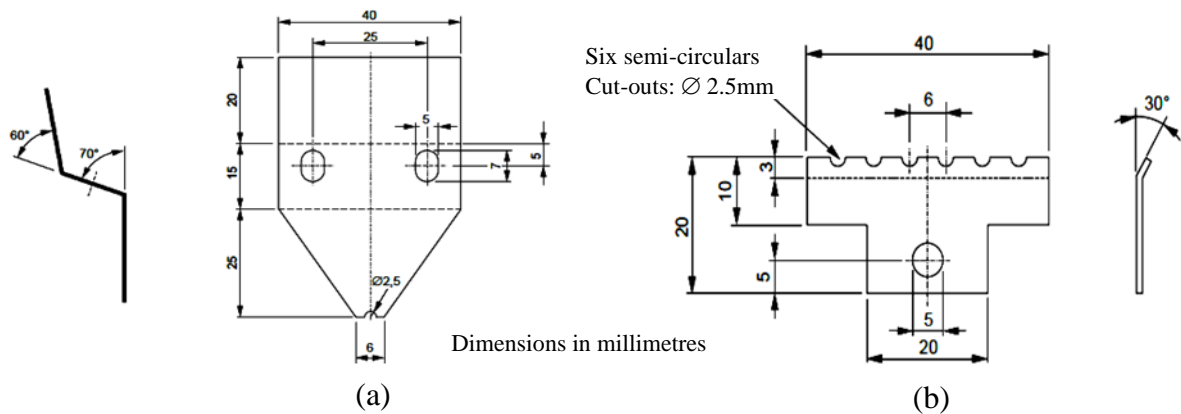
Figure 3.6 Electrodes dimensions (a) High-voltage electrode, (b) Ground electrode
[19]

The constant tracking voltage (CTV) (method 1) and stepwise tracking voltage (method 2), also known as initial tracking voltage (ITV) are the two standard procedures used in the inclined plane test method [19]. In the CTV method, a constant voltage and a specified flow rate as per the standard are used for six hours or until the insulator fails. In the stepwise tracking method, a lower initial voltage is selected first and then incremented by 250 V in every hour for six hours or until failure is established.

Depending on the selected voltage, a series resistor and contaminant follow rate shall be taken from Table 3.2. Preferred test voltages are 2.5 kV, 3.5 kV and 4.5 kV for, method 1.

In both methods, the failure criteria are the same. The end-point criteria as given in the IEC-60587 standard [19] are when the magnitude of the leakage current exceeds 60 mA ± 6 mA for 2 to 3 seconds or when the surface track, measured from

the ground electrode reaches 25 mm. In addition, the test is terminated if a hole develops through the insulation due to intensive erosion or the sample ignites. In the absence of the above failure criteria, the material is accepted as having passed the test [19].

Table 3.2 Values of the test voltage, series resistance and contaminant flow rate (Table taken from [19])

Test voltage (kV)	Preferred test voltage for method 1, (kV)	Contaminant flow rate, (ml/min)	Series resistor, resistance, (kΩ)
1.0 to 1.75	−	0.075	1
2.0 to 2.75	2.5	0.15	10
3.0 to 3.75	3.5	0.30	22
4.0 to 4.75	4.5	0.60	33
5.0 to 6.0	−	0.90	33

3.4. Tracking and erosion of silicone rubber materials under AC and DC voltages

Previous studies of DC tracking and erosion tests on SIR insulation have concluded that tracking is more severe under DC conditions than for AC. One of the first observations of the increased severity of DC over AC stress on polymeric materials was observed in 1988 in salt-fog chamber studies. In these tests, it was clear that −DC stress caused a marked reduction in the tracking and erosion resistance as compared to AC and +DC which seemed to perform similarly [128]. In 1998, Guan used DC instead of AC voltage in the IPT and reported the damage level of samples tested by +DC was greater than −DC [129].

Moreno and Gorur [130] performed AC and DC IPTs on polymeric materials. They only used positive polarity DC as it is generally considered to be more severe than negative polarity. They noted that a substantial reduction in the tracking and erosion resistance of the polymeric materials tested with DC stress, in comparison to AC. The poorer material performance stressed with DC voltage was attributed to higher magnitudes and longer duration times of the discharge current pulses. Gustavson et al. [131] tested cylindrical silicone rubber samples in a coastal environment under AC and DC voltage. The DC stressed samples showed higher leakage currents and exhibited larger surface degradation compared with samples

exposed to AC voltage.

The standard inclined plane test incorporates testing by AC voltage only, there is no standard test exists for the IPT under DC voltage. In previous years, most of the studies have considered applying equal voltages of rms AC and DC. Table 3.3 summarizes the researches results for the inclined plane tests in AC and DC applications and those that use DC voltages only. Generally, leakage current, mass loss and time to track or failure are the parameters stipulated in the IEC-60587 standard used to assess the quality of SiR insulators. However, some of the researchers were not recorded these all parameters as indicated in the table below.

Another observation made in the literature review is that the results are presented in relative qualitative terms (either 'higher' and 'lower or better') and not as quantitative values. For example, Vas et al [132] have reported that the performances of SiR insulators were better under negative DC as compared to positive DC. Heo et al [135] stated that under AC voltage was occurred a slight arc, whose duration was not long. On the other hand, under DC voltage showed a constant arc fixed at the ground electrode caused a greater loss of materials. The magnitude of the leakage current was not given in [135].

In studies [133, 136, 137] only the magnitude of the leakage currents were reported, and not indicated the mass loss. The positive DC showed higher levels of current than the negative tests, and the erosion is more severe [137]. Heger [134] reported that the DC test is more severe than the AC test for all materials. Finally, the findings by [133] stating that the tracking resistance was low for positive DC and much lower for negative DC this contradicts the results of other studies. In general, the above studies showed the severity of the DC inclined plane test when compared to AC in terms of leakage current magnitude and the damage of the material.

From the above studies, it can conclude that there is no uniform methodology for SiR tests. Where many researchers have used different voltages than those recommended in IEC-60587. The selection of DC voltage levels equivalent to the corresponding standard AC voltages is desirable and an important aspect while investigating erosion under DC as compared to AC [138].

Table 3.3 Summary of inclined plane test results.

Researchers	Voltage magnitude and type	Leakage Current (mA)			Mass Loss (g)			Time to Track (min)			Testing Method
		AC	+DC	+DC	AC	+DC	−DC	AC	+DC	−DC	
Vas et al. [132]	±2.5 kV DC	——	9	4.4	——	0.7	0.1	——	——	——	CTV
Rajini et al.[133]	5 kV AC & ±5 kV DC	20	15	25	——	——	——	——	——	——	CTV
Heger et al [134]	4 kV AC & ±4 kV DC	11	13	8	0.1	3.4	0.1	——	——	——	CTV
Heo et al [135]	4.5 kV AC & ±4.5 kV DC	——	——	——	0.3	2.91	1.36	360	45	76	CTV
Sarathi et al [136]	4 kV AC & ±4 kV DC	——	30	40	——	——	——	353	353	353	CTV
Mahatho et al [137]	±4.5 kV DC & ∓6.5 kV DC	——	47.6	27.3	——	——	——	——	95	112	CTV
remark	A variety of test voltages that are not specified in the IEC-60587 standard were used	Generally, +DC leakage currents is highest, followed by − DC and then AC.			Mass loss is lower at AC than DC. Positive DC has a higher mass loss than negative DC.			Time to track is longest for AC than for DC.			Common method used is the CTV.

Some researchers proposed different equivalent DC voltages of the corresponding RMS AC voltage. Bruce et al [139, 140], found that the equivalent DC voltages for the inclined plane test to be 90% of the corresponding AC voltages. The equivalent DC value was calculated such that the area under the voltage waveforms is equal for AC and DC. In another search, Rowland et al [141] have used for the equivalent +DC and −DC IPT voltages equal to ± 2.7 kV. In addition, Ghunem et al [142, 143] it was suggested that the equivalent +DC and –DC IPT voltages in the constant voltage methods have to be 67% and 84%, respectively, of the standard AC (rms). The values of the DC voltages proposed by the researchers are summarized in Table 3.4.

Table 3.4 Equivalent DC voltages of the inclined plane test

Researchers	Equivalent DC voltages	Testing Method
Bruce et al [139, 140]	± 2.25 kV ± 3.15 kV	CTV
Rowland et al [141]	± 2.7 kV	CTV
Ghunem et al [142]	+2 & −2.5 kV DC for ITV, +2.25 & −3 kV DC for CTV.	CTV/ITV
Ghunem et al [143]	+2 kV DC & −2.5 kV DC	ITV

Waters et al. [21] have studied the erosion and tracking of different textured SIRs in a series of AC inclined-plane tests. Contiguous hexagonal pattern, hexagonal intersections of overlapping protuberances and intersecting square arrangements all passed the inclined-plane test successfully, but non-textured SIR surfaces failed.

Sarkar et al. [20] found that the textured sample with 4mm square pattern gives insignificant material losses and best performance compared with the other texture patterns. Haddad et al. [16] studied the effect of a non-contiguous hemisphere texture, which gives a 1.49 times larger surface area for the smooth surface of SIR. Fog tests were also performed on the samples to study the performance of the textured SIR under polluted conditions. Lower tracking and erosion rates as well as smaller and more mobile partial arcs were observed on the textured SIR surface indicating better anti-fog properties.

Nekeb et al. [144] have studied the effect of UV irradiation on textured and non-textured SiR insulating samples. Laboratory tests were carried out in two stages: a)

applying the UV radiation in accordance with ISO 4892-2 [145], with variable exposure/condensation cycle; b) IPT to evaluate tracking and erosion performance under AC voltage of both kinds of insulation samples. The results showed that the textured design exhibiting improved surface properties in terms of resistance to tracking and erosion with only minimal loss of material.

3.4.1. Modelling of polymeric outdoor insulator

Practical experience and laboratory observations have indicated that corona and electric discharges, due to the high electric field, can severely deteriorate the insulation material. Control of high electric fields on polymeric insulators, particularly near both insulator terminals, is extremely important to minimise such undesirable effects, ensuring satisfactory performance during the period of service. A lot of research, therefore, has focused on the determination of the electric field distribution along the creepage path of the polymeric insulator [146].

Due to the limitations of laboratory equipment, materials and safety concerns, scientists and researchers are shifting their focus to numerical analysis. Kovalev et al. [147] highlighted the importance of the implementation of numerical analysis in high voltage industries, in order to understand the performance of high voltage equipment. This alternative method provides faster results at a lower cost. The numerical study is useful for design optimisation and power system application.

There are numerous factors that influence the E-field distribution [148]. The most important of these include:

- Geometry of insulator; including weather-shed system, fiberglass rod and end fittings;
- Dimensions and position of the corona rings and their attachment method;
- Value of the energized line voltage;
- Environmental aspects such as pollution and water droplets on the insulator surface.

3.4.1.1. Study of electric field strength along the insulators under wet and contaminated conditions

Modelling of a polymeric insulator covered with a pollution layer is useful in representing realistic outdoor insulators which are subjected to various inland and sea contaminants with different severity. It is found that naturally aged insulators have shown a near-uniform deposition of pollutants over the insulator surface [149]. Many researchers have, therefore, created a pollution layer with a uniform thickness when modelling polluted outdoor insulator [150]. Electrical properties such as permittivity and conductivity of the pollution were normally assigned with constant values, obtained from simplified assumptions and sometimes from experimental measurements.

In an attempt to provide a better and more realistic outdoor insulator model, some researchers have considered various practical conditions for representing/ characterising the pollution layer on the insulator surface. For example, El-Hag et al. [13] have modelled polluted insulators based on wetting action. The uniform pollution layer on the insulator surface was classified into three main regions, which were specified with different conductivity values obtained from equivalent salt deposit density (ESDD) measurement. In another investigation, Yong et al. [151] have modelled a non-uniform pollution distribution where the cylindrical insulator was divided axially into four equal regions, which were assigned with different resistivity to represent heavy, moderate and no pollution on the insulator surface. They also studied asymmetric top and bottom surface contamination.

Simulation results of E-field and potential distributions along the surface of silicone rubber polymer insulators under clean and various contamination conditions with/without water droplets in [152] have pointed out that contaminants and water droplets cause highly non-uniform electric field distributions.

However, dry contaminants have no effect on electric field distribution when compared with that of clean conditions [152]. El-Kishky et al. [153] found that the maximum E-field intensification of an ellipsoidal water droplet is about 60% higher than that observed with spherical droplets. These investigations have been performed later on by Guan et al. [154] showing only about 25% higher maximum E-field

intensification especially for large volumes of water droplets.

A large number of deformed water droplets on an insulating surface stressed by an electric field have been simulated by Feier-Iova [155]. The electric field enhancement is analysed on the insulator surface along a path 0.1 mm above the insulator surface. Figure 3.7 shows the summarized results of maximum calculated E-field enhancement factors for different shapes of a single water droplet on the surface. It is concluded that the deformed water drops can intensify the electric field at the triple points up to seven times [155]. The simulation results of the initial and elongated water droplets on a SiR surface by Zhu et al. [156] showed that the maximum E-field of the initial hemispherical and elongated shapes of a water droplet can be four or five times, respectively, and higher than that of without water droplet on the surface.
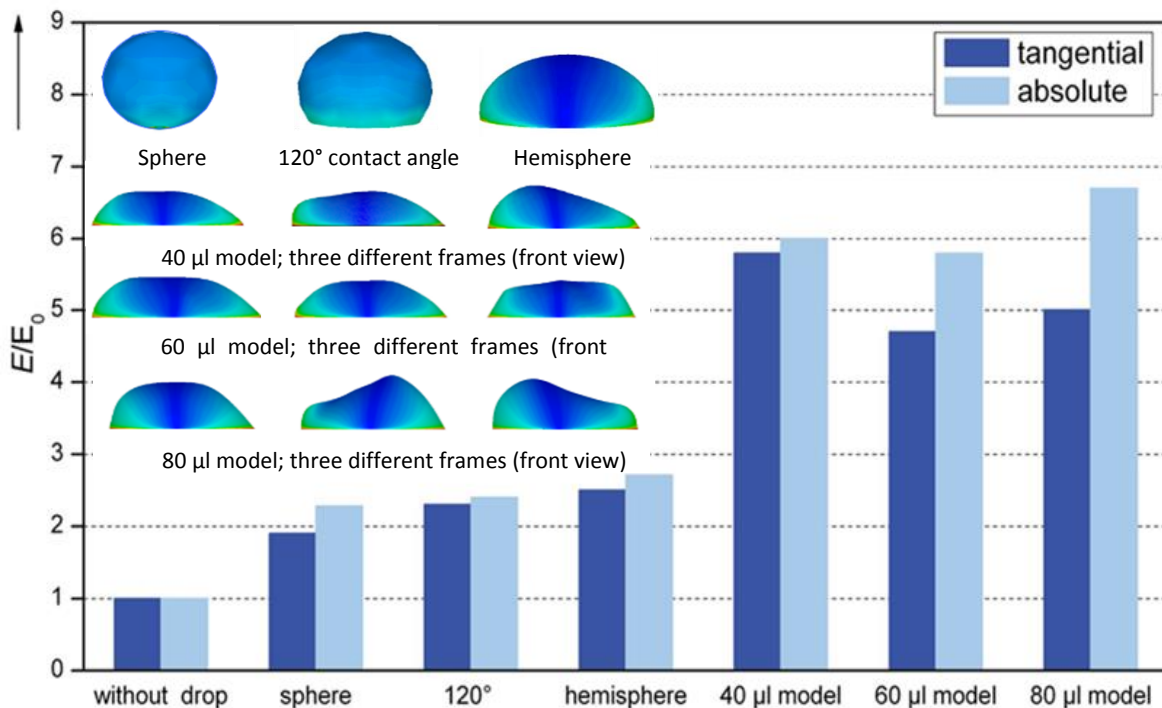
Figure 3.7 Maximum electric field intensification at different water drops [155]; for deformed droplets a mean value for E_{tan} and E_{abs} at three different frames are considered

Weigue et al. [157] have introduced a more realistic droplet model, based on photographs captured during the wetting of a polymeric insulator in a fog chamber, shown in Figure 3.8. The droplets were categorised according to the hydrophobicity classification (HC) recommended by the Swedish Transmission Research Institute (STRI) [108]. From the simulation results, it was demonstrated that the field

enhancement factor varies depending upon the shape and distribution of water droplets on the polymeric surface.

Case 1: HC1	Case 2: HC2	Case 3: HC3
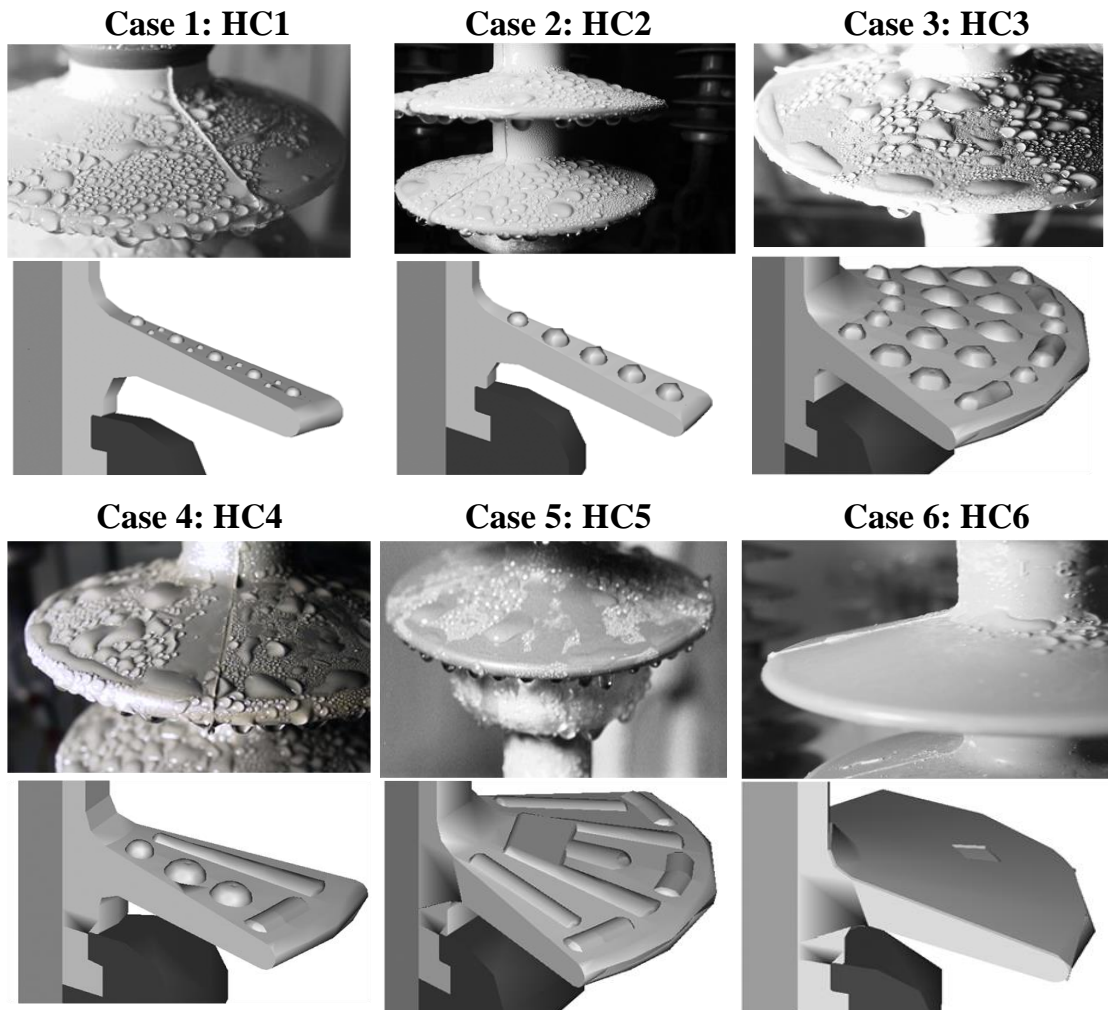
Figure 3.8 Photographs of water droplets on the insulator surface, and the corresponding droplet models used in the numerical simulations [157]

3.4.1.2. Control of electric field distribution

There are various concepts employed in insulator design to limit electric field strength near the surface of the weather shed which is responsible for tracking, erosion and flashover. These include:

a. Weather shed insulation:

Chakravorti and Steinbigler [158] studied the relationship between the shape of the insulator and the maximum electric field strength around it with or without pollution. The parameters studied in their work are the slope angle of the insulator

weather shed, the shed radius, the core radius, the axial height, and the electrode radius. The results from the numerical calculations were as follows:

- The higher slope angle does not yield a notable reduction in the maximum electric field strength.

- Increasing the shed radius from 6 cm to 10 cm significantly lowers the maximum electric field strength.

- The increase of the core radius has little effect on the maximum electric field strength reduction.

- The higher the axial height, the lower the maximum electric field strength.

El-hag et al. [13] have also studied the effect of insulator design parameters such as shed spacing, shed diameter, alternate shed design and shed shape. Insulator profile is shown to greatly influence the aging performance of SIR insulators. Shed shape proves to be the most important parameter to be considered in designing polymeric insulators profiles. Also, as the shed spacing decreases, the performance of SIR insulators improves.

b. End fitting design

The design of the end fitting has an influence on the E-field distribution within the composite insulator, on the surface of the weather-shed material and on the surface of the metallic end-fittings. Large end fittings with rounded edges tend to reduce the peak magnitude of the E-field values in close proximity of the end fittings [159]. Figure 3.9 below shows the distribution of E-field for three different end fittings designs. The area in black is the area where the field is greater than 2kV/mm. Type "B" fitting has a much larger diameter at the top of the end-fitting than the rest of the fittings. This acts like a mini corona ring, reducing the field on the sheath at the beginning of the insulation distance. The type "A" end-fitting does not have a diameter as large as the type "B" fitting, however, it has the first shed connected directly above the end fitting. This greatly reduces the field on the sheath. The type "C" fitting is not as effective in reducing the field, because its diameter is smaller than that of the previous two types.

- Design A: End fitting close to the last shed.
- Design B: End fitting at a short distance away from the last shed.
- Design C: End fitting partly covered by silicone rubber.
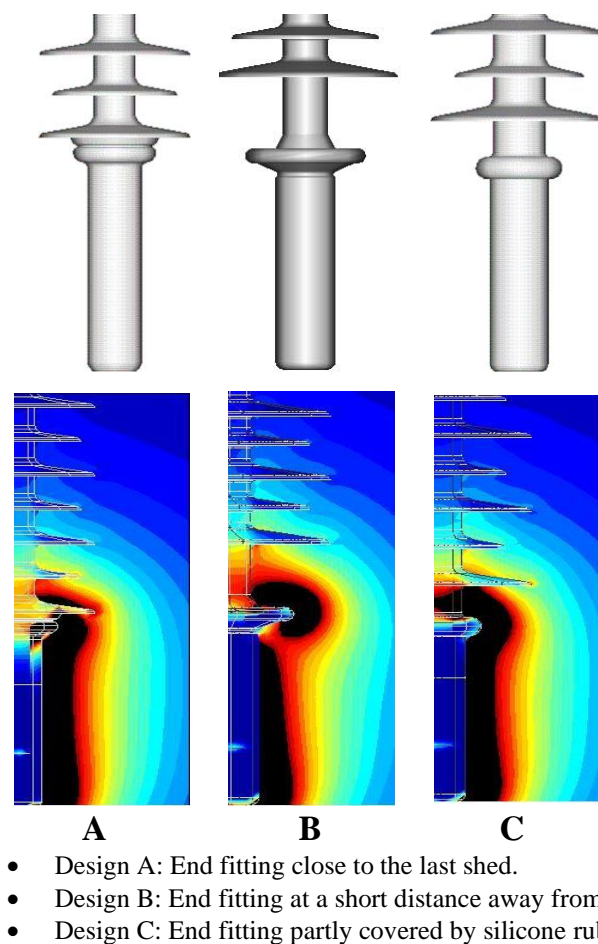
Figure 3.9 Examples of the E-field distribution surrounding three
different designs of composite insulator end fittings [159]

c. Corona ring application

The installation of the corona rings is adapted to reduce the electric field and thus to reduce the failure appearing in transmission systems operating at 230 kV and above and to extend the life duration of the insulators. The plot in Figure 3.10 illustrates the maximum electric field norm versus the line voltage for both cases without corona ring and with the corona ring for the 230 kV composite insulators under dry and clean conditions [160]. It is concluded that the installation of corona ring leads to a significant reduction of the electric field strength. There are many corona rings parameters that should be considered during the design. These parameters include: the radius of the ring tube, the radius of the corona ring and the vertical position of the ring [161]. M'hamdi et al. [160] have used particles swarm optimization (PSO) with a dynamic population size to identify the optimal design parameters of corona ring on HV insulators. Normally, corona rings are installed at both ends of the

insulator (HV and ground end) in voltage level above 345 kV. However, only one corona ring is required at HV ends in voltage level between 230 and 345 kV. The crown ring is seldom used at a voltage below 230 kV.
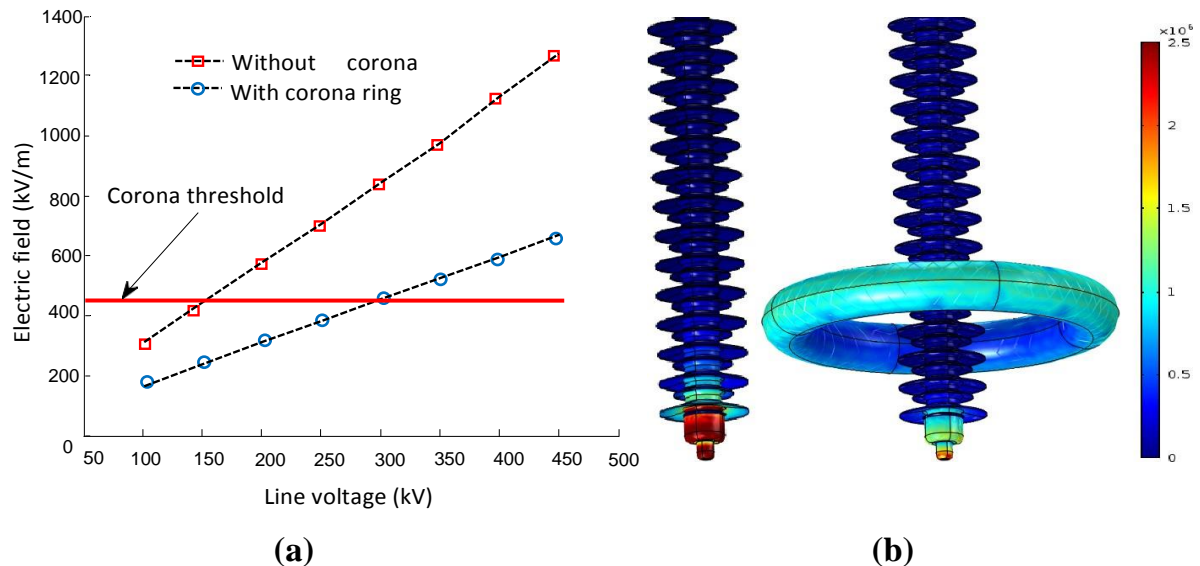
Figure 3.10 Electric field. (a) Maximum electric field norm as a function of system voltage under dry conditions considering the effect of corona rings. (b) Electric field distribution on the surface of composite insulator with and without corona ring

3.5. Conclusion

The literature has provided useful information about the performance of SiR insulators energised by AC, +DC and −DC voltages. The polarity effect has been confirmed relating to the pollution performance and the aging of SiR insulators. The severity of DC testing compared with AC has also been noticed. The absence of a standard test for the IPT under DC voltage leads to the search for an answer to the following question: Can be evaluated the quality of the SiR insulation under the DC voltage in the same method as that of the AC inclined plane test?

Recently, efforts are towards modifying the AC inclined plane test so that it can be used for the DC test.

Textured SIR surfaces have been designed and patented to improve the anti-dry band as well as the anti-fog properties of the insulators in polluted areas. The behaviour of this novel insulator design was investigated by using the inclined plane test methods under AC voltage. However, no research has been carried out to

investigate the behaviour of textured insulators under DC voltage according to the IPT. Also, no numerical models regarding textured insulator based on the FEM method were developed to the determination of field distribution along the creepage path. The next chapter presents the measurement procedure of the inclined plane test based on IEC 60587 to evaluate the tracking and erosion resistance, of non-textured and textured SiR materials at DC and AC voltages.

Chapter 04

COMPARATIVE PERFORMANCE OF SILICONE RUBBER POLYMERIC INSULATORS UNDER HVDC AND HVAC VOLTAGES USING THE INCLINED PLANE TEST

4.1. Introduction

For long-distance electric power transmission and distribution systems, the high-voltage direct current (HVDC) technology is viewed as the most widespread and economically appealing option. To ensure the reliability of direct current electrical networks, it is necessary to know the behaviour of electrical equipment such as insulators. Although SiR insulators are generally accepted to have a superior electrical performance over the traditionally used glass and porcelain insulators [35, 162, 163], they are susceptible to degradation effects of tracking and erosion due to their organic nature. This may result in insulation failure and poses a greater challenge in maintaining the reliability of the power system. For this reason, materials used in high voltage insulation systems should be tested to determine their adequacy to resist erosion and tracking. Different international standard methods have been developed in order to test polymeric insulator materials. One of the most important test techniques is the Inclined Plane Test (IPT). The standard test incorporates testing by AC voltage only, there is no standard test exists for the IPT under DC voltage. While some researchers used equivalent DC voltages of the corresponding RMS AC voltage. Bruce et al [139, 140], found that the equivalent DC voltages for the inclined plane test to be 90% of the corresponding AC voltages. The equivalent DC value was calculated such that the area under the voltage waveforms is equal for AC and DC.

Four samples for each type of insulators (textured and conventional) at both AC and DC positive voltages were tested in this study. The SiR samples were manufactured in Cardiff University. A 3.5 kV AC and 3 kV positive DC voltages were

applied on conventional and textured insulators to compare the material behaviours. Physical damage in terms of erosion, weight loss of the samples and electrode, and current magnitudes were the main parameters evaluated in this research. In addition to the use of image analysis of discharge activity to enable more information concerning the discharge processes which are ageing the polymer surface during testing.

4.2. Rectangular silicone rubber samples

Silicone rubber rectangular samples were manufactured in the high voltage laboratory at Cardiff University. The dimensions were in accordance with the IEC-60587 standard, 120mm x 50 mm x 6 mm. The steps and techniques of manufacturing of these samples are explained in detail in the references [164, 165]. The same material and casting techniques were used for conventional non-textured sample and textured samples. Figure 4.1 shows a conventional non-textured sample containing holes to attach the electrical electrodes. With regard to the texture patterns, the intersecting hexagonal "B", intersecting square "C" patterns were used to be experimentally explored consisted of an array of hemispherical protuberances of diameter 4 mm (Figure 4.2). Table 4.1 presents the mechanical and electrical properties of the silicone rubber material used in this investigation.
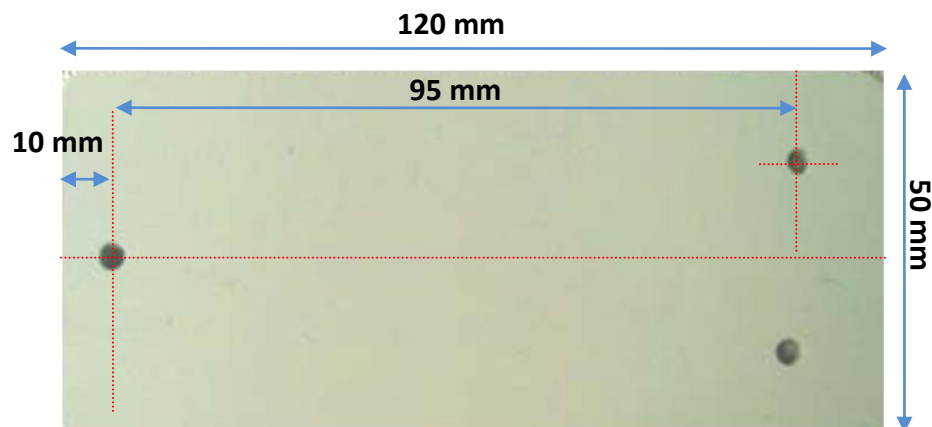
Figure 4.1 Conventional non-textured sample
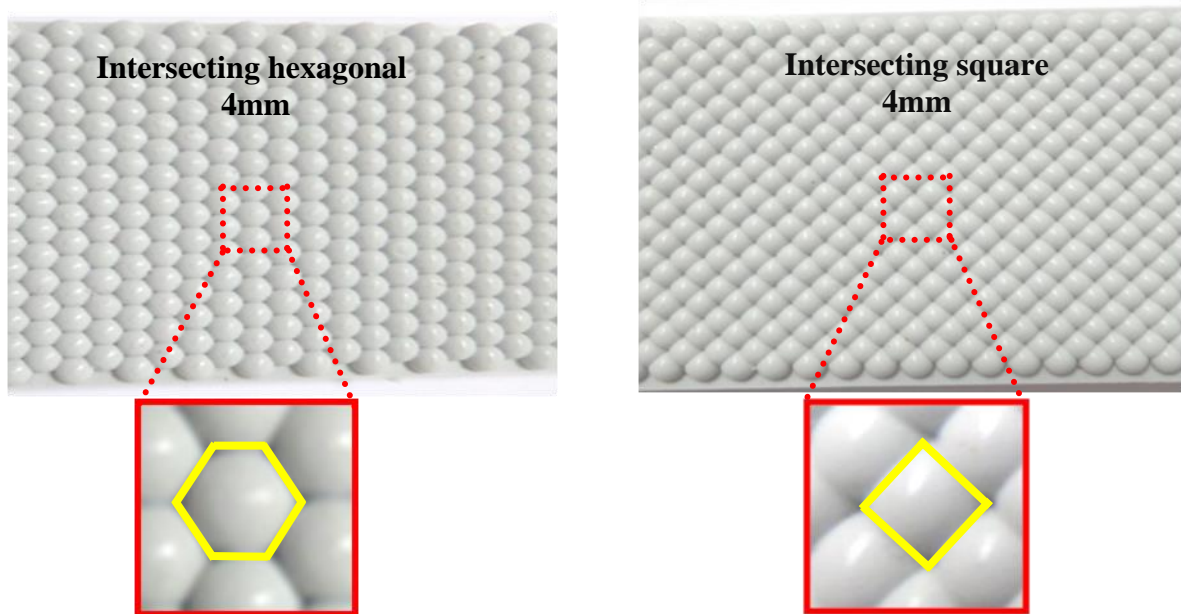
Figure 4.2 Zoomed detail of the 4mm intersecting hexagonal and intersecting square
samples.

Table 4.1 Properties of silicone rubber materials [126].

Property	Inspection Method	Value
Dielectric strength	IEC 60243	23 (kV/mm)
Permittivity	IEC 60250	2.9
Dissipation Factor	IEC 60250	0.00031
Elongation at break	ISO 37	500 (%)
Hardness Shore A	DIN 53505	30
Tear-strength	ASTM D624 B	25 (N/mm)
Tensile strength	DIN 53504	6.5 (N/mm^2)
Tracking resistance	IEC 60587	1A
Density	ISO 1183-1 A	1.13 (g/cm^3)
Arc resistance	IEC 61621	> 300 s
Volume resistivity	IEC 60093	10×10^{15} (Ω cm)

4.3. DC-AC High voltage tracking testing machine

The DC-AC high voltage tracking testing machine is a metal enclosure consisting of a test compartment at the top of the unit and the equipment for the high voltage supply located on the lower part of the machine.

The DC-AC high voltage tracking testing machine is shown in Figure 4.3. The top compartment consists of five test bays that can allow the simultaneous testing of five rectangular samples at a 45° inclined position.

Chapter 04

Comparative performance of silicone rubber polymeric insulators under
HVDC and HVAC voltages using the inclined plane test

(1) D.C. Voltmeter.
(2) A.C. Voltmeter.
(3) D.C. Ammeter.
(4) A.C. Ammeter.
(5) Scram Button.
(6) Power Switch.
(7) Printer.
(8) Touch Screen.
(9) Contaminant.
(10) Ground electrode.
(11) Plastic basin.
(12) Tubes.
(13) Pump.
(14) HV electrode.
(15) Test sample.
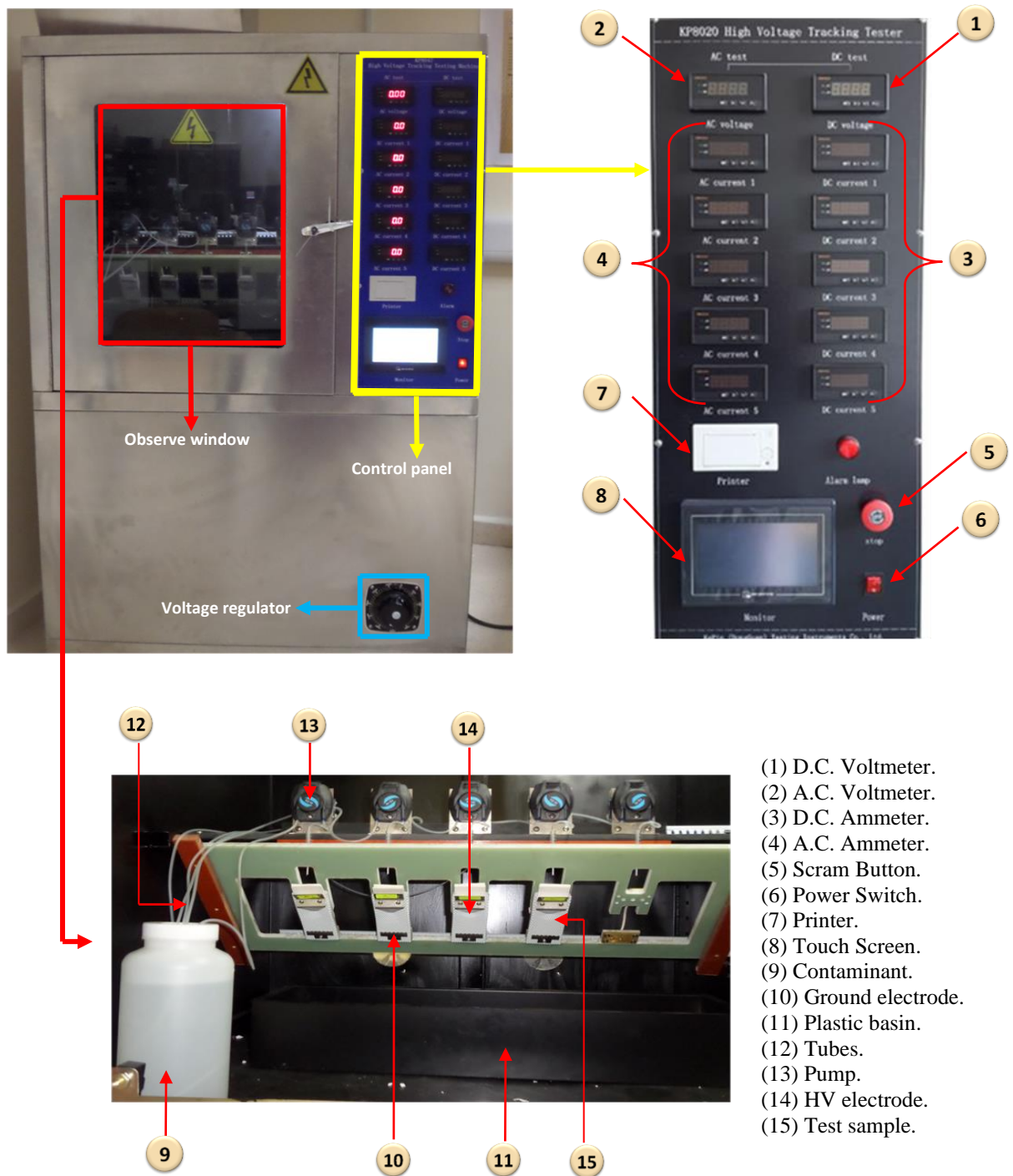
Figure 4.3 DC-AC High voltage tracking testing machine.

The contaminant is supplied by five pumps that are attached at the top of each test bay.   A peristaltic Lei fluorine pump transports the saline contaminant from large cup to the test samples. The pump can achieve flow rates from 0.0016 ml/min to 1.5 ml/min. A plastic basin at the bottom of the test compartment to accumulate the

contaminant that drips from the samples and the material lost due to erosion. The top of the test compartment contains holes to allow ventilation.

A touch screen (Figure 4.4) allows us to control the machine and to insert the parameters we need. Functional buttons are described as follows:

- Test time (s): to enter the test time in seconds (s) for the five samples. The machine stops working when the specified time expires.

- Alarm indication: to indicate all kinds of alarms, for example, a low level of polluted liquid, and when the door of a test compartment is opened.... etc.

- Test parameters: - To enter the flow rate value of the contaminated liquid.

                              - To choose the voltage type AC or DC.

Figure 4.4 Touch display of the DC-AC High voltage tracking testing machine.

4.4. Preparation of pollution suspension used for IP tests

The sample surface is continually wetted with a contaminant consisting of 2g of ammonium chloride (NH_4Cl) and 0.4g of iso-octylphenoxypolyethoxyethanol (triton X-100) diluted in 2000g of distilled water (Figure 4.5). The conductivity of the contaminant should be 0.253 S/m according to IEC 60587. The liquid contaminant flows from the HV electrode along the sample surface towards the ground electrode.

The contaminant flow rate was adjusted according to IEC 60587. The flow was

monitored for at least 10 minutes to ensure that the contaminant was stable on the sample surface and reached the ground electrode before the application of the test voltage.
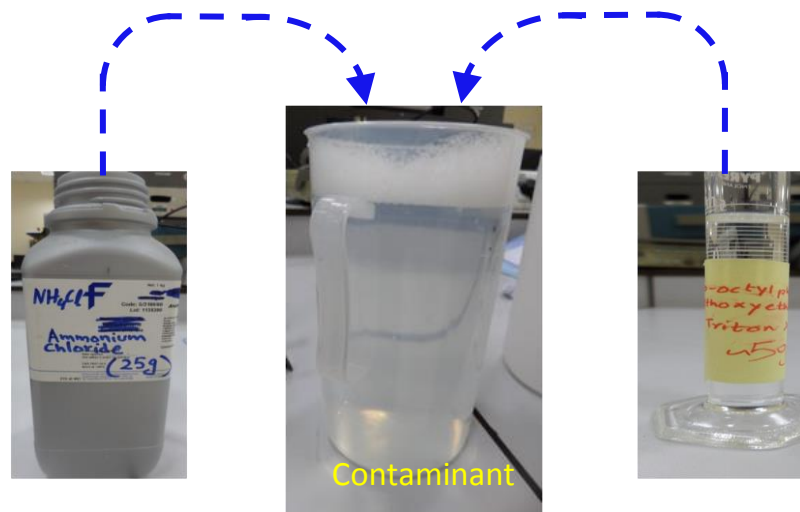
Figure 4.5 Ammonium chloride and isooctylphenoxpolyethoxyethanol

4.5. Test procedures

The IEC standard advocates two test methods: the application of a constant voltage (Method 1) and the application of a stepwise voltage (Method 2), as described in section 3.3. In the present work, method 1 was followed. All samples were cleaned with distilled water to remove any external contamination. The weight of the samples was measured before the test. A pair of stainless-steel electrodes separated by a 50 mm gap was attached on the surface of the SiR sample (Figure 4.6 a). Eight filter papers clamped between the top electrode and the sample was used so that a steady flow of the liquid contaminant on the face of the sample between the electrodes would be established. The filter papers were cut using the allocated cutting mould (Figure 4.6 b). Then, the samples were placed in the DC-AC High voltage tracking testing machine.

The preferred voltages for the constant tracking methods (Method 1) are 2.5 kV, 3.5 kV and 4.5 kV rms with a corresponding flow rate in ml/min of 0.15, 0.30 and 0.60 respectively [19]. In this research, the selected AC voltage was 3.5 kV. The equivalent positive DC voltage is 3 kV. Depending on the selected voltage, the series resistor was set to 22 kΩ and contaminant follow rate at 0.3 ml/min, as was shown in Table 3.2.

(a)   **(b)**
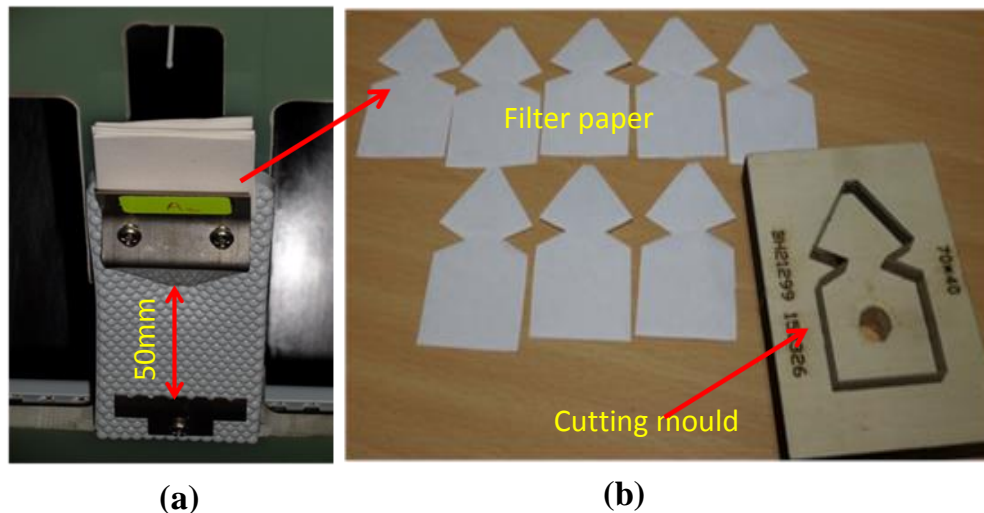
Figure 4.6 (a) A close-up of a rectangular sample in the test compartment, (b) Filter-
paper

Four specimens were used for each test, textured (intersecting hexagonal and square) and non-textured samples were exposed to AC and positive DC voltages. Figure 4.7 shows a diagram for performed inclined plane tests under various voltage types. Once the contaminant was flowing uniformly on the sample surface, a preselected high voltage level was applied to the samples by adjusting the regulator voltage. The duration of each test is 6 hours, unless a) the leakage current reached 60 mA for 2 seconds, or b) samples were ignited. A flow chart of the procedure used in the data collection phase of the experiments is shown in Figure 4.8. Visual camera was employed to monitor the samples during the test time. The leakage current was monitored using AC and DC Ammeter and manually recorded every 5 minutes. At the end of each test, samples were removed from the IPT unit, and the material loss calculated from the differences in the sample weight before and after performing a test.

4.6. Results analysis and discussion

This section analyses the results of the DC and AC tests. These findings included the following: Visual images of the discharge and arcing, visual images of the eroded areas of samples, data relating to samples mass loss and the leakage current characteristics.
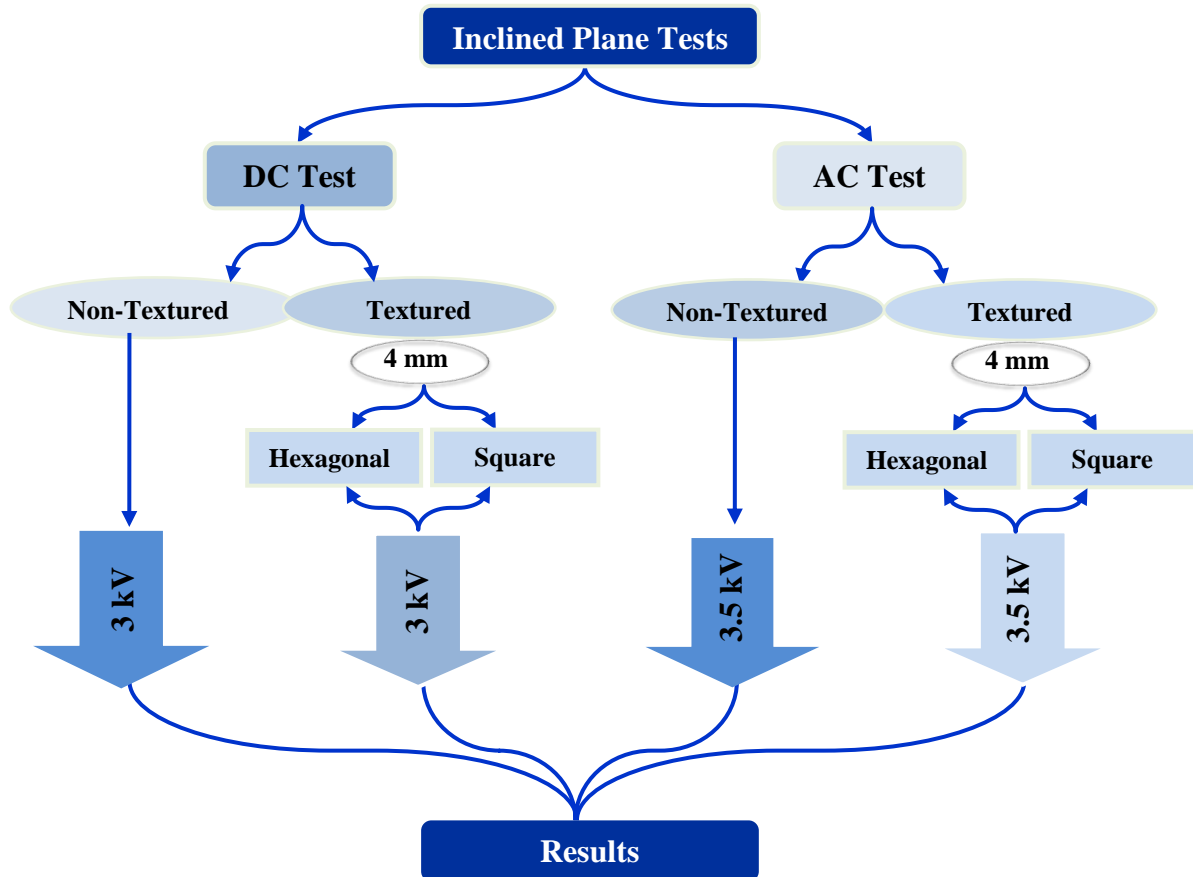
Figure 4.7 Schematic representation of comparison methodology.

4.6.1. Visual Observations

The discharge activity processes during the tests were carefully monitored by a video camera, in addition to visual observations, which lasted for a duration of 6 hours of the test, to enable more information concerning the discharge processes which are ageing the silicone rubber surface during testing. The visual images collected during the tests can be used to determine the discharge intensity, shape, and colour. Also, to monitor changes in surfaces of the samples as well as electrodes.

4.6.1.1. Visual Observations of intersecting square samples tested at DC voltages

During the early stages (especially in the first quarter-hour) of the test, the water vapour can be seen and that indicate the heating of the surface by joule heating. As a result, the dry bands begin to develop in some parts of the contaminant flow path, producing small discharges which have an orange and violet colour distributed

Chapter 04

Comparative performance of silicone rubber polymeric insulators under
HVDC and HVAC voltages using the inclined plane test

randomly on the surface of the samples. The discharges are unstable and quickly suppressed.

```
                    ┌─────────────────────┐
                    │  Inclined Plane Test │
                    └─────────────────────┘
```

Put the sample in the DC-AC High voltage tracking testing machine

Mix the liquid pollutant as per the IEC-60587 Standard

Permit the pollutant to wet the samples uniformly for 10 minutes

Switch on the supply voltage using the constant tracking method

Record the leakage current

Has the leakage current reached 60 mA? — Yes → Terminate the test

No

Have the samples caught fire? — Yes → Terminate the test

No

Continue this test until the 6 hours have elapsed

Analysis of materials after ageing and discuss the results

Figure 4.8 Flowchart of the test procedure.

Chapter 04

Comparative performance of silicone rubber polymeric insulators under
HVDC and HVAC voltages using the inclined plane test

During the advanced hours of testing and exactly at the third hour (3h), a dry-band was observed above the ground electrode. The discharge activity in this area was bright, more intense and stable. The stable discharge phenomenon releases sufficient heat energy to decompose the test samples and develop the damaged areas. The arcing is localised at certain points along the ground electrode and continues for several seconds. In the final hours of the test, the arcing becomes brighter more, and hot spots are stabilized and cause damage on the sample surface in the vicinity of the ground electrode. Table 4.2 shows the discharge phenomena in the samples during the test.

Figure 4.9 shows the top and bottom electrodes before and after 6 h of IP test under DC voltage. It can be seen that there is erosion on the top electrode (Figure 4.9. (a)). Whereas in Figure 4.9. (b), there is a solid brownish material deposition was observed on the surface of the bottom electrode. The difference in electrode mass was measured before and after testing, these data are shown in Table 4.3. The average mass loss value of the four top electrodes is 0.055 g, whereas the bottom electrodes show an increase in mass due to the formation of the solid layer.

(a)   **(b)**
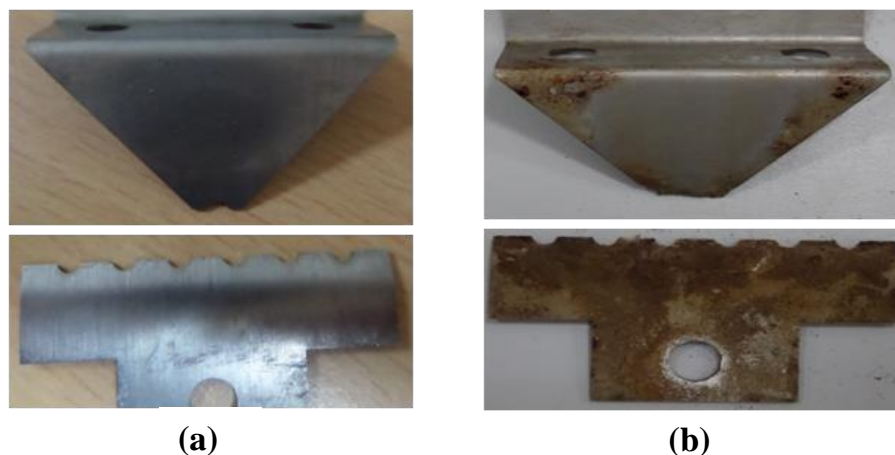
Figure 4.9 Pictures of the electrodes. a) before IP test, b) after 6 h of IP test for intersecting square sample under DC

Figure 4.10 shows the surface condition of each sample after the end of the IP test. The degraded area is only prominent in the bottom half of the samples (near ground electrode), because the discharge activity was more intense in this area, resulting in mass loss of material due to erosion.

Chapter 04

Comparative performance of silicone rubber polymeric insulators under
HVDC and HVAC voltages using the inclined plane test

Table 4.2 Discharge phenomena on the intersecting square samples during the test

Time	Photographs of specimen during the IP test
15min	
60min	
150min	
300min	

Chapter 04

Comparative performance of silicone rubber polymeric insulators under
HVDC and HVAC voltages using the inclined plane test

Table 4.3 Mass of the top and bottom electrodes before and after IP test for
intersecting square sample under DC

	Top electrodes				Bottom electrodes			
Sample	Mass before IPT (g)	Mass after 6h (g)	Mass loss (g)	Avg (g)	Mass before IPT(g)	Mass after (g)	Mass loss (g)	Avg (g)
1	9.894	9.836	0,057		3.590	3.605	-0,015	
2	9.845	9.790	0,055	0,055	3.574	3.592	-0,018	-0,0165
3	9.877	9.820	0,057		3.586	3.604	-0,018	
4	9.710	9.656	0,054		3.580	3.595	-0,015	

The visual images show coloured areas such as brown (spot 1) and gray region
(spot 2). To observe the chemical composition of the spots formed on the surfaces,
physical and chemical techniques can be used. Energy-dispersive X-ray spectroscopy
(EDX) is one of the most suitable techniques for studying the fine chemical changes
that occur on the surface of materials as a result of ageing. In this work, we did not use
this technique. Joseph Vimal Vas et al [132] have used the EDX technique to
understand the changes in the smooth surface of silicone rubber samples which have
been tested using inclined plane tests under DC voltage. The results showed that
colored areas are the accumulation of iron, chromium and chlorine. These elements
though not originally present could have migrated from the metal electrodes and the
pollutant used for the test due to electrolysis.

Figure 4.10 Photographs of intersecting square samples tested at 3 kV DC showing
the discolorations on the surface

The samples were cleaned, and the material loss calculated from the differences in the weight of the samples before and after performing a test, as shown in Table 4.4. Figure 4.11 shows close-up images of the eroded areas of silicone rubber textured samples (intersecting square) tested at DC voltage.

Table 4.4 Mass of intersecting square samples before and after IP test

Sample	Mass before test (g)	Mass after test (g)	Mass loss (g)	Avg (g)
1	48.811	48.522	0,289	
2	48.883	48.595	0.288	0,292
3	48.858	48.588	0,270	
4	48.867	48.546	0.321	

Sample 1

Sample 2
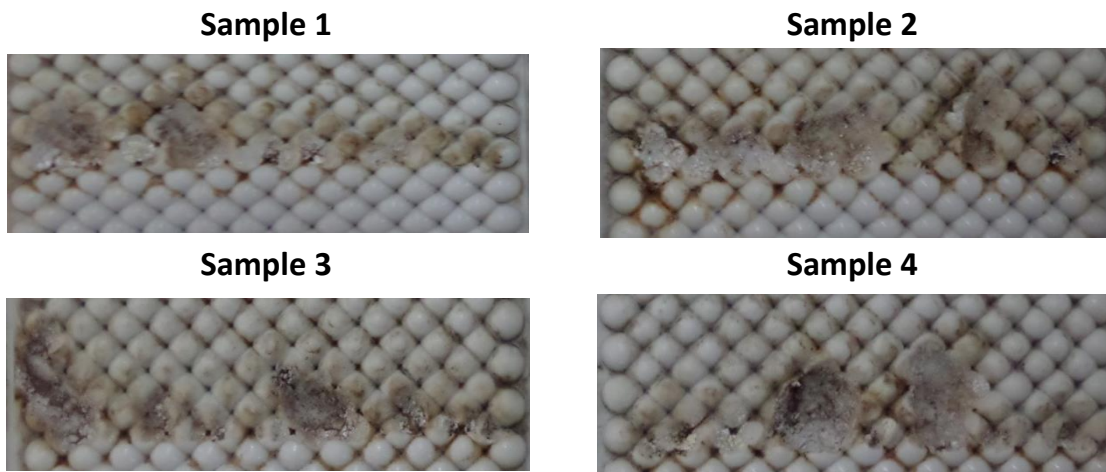
Sample 3

Sample 4

Figure 4.11 Close-up images of the eroded areas of silicone rubber textured samples (intersecting square) tested at DC voltage

4.6.1.2. Visual Observations of intersecting hexagonal samples tested at DC voltages

The behaviour of the discharge of the intersecting hexagonal samples was very similar to that of the intersecting square samples. The evolution of the discharge phenomenon on the samples was in three stages: (a) Mobile discharge: In the early hours of the test, there were small and fast dynamic discharges and they do not stay rooted on any particular point. (b) Localized arcing: As the damaged area develops, the arcing is localized at a particular point. This kind of arcing stays rooted normally at the top point of existing damage and lasts for 2 to 3 s. (c) Brighter localized arcing:

Chapter 04

Comparative performance of silicone rubber polymeric insulators under
HVDC and HVAC voltages using the inclined plane test

When the localized arcing develops brighter discharges have been observed, and hot spots are stabilized and cause damage on the sample surface in the vicinity of the ground electrode. Interestingly, the localized arcing arc seemed more intense and was more glows compared to the intersecting square samples. Table 4.5 shows the discharge phenomena on the intersecting hexagonal samples during the test.

The difference in electrodes mass was measured before and after the test, these results are given in Table 4.6. It has been observed that there an erosion on the HV electrode after 6 hours of DC test, while a solid brownish layer was formed on the ground electrodes, where the amount was lower compared to the ground electrodes of the intersecting square sample. The average mass loss value of the HV electrodes is 56 mg, whereas the ground electrodes show a slight increase in mass an about 8.5 mg.

For the intersecting hexagonal samples, there are different coloured regions (see Figure 4.13) like light brown (spot 1) and the yellow coloured region (spot 2) away from the eroded region and close to the HV electrode, the gray coloured region close to the eroded area (spot 3). The degraded area is only prominent in the bottom half of the samples (near ground electrode), because the discharge activity was more intense in this area, resulting in mass loss of material due to erosion. As discussed earlier in the su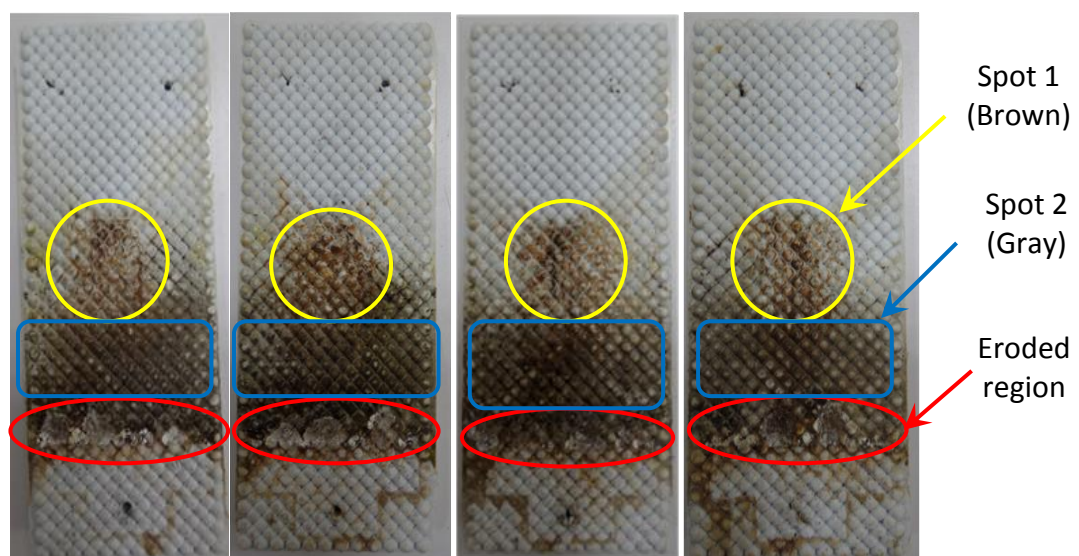rface condition of the intersecting square samples, the coloured areas are the accumulation of iron, chromium and chlorine.
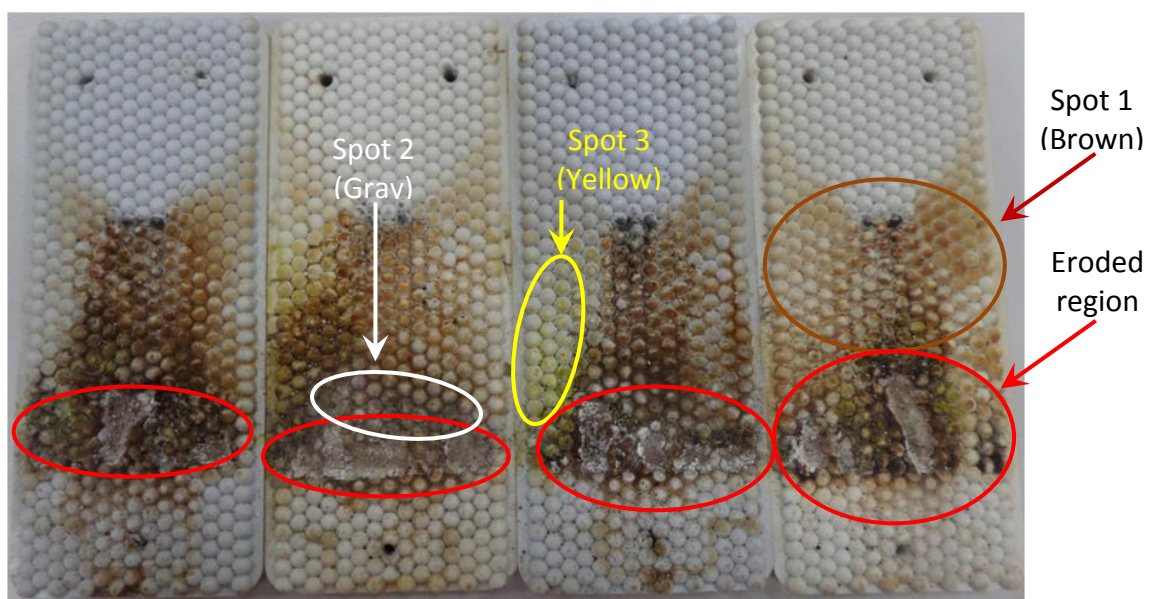
Figure 4.12 Photographs of intersecting hexagonal samples tested at 3 kV DC showing the discolorations on the surface

Chapter 04

Comparative performance of silicone rubber polymeric insulators under
HVDC and HVAC voltages using the inclined plane test

Table 4.5 Discharge phenomena on the intersecting hexagonal samples during the test
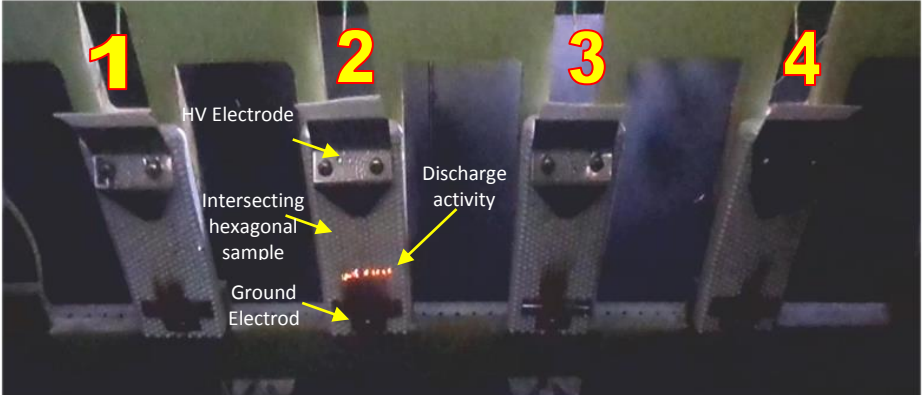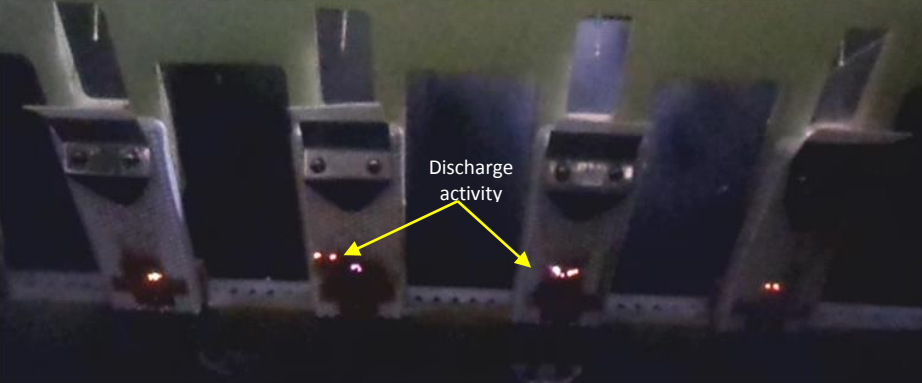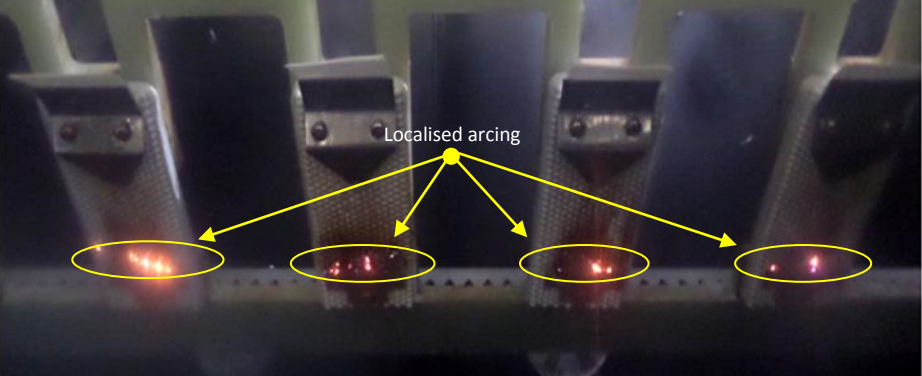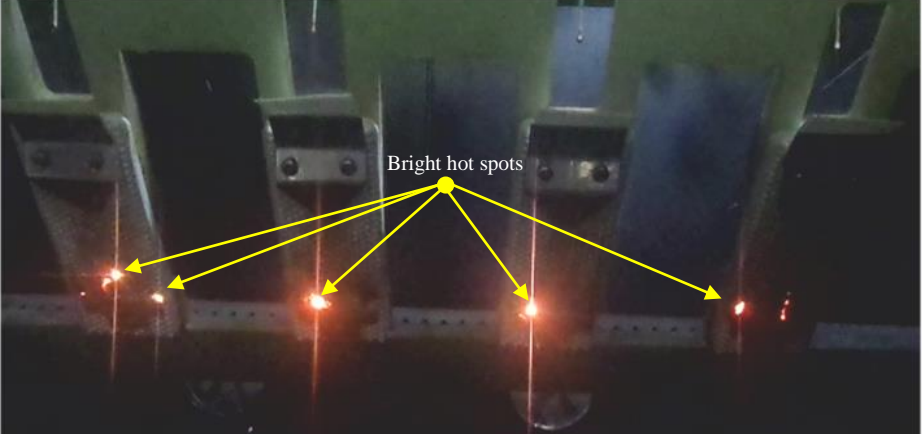
Time	Photographs of specimen during the IP test
15min	
60min	
150min	
300min	

Chapter 04

Comparative performance of silicone rubber polymeric insulators under
HVDC and HVAC voltages using the inclined plane test

Table 4.6 Mass of the top and bottom electrodes before and after IP test for
intersecting hexagonal sample under DC

	Top electrodes				Bottom electrodes			
Sample	Mass before IPT (g)	Mass after 6h (g)	Mass loss (g)	Avg (g)	Mass before IPT(g)	Mass after (g)	Mass loss (g)	Avg (g)
1	7.202	7.147	0,055		3.602	3.610	-0,008	
2	6.548	6.490	0,058	0,056	3.588	3.597	-0,009	-0,0085
3	7.248	7.191	0,057		3.894	3.902	-0,008	
4	7.256	7.202	0,054		3.562	3.571	-0,009	

Figure 4.12 shows close-up images of the eroded areas for intersecting
hexagonal silicone rubber samples after cleaning. The samples were weighed before
and after the tests to calculate the weight loss of the material. These results are shown
in Table 4.7.
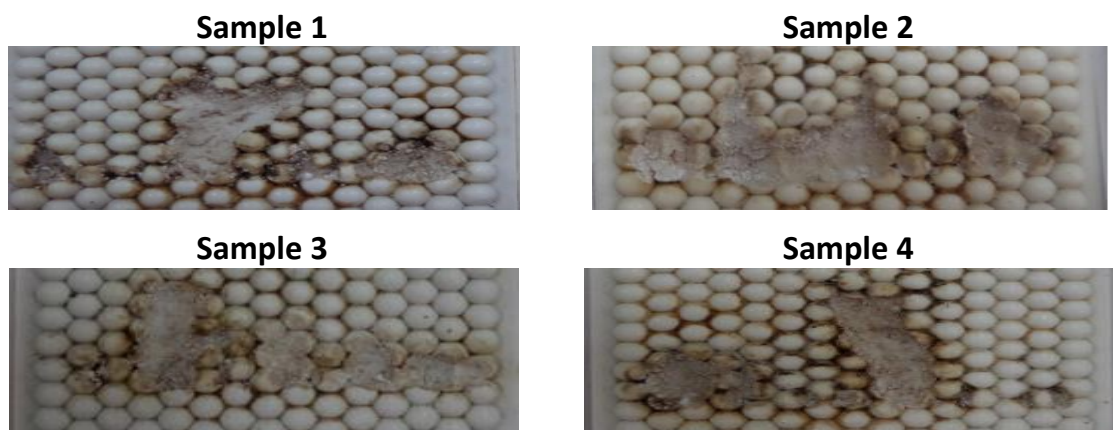
Figure 4.13 Close-up images of the eroded areas of silicone rubber textured
samples (Intersecting hexagonal) tested at DC voltage

Table 4.7 Mass of silicone rubber textured samples
(Intersecting hexagonal) samples before and after IP test

Sample	Mass before test (g)	Mass after test (g)	Mass loss (g)	Avg (g)
1	47.689	47.245	0,444	
2	47.549	47.100	0.494	0,401
3	47.738	47.442	0,296	
4	48.460	48.090	0.37	

4.6.1.3. Visual Observations of intersecting hexagonal and square samples tested at AC voltages

The dynamics of surface discharges for intersecting hexagonal textured samples in the AC test were significantly different from the DC test.

The visual observations have shown that the discharge channels originate in the upper high-voltage electrode. A line of the short and parallel discharges channels was observed in a violet colour (Figure 4.14) formed along the intersecting edges of the hemispheres and spread across the width of the sample to form a half-ring.

Figure (4.15) shows the line of discharges channels on the intersecting hexagonal sample moving in the direction of the polluted flow to reach the ground electrode after a few seconds; the discharge phenomenon can last for about 15 seconds.

This process for the movement of the discharge activity on the sample was frequent. Sometimes, the channels line of the discharges is turned off while moving along the sample surface, indicating a temporary blockage of the dry band through the contaminant flow.

It was also observed that near the ground electrode, the discharges transform to arcs that are mobile, unstable and distributed along the width of the sample as shown in Figure (4.16), which explains little erosion of the sample in that area. At some moments of the test, there was no activity (dark periods) and the leakage current was minimal.
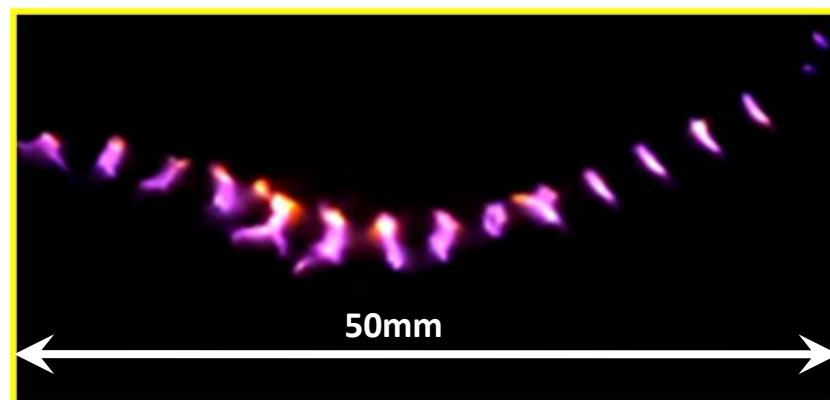
Figure 4.14 Line of short and parallel discharge channels

The intersecting square samples had overall a very similar behaviour to that of the intersecting hexagonal samples. The parallel discharges channels were once again

Chapter 04

Comparative performance of silicone rubber polymeric insulators under
HVDC and HVAC voltages using the inclined plane test

observed spreading across the width of the sample and advancing towards the ground electrode. The discharges channels formed along the intersecting edges of the hemispherical protuberances in the square sample are shown in Figure 4.17 (a). It was also observed that near the ground electrode, the discharges transform to arcs that are mobile, unstable and distributed along the width of the sample as shown in Figure 4.17 (b).
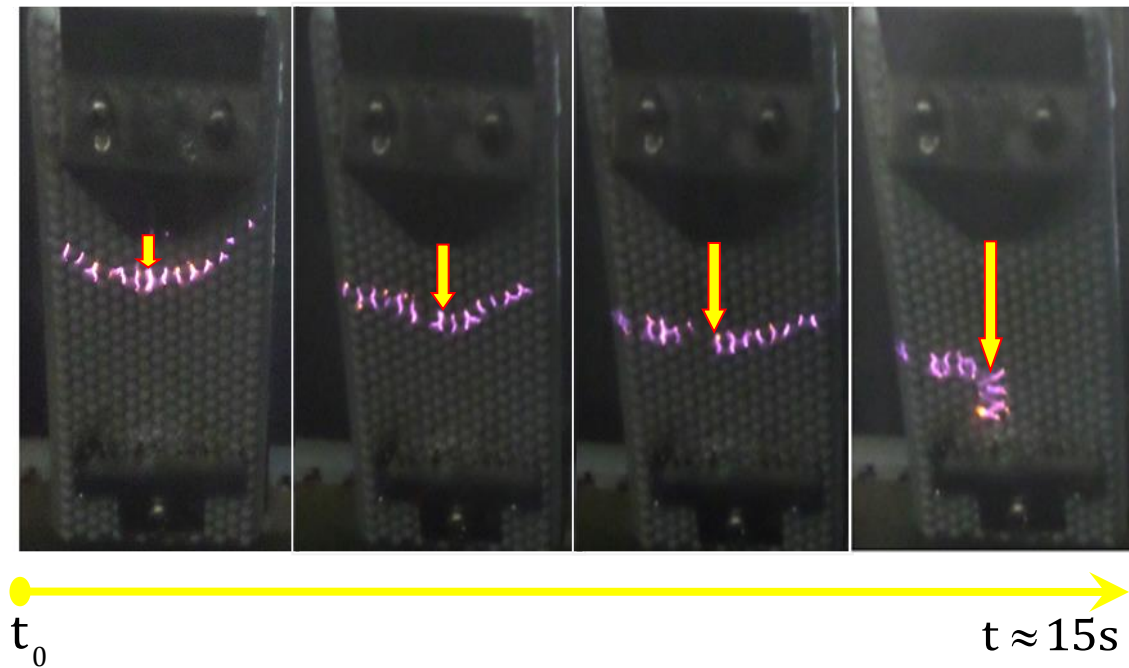
Figure 4.15 Progression of the discharge's activities on the surface sample
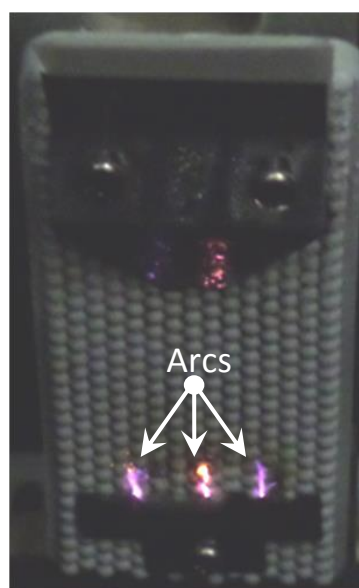
Figure 4.16 Distribution of arcs near the ground electrode

(a)   **(b)**
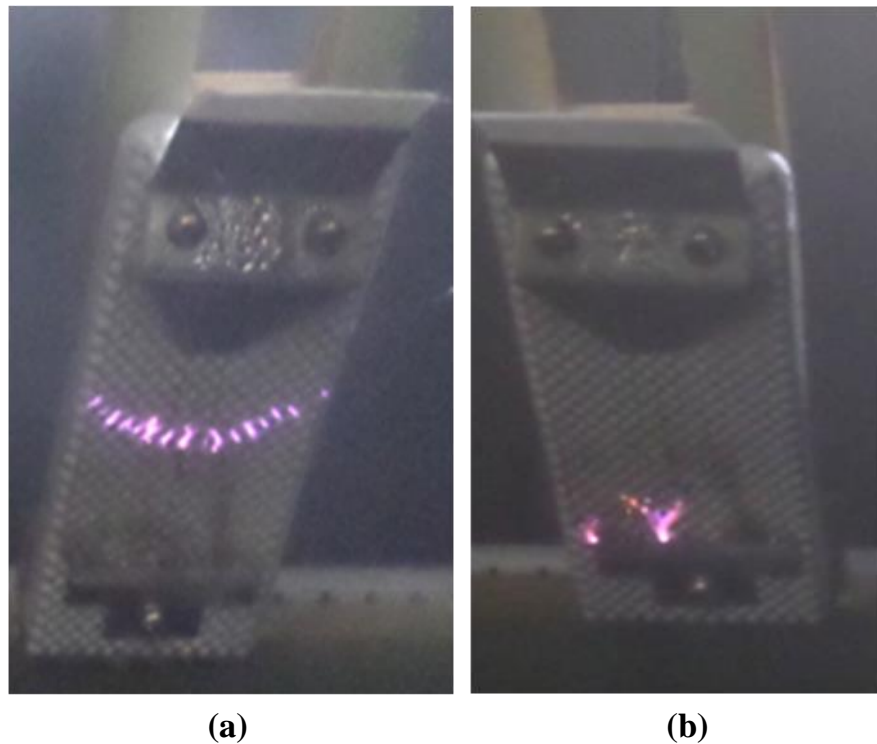
Figure 4.17 Discharge activity distribution. (a) Line of short and parallel discharge
channels, (b) Arcs near the ground electrode

Figure 4.18 shows the eroded areas for textured silicone rubber samples tested
at AC voltage. The intersecting square samples have the highest resistance to tracking
and erosion. From Table 4.8 this is indicated by a significantly lower mass loss than
the intersecting hexagonal samples. There was no significant change in the top and
bottom electrodes, as we consider that the values of mass loss are negligible.

Table 4.8 Mass loss of textured silicone rubber samples and electrodes at AC test

Sample		Mass loss of samples (g)	Avg	Mass loss of electrodes (g)			
				Top electrode	Avg	bottom electrodes	Avg
Intersecting square	1	0,052	0,044	0	negligible	-0,002	-0.0016
	2	0,053		0.001		-0,001	
	3	0,029		0		-0.002	
Intersecting hexagonal	1	0,203	0,1435	0.003	0.0025	-0,002	-0,002
	2	0,084		0.002		-0,002	

Intersecting hexagonal sample (1)   **Intersecting hexagonal sample (2)**

Intersecting square sample (1)   **Intersecting square sample (2)**

Intersecting square sample (3)
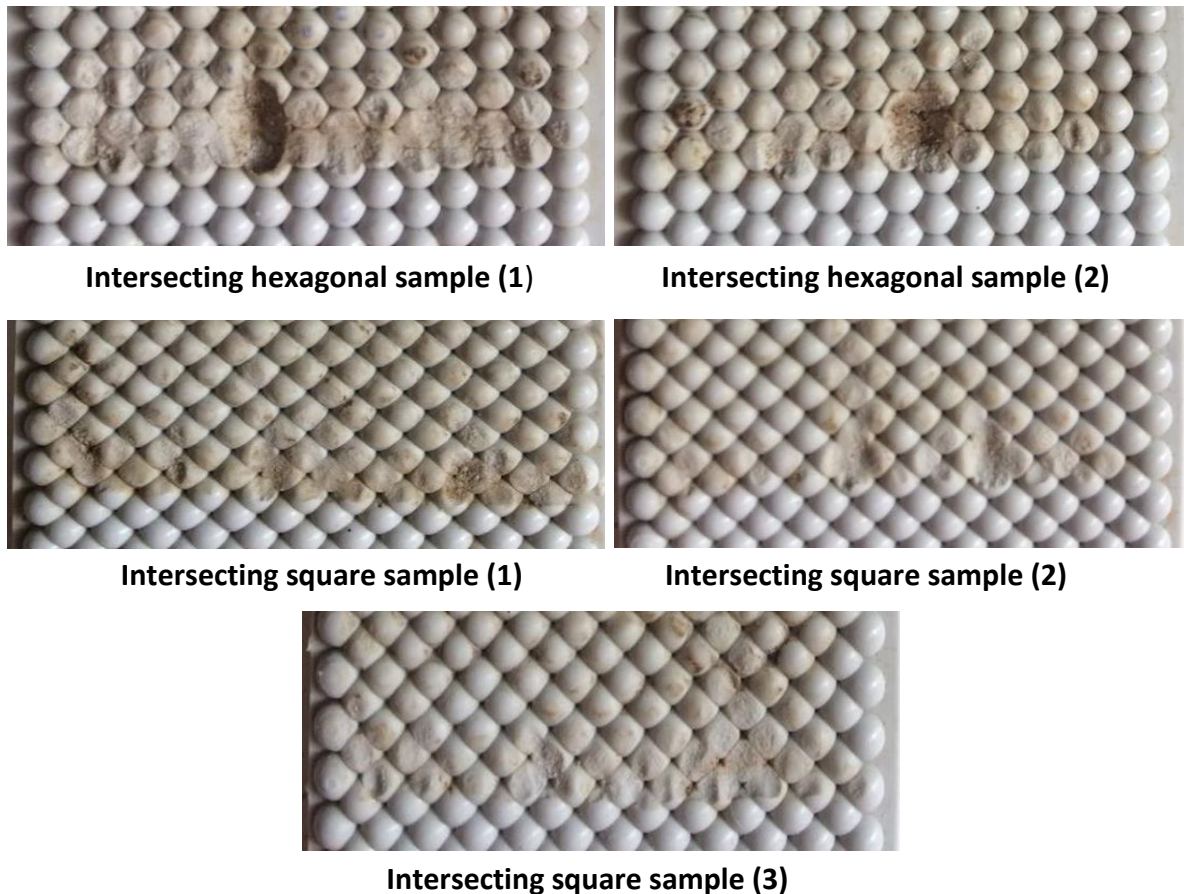
Figure 4.18 Close-up images of the eroded areas of silicone rubber textured samples (Intersecting hexagonal and square) tested at AC voltage

4.6.1.4. Visual observations of smooth samples tested at DC and AC voltage.

The liquid contaminant flows from the HV electrode along the sample surface towards the ground electrode. Over a few minutes, small drops started forming along the path of the contaminant, see Figure 4.19. The leakage current begins to flow along the contaminant's path, which causes the contaminant liquid to heat up and evaporate. Consequently, dry-bands start to develop in some parts of the pollutant flow path, resulting in discharges activity. The visual observations in the first few minutes of the DC test have shown that the discharge activity was intense, rapid, frequent and randomly distributed on the all over the smooth surface, see Figure 4.20. After 30 minutes of the test, a dry-band formation was concentrated near or at the ground electrode region. Local arcing in bright yellow was observed to be stable at specific locations for 2 to 5 seconds. At the same time, the movement of random discharges

Chapter 04

Comparative performance of silicone rubber polymeric insulators under
HVDC and HVAC voltages using the inclined plane test

continued over the other regions of the smooth surface. As the test progressed, a build-up of visible dark brown tracking that started from the ground electrode was observed. The arcing becomes brighter were mainly concentrated near the ground electrode, further leading to deep material erosion in this region. After approximately 60 minutes of the test, "track" marker was observed on the surface of the non-textured sample and heading toward the HV electrode on a straight path. After about 120 minutes of testing, where the rate of progress was approximately 70 % of the distance between electrodes.
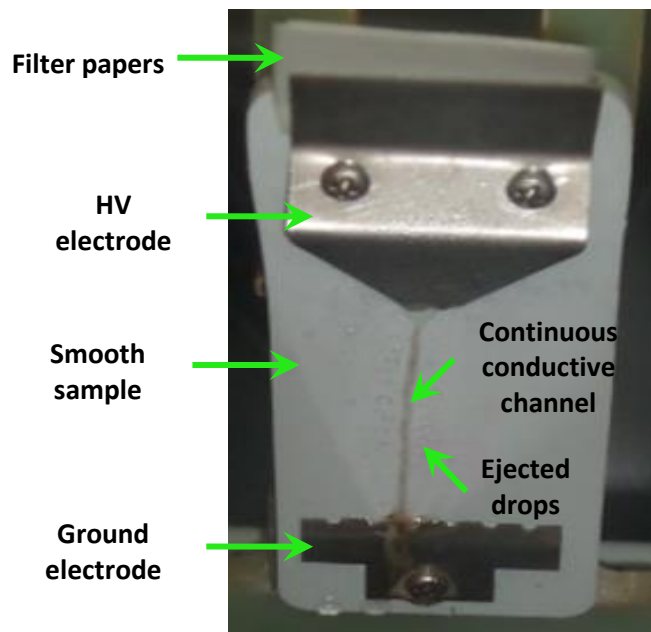
Figure 4.19 Zoomed view showing expulsion of droplets of the liquid contaminant at the smooth sample under IPT
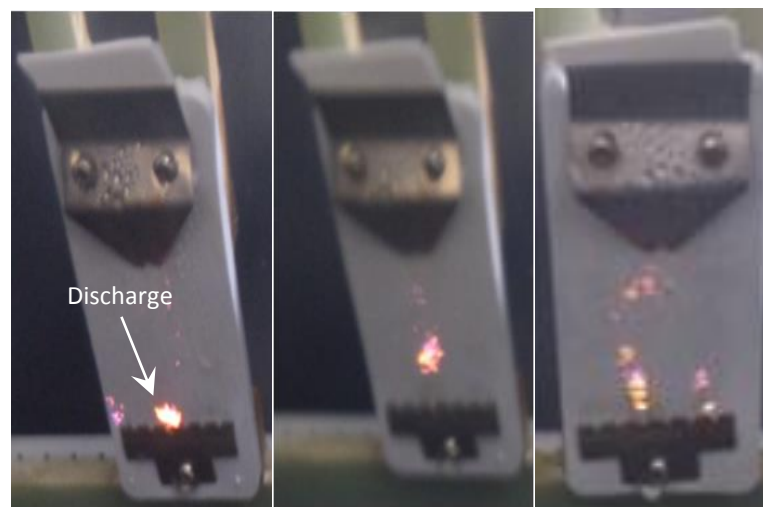
Figure 4.20 Visual images showing different cases of discharges distribution at the smooth surfaces during the early stages of the DC test

After 136 minutes, the track finally reaches the HV electrode (see figure 4.21) and the non-textured sample caught alight and "failed" according to the IEC 60587 standard [19], at which point the system was switched off. The sample was measured after the test to determine the severity of the erosion, the weight of the eroded mass was about 1,536 g.
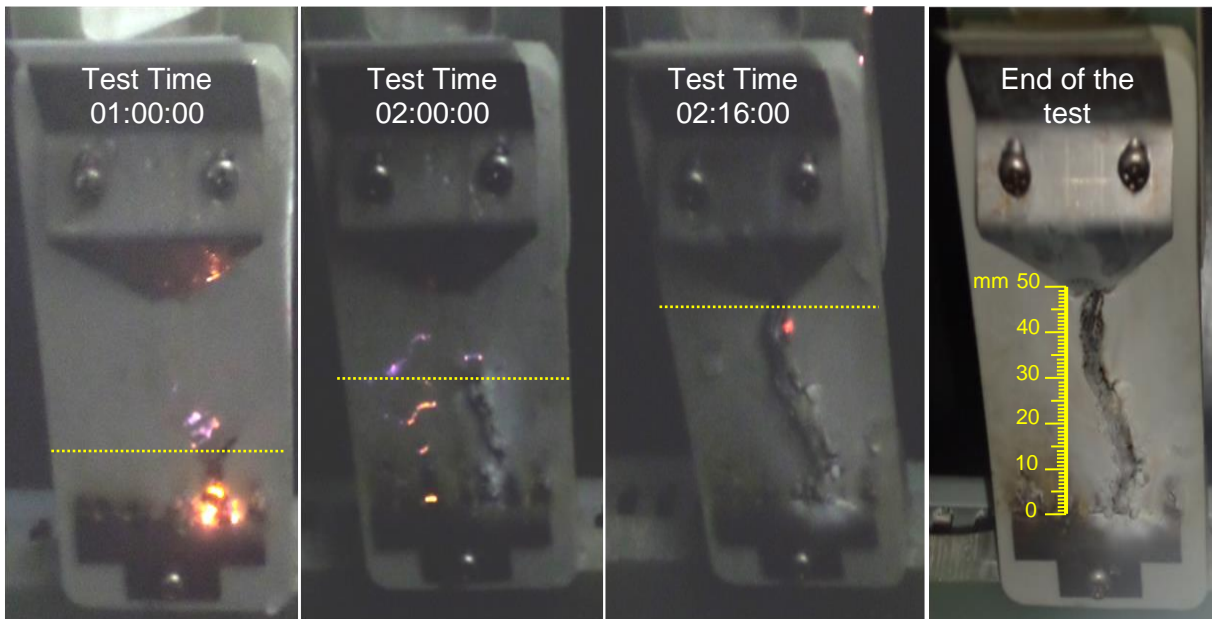
Figure 4.21 Evolution of tracking on the non-textured sample at the DC test

Concerning the behaviour of the smooth sample under AC voltage, the visual observations in the first few minutes of the test have shown that the discharge activity was rapid, frequent and randomly distributed over the entire surface, see Figure 4.22.
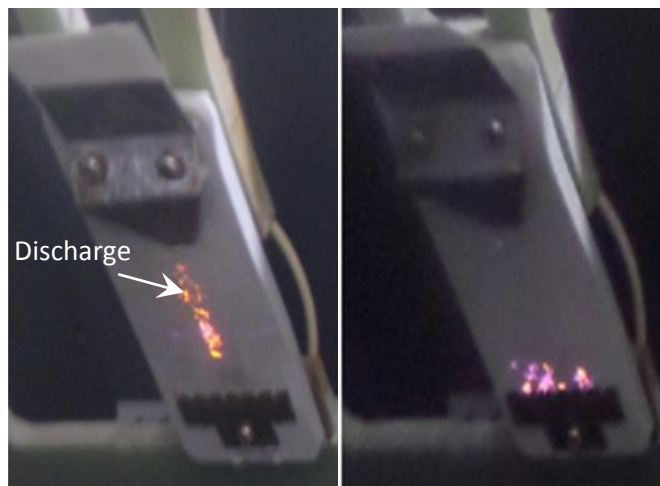
Figure 4.22 Visual images showing different cases of discharges distribution at the smooth surfaces during the early stages of the AC test

After about 60 minutes of testing, there were visible "track" marks on the non-textured sample surface and reached about 30% of the distance between the electrodes, see Figure 4.23. After about 90 minutes of testing, it was noted that the tracking became broader and brighter. After approximately 150 minutes, the sample "failed" according to the IEC 60587 standard [19], where the sample displayed intensive erosion and a burning hole near the ground electrode, shown in Figure 4.23. Figure 4.24 shows a close-up image of the extensive erosion caused by discharges activity on a smooth surface, where the weight of the eroded mass was about 0,637 g and the erosion depth was about 5mm.
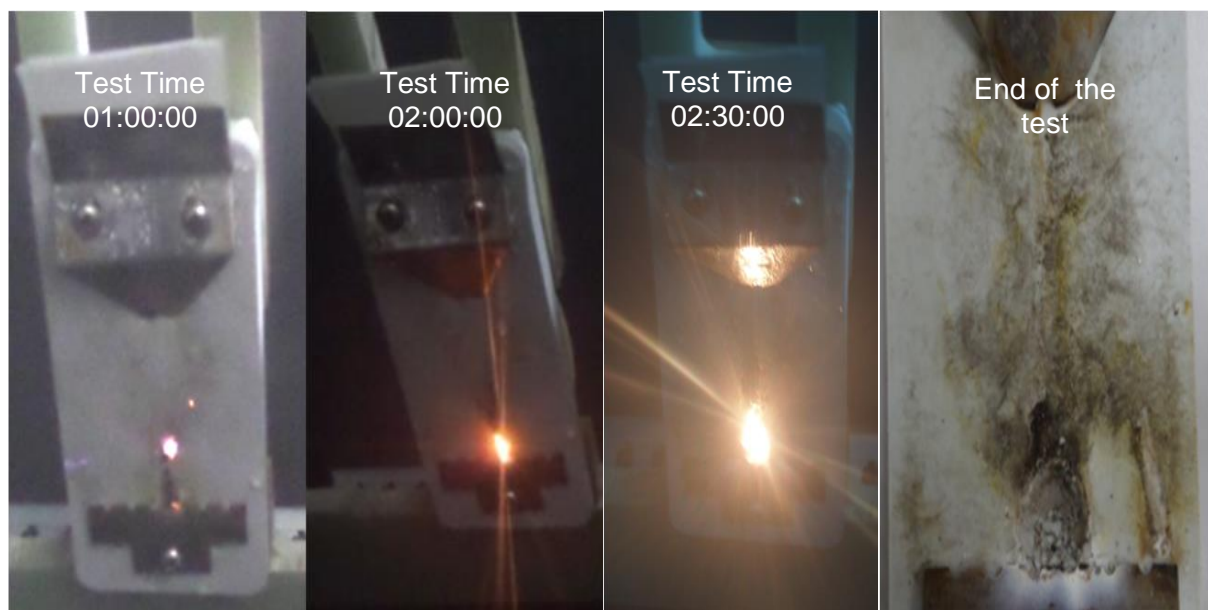
Figure 4.23 Evolution of erosion on the non-textured sample at the AC test

Figure 4.24 Close-up images of the eroded areas of non-textured sample tested at AC voltage

4.6.2. Leakage currents analysis

Leakage current is one of the most important parameters for monitoring and investigating the surface electrical activity. The results of measuring leakage current during IP tests for textured and conventional SiR insulators under DC and AC voltages are analyzed and discussed in this section. The leakage current was monitored using AC and DC Ammeter and manually registered every 5 minutes.

Leakage current values were recorded for 6 hours of testing. The voltage fluctuation remained within the 5% range indicated in the standard. Figure 4.25 shows the average leakage current values of four intersecting square samples in AC and DC tests. It can be seen that the leakage current gradually increases with time as the IP test progresses for both positive DC voltage. The alternating leakage current shows a high fluctuation over the duration of the test. Where was observed fast rising and fast falling and it did not stabilize in certain values, and this is what was noted during the visual observations of the discharge phenomenon that did not settle in a particular location and was extremely moving.
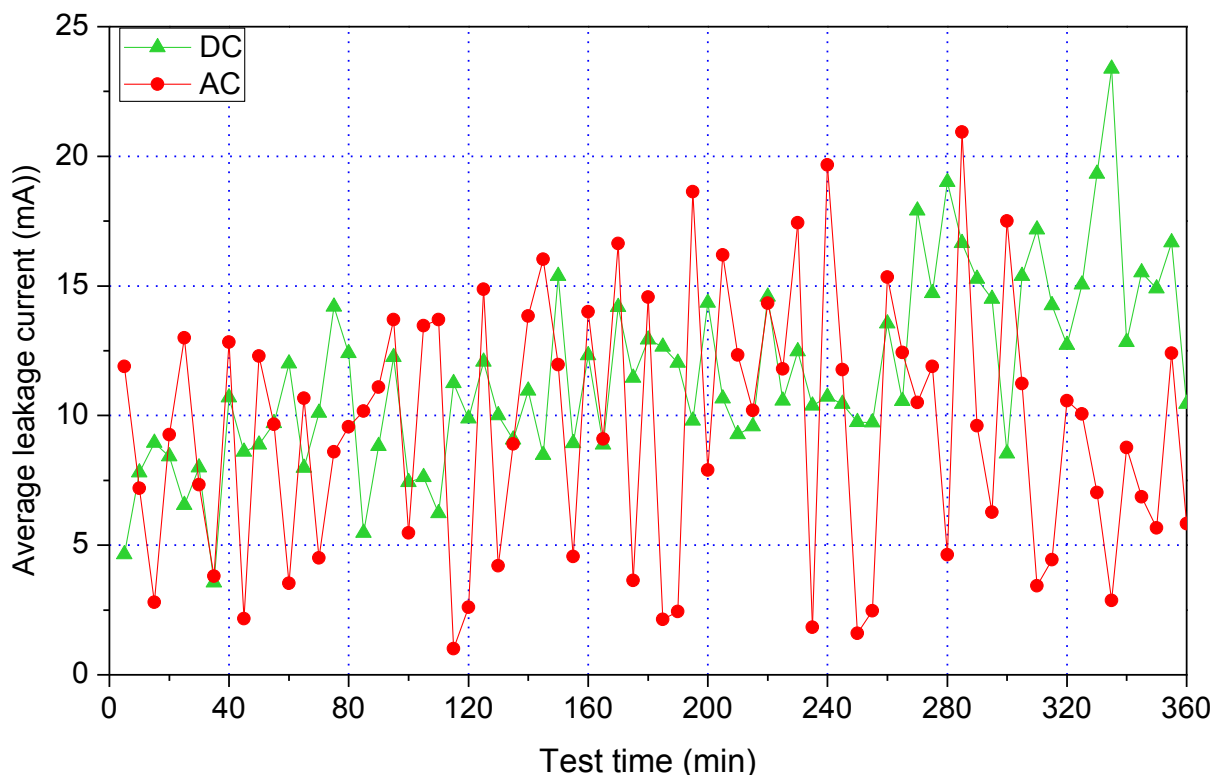
Figure 4.25 Leakage currents measured during the IP tests for intersecting square samples under DC and AC voltages

For diagnosis and a better understand the difference between DC and AC leakage currents, the average leakage current in each hour was analysed by using a box and whisker plot, as shown in the diagram in Figure 4.26. This statistical analysis identifies the:

1. Minimum current in that hour.
2. Mean minus the standard deviation.
3. Average current for that hour.
4. Mean plus the standard deviation.
5. Maximum current in that hour.

The Figure 4.26 indicates that the hourly average current leakage in the DC test is gradually increasing, indicating that the surface resistance of the insulator is decreasing. An increase was also observed in the last hour of the test, which explains the apparent deterioration of the materials which had a direct correlation with the duration of the insulator exposure to the DC leakage current.
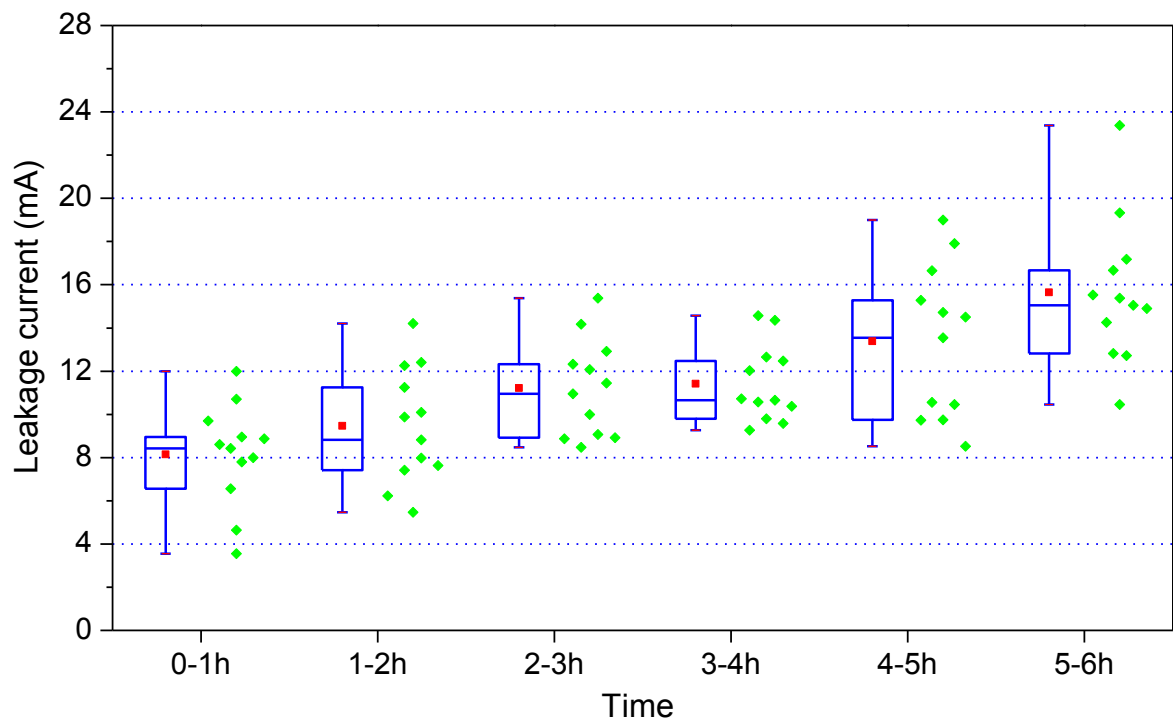
Figure 4.26 Box and whisker plots for each hour of the DC test on intersecting square samples

In contrast, the average leakage current per hour in the AC test increases and decreases during the duration of the test (see Figure 4.27). The leakage current value

on one intersecting square sample in many cases was less than 1 mA, as shown in
Figure (4.28). In this case, the discharge phenomenon does not occur (dark period) and
the sample was non-conducting [140]. This is consistent with the observed physical
damage where the samples showed minor damage in the AC test compared to the DC
test.
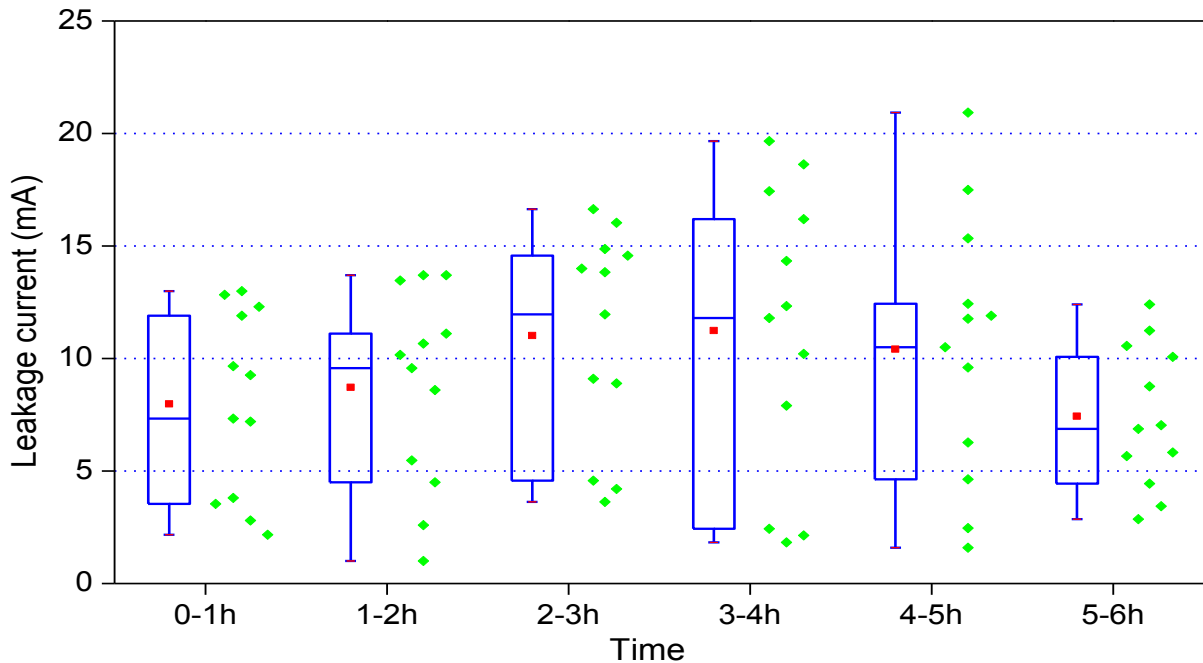
Figure 4.27 Box and whisker plots for each hour of the AC test on intersecting square
samples

Figure 4.29 highlights the differences in average leakage current values
between DC and AC test of four intersecting hexagonal samples. Leakage current
values measured at every hour for DC and AC tests are shown in Figures 4.30 and
4.31, respectively. It can be seen that in the DC test, the average leakage current
gradually increases with time as the IP test progresses. For the AC test, the average
leakage current increases and decreases during the duration of the test.

Results of the studies by Meyer et al [166] have shown a correlation between the
surface temperature of the silicone rubber samples and the eroded mass. The leakage
currents for DC showed the current values more stable and gradually increased
compared to AC. An increased leakage current would lead to a higher in the
temperature of the same surface profile, which is reflected in the erosion depth and
mass loss.
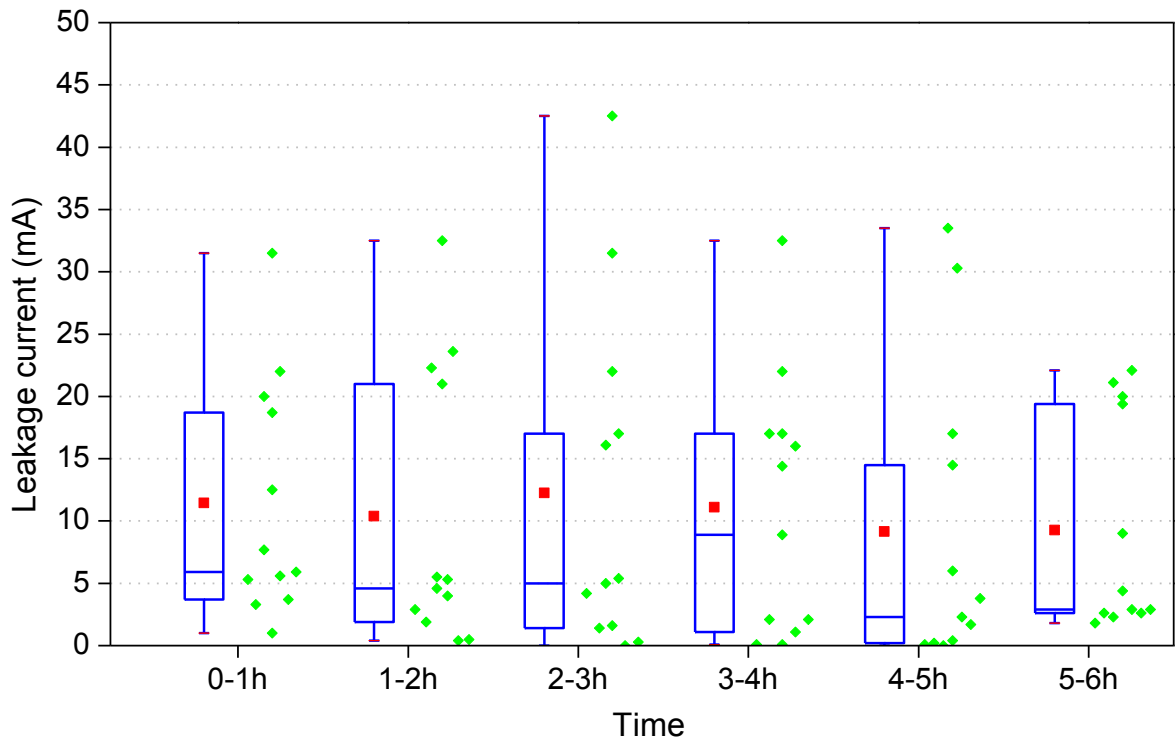
Figure 4.28 Box and whisker plots for each hour of the AC test on one intersecting
square sample
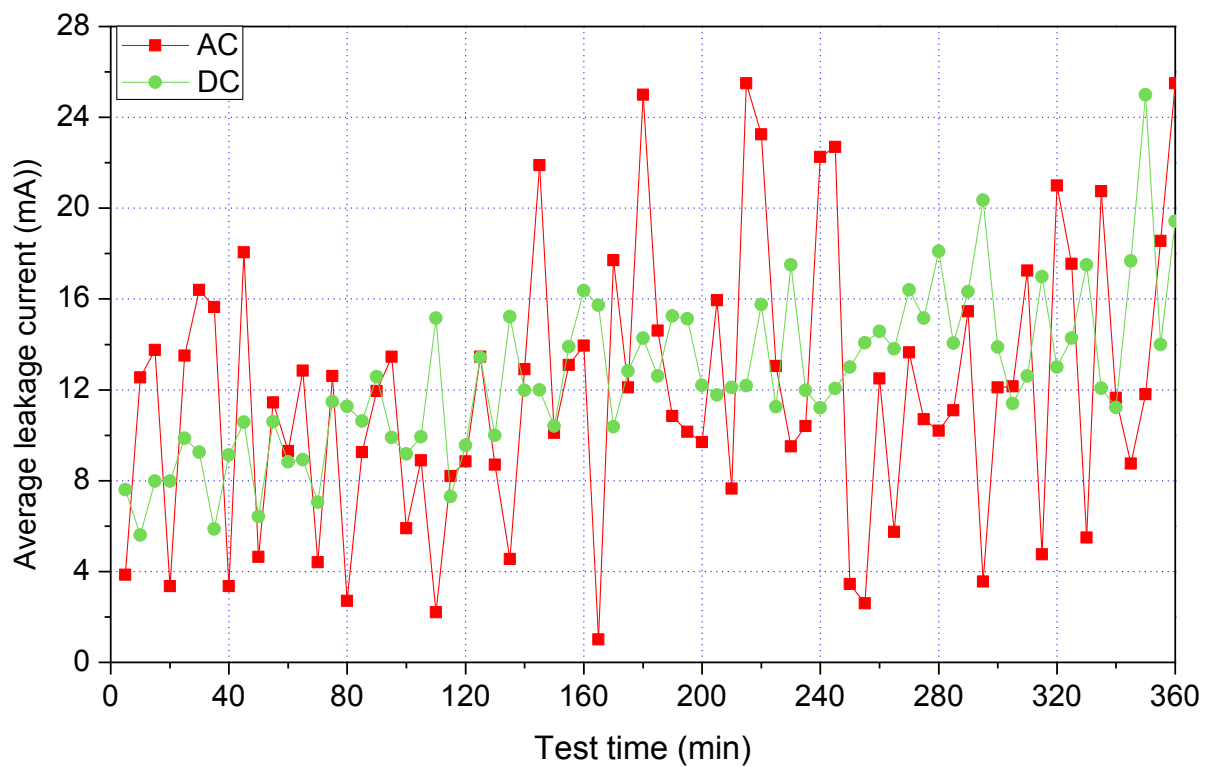
Figure 4.29 Leakage currents measured during the IP tests for intersecting hexagonal
samples under DC and AC tests
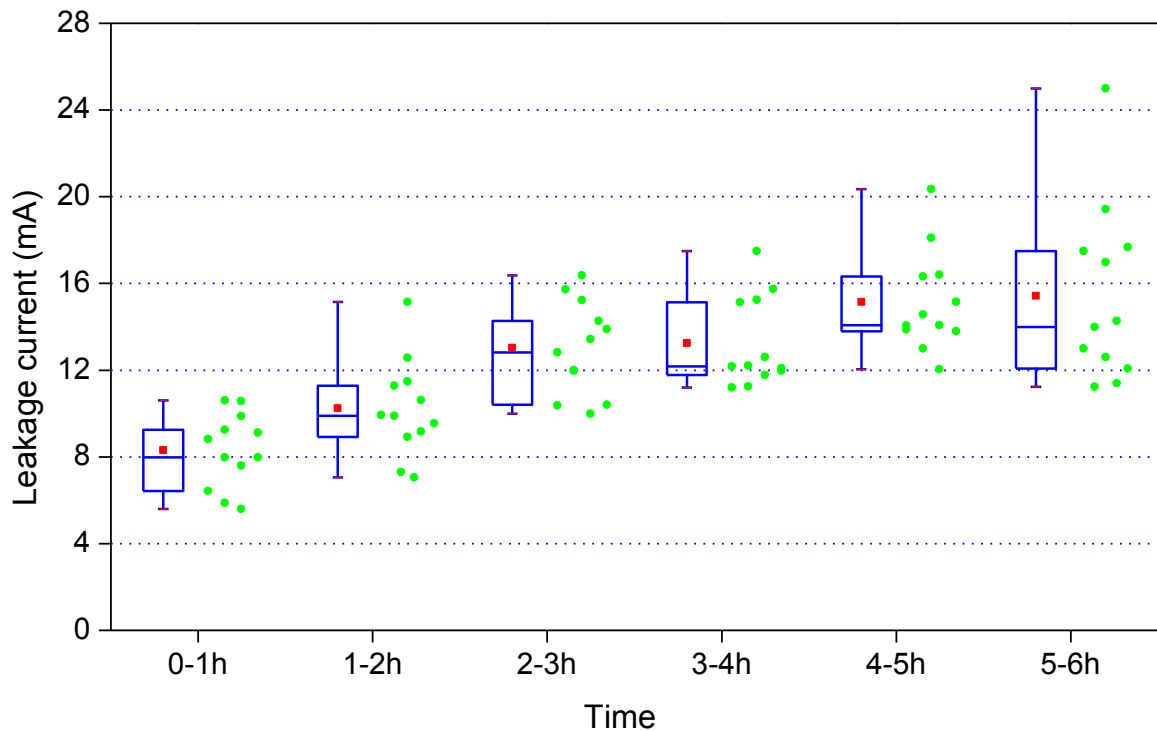
Figure 4.30 Box and whisker plots for each hour of the DC test on intersecting
hexagonal samples
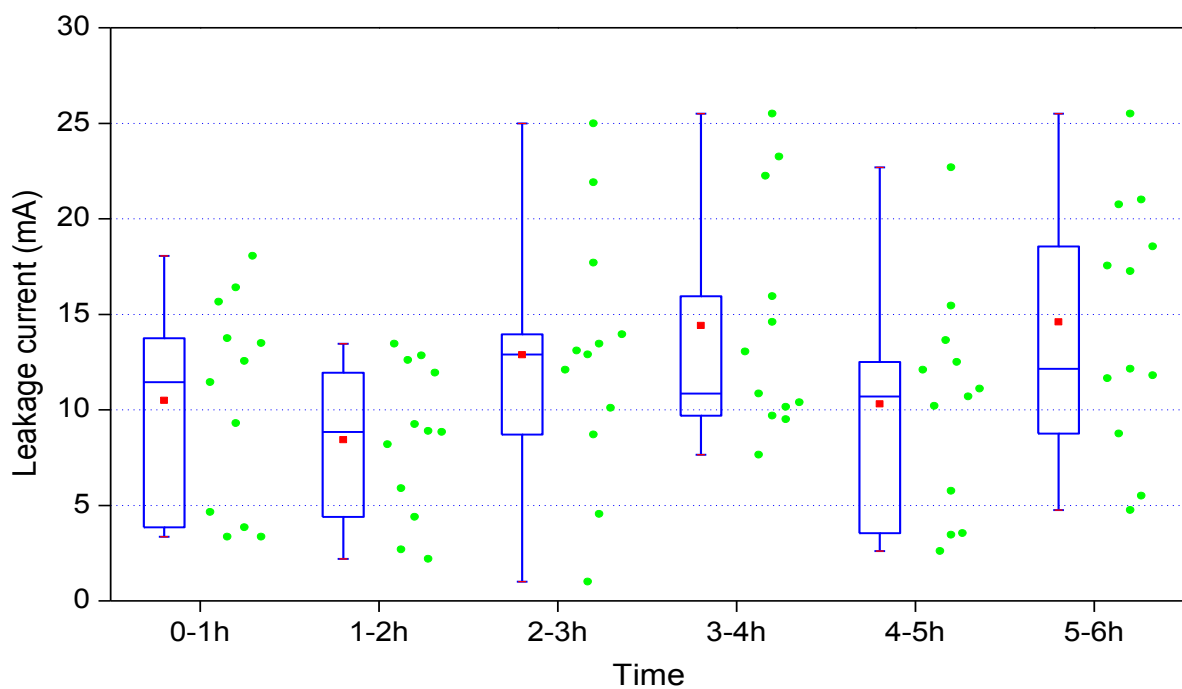
Figure 4.31 Box and whisker plots for each hour of the AC test on intersecting
hexagonal samples

The eroded mass for the DC tests is much more than those under AC. The
possible reason for such behaviour could be the electrolysis occurring during the test
duration. Bruce et al. [140] have stated that electrolysis could have caused the erosion

Chapter 04

Comparative performance of silicone rubber polymeric insulators under
HVDC and HVAC voltages using the inclined plane test

of the HV electrode for positive DC voltage, and this has also been confirmed by this study. The ion migration from the electrodes into the electrolyte could have increased the electrical conductivity on the surface of the SiR material. This increased conductivity leads to increased leakage current and hence an increased erosion in the case of DC.

4.6.3. Discussion of results

This section highlights the mechanism of tracking and degradation observed in this study, as well as discussing the most important results obtained.

When the polluted droplets flow from the top electrode along the inclined insulator surface, it creates a continuous wet film. The leakage current begins to flow along the contaminant's path, when the LC reaches a certain value, in the order of few µA to a few mA, heat is produced due to the Joule effect and the water in the path of leakage current evaporates, thereby, leads to drying portions of the surface and forming dry-band area, which interrupt the current. When the LC is interrupted, much of the voltage is applied across the dry area, and if this voltage is high enough, small arcs bridge the areas. Dry bands were more likely to form at the bottom of the water film, so the dry band arcing is mainly concentrated near the bottom electrode, which was the main discharge process of the test. Dry band arcing can increase the local temperature rapidly. The heat generated by discharges could bring the temperature on the specimen surface to 400 ºC or more, which is sufficient to cause the silicone rubber backbone to break into low chain polymers and induce tracking and erosion [66]. The degradation mechanism is illustrated in Figure 4.32.

In general, for textured samples, the discharges dynamics of the DC test was significantly different from the AC test. Visual observations showed that the discharges activity during the AC test were started from the HV electrode and moving in the direction of the polluted flow to reach the ground electrode. Also, the discharges activity was highly mobile, frequent and unable to stable at any one single point on the area near the ground electrode. While the discharges activities on the samples at DC test were more intense and not mobile and located in the area near the ground electrode.

Chapter 04

Comparative performance of silicone rubber polymeric insulators under HVDC and HVAC voltages using the inclined plane test

Start   Time

HV electrode

Sample

Contaminant flow

Discharges

Localised Bright spot

Large erosion

Bottom electrode
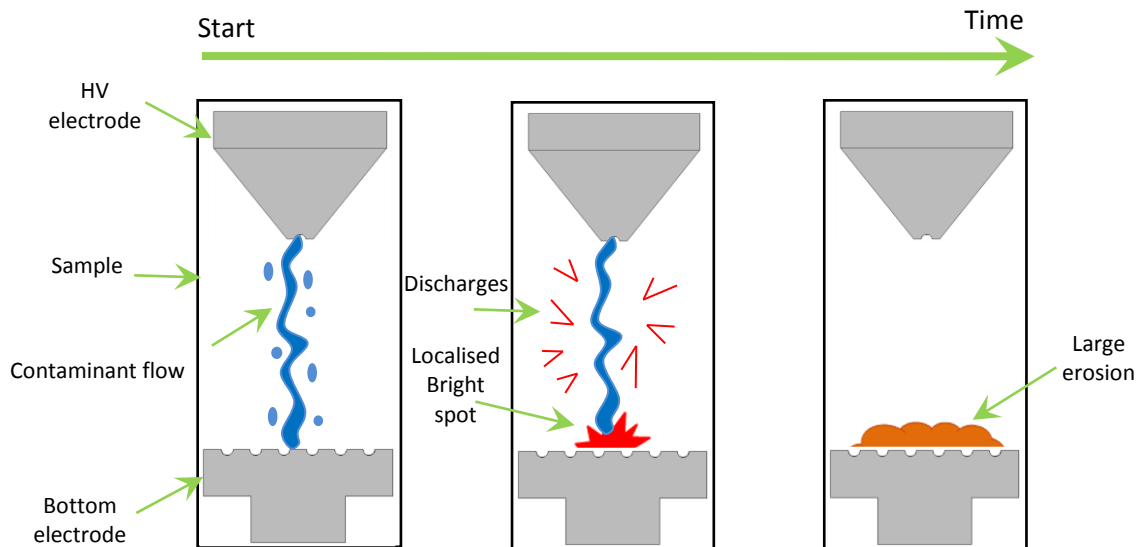
Figure 4.32 Illustration of the insulator surface ageing mechanisms under inclined plane test

The concentrated burning point was formed more clearly at the DC test, it is a very hot and bright point and it's the cause of destroying the surface of the textured sample. The temperature of the bright points much exceeds the pyrolytic temperature of silicone rubber materials which leads to the intense erosion.

In DC tests, the eroded mass of the HV electrodes was observed, while there is an increase in the mass of ground electrodes due to the formation of a solid layer on its surface, where this phenomenon has been also reported in similar DC tests [140, 167]. In this case, the oxidation occurs at the anode (HV electrode), where solid metal atoms turn into ions while they lose electrons, see Figure 4.33. Therefore, the loss of mass occurs at the anode and its mass is decreasing. On the other hand, the reduction occurs at the cathode in which ions take up the electrons to form solid atoms and hence the mass of cathode increases [135]. Due to the corrosion of electrodes, they are unsuitable for use in further tests, for this it should be used only once. On the contrary, during the AC test, we did not observe any change in both electrodes.

In the case of DC voltage, the current is stable and generates more heat than the AC voltage. Furthermore, when the electrode corrodes under the influence of DC voltage, the metallic ions dissolve in the pollutant and further increase the contaminant conductivity. In the AC voltage, because of the voltage changes periodically in magnitude from peak to zero, the discharges and arcs may not always be stable in

comparison to the DC condition.
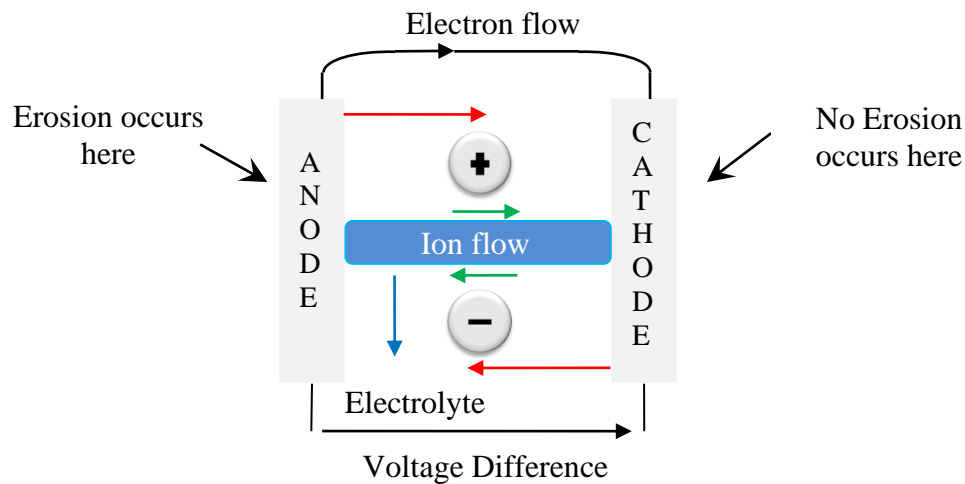
Figure 4.33 Erosion process

The leakage current failure criterion is used to compare the performance of silicone rubber insulators at DC and AC inclined plane test. The leakage current does not reach the 60 mA threshold value of failure criterion for the textured sample at AC and DC test. While, the current leakage values of the non-textured sample amounted to 60 and 50 mA in AC and DC testing, respectively. For the textured sample, the intersecting hexagonal has higher average leakage current compared with intersecting square. This increase in average leakage current would suggest a more severe test, which is reflected in the erosion depth and mass loss. Also, through the results, it was observed that the DC tests have a higher average leakage current, while the AC tests have a higher peak current.

According to the failure criterion of IEC 60587 standard, the textured samples successfully passed the inclined- plane tests in-contrast to non-textured samples.

The application of DC voltage resulted in a significant erosion of textured and non-textured materials. As well, for the textured samples, the intersecting hexagonal samples showed extensive erosion over large areas compared with the intersecting square samples in both AC and DC tests. The intersecting square samples were the most successful as they managed to suppress erosion and tracking damage with the least material loss compared with the other samples.

4.7. Conclusion

The Inclined Plane Tests performed in this investigation yielded useful information about the performance of textured silicone rubber insulators when energized by DC and AC voltages. There is a clear difference between AC and DC test conditions, at DC tests have higher average leakage current and produce deeper erosion and greater sample mass loss as compared to their AC test. The observed surface degradation pattern is also considerably different in each case. The likely contributing factors to the above are the shape of insulators surface and the effects of electrolysis.

In DC tests, there is evidence of: erosion of the positive electrode (anode) from electrolysis and oxidation of the bottom electrode due to high temperature arcing.

The tests showed that all textured samples successfully passed the inclined-plane test, whereas none of the conventional non-textured samples made of the same material passed the same test. In particular, the intersecting square configurations were the most successful as they managed to suppress erosion and tracking damage with the least material loss compared with the intersecting hexagonal patterns.

As the electric field is considered the drive of the electric current on the surface of the insulators which in turn responsible for surface damage, the following chapter investigating the distribution of the electric field on the textured and non-textured surface of the insulators.

Chapter 05

INVESTIGATIONS OF ELECTRIC FIELD AND POTENTIAL DISTRIBUTION OVER THE SURFACE OF TEXTURED SILICONE RUBBER INSULATORS

5.1. Introduction

A thorough understanding of problems such as corona and electric discharge activity can only be achieved through accurate determination of electric field distribution along the insulator surface under a range of atmospheric conditions. The performance of a dielectric depends strongly on the electric field distribution and the electric field stress. For this reason, the electric field determination is important in predicting high-stress regions on the insulator surface. The recent research on the polymeric insulator failure shows insulator ageing and degrading were caused by a high electric field. Simulations of the electric field over the surface of the insulators are intended to determine the high-stress regions on the surface of the insulator. A commercial finite element package is employed for insulator modelling to determine the electric potential and the electric field distribution along the creepage distance of the insulator.

In this chapter, we combine the finite element method with the design of experiment method to investigate and describe the behaviour of textured silicone rubber insulators.

First, a 3D FEM model of different silicone textured surfaces is developed. The potential and the electric field distributions are calculated taking into account various available patterns of hemispherical protuberance having different diameters. Then the design of experiment methodology is adopted to reduce the number of simulations and to give more significance to the results. Various influencing factors were considered in this stage. Finally, the analysis of variances (ANOVA) is used to evaluate the contribution of the studied factors and their interaction on the total variation of the studied responses.

Thorough understanding of the mathematical approach (The finite element and the design of experiment method) was not the main objective of the present study, as this can be explored in great detail in many textbooks, for example [168-172]. Instead, this study is more focused on modelling procedures and simulation results. The computed electric field and voltage distribution over the textured silicone rubber insulator under both dry-clean and polluted surface conditions are compared and discussed.

5.2. Numerical analysis through finite element method (FEM)

FEM is a numerical technique for solving partial differential and integral equations met in many practical engineering problems. The basic feature of the FEM is to divide the entire problem space, including the surrounding region, into a number of non-separated, non-overlapping sub-regions, called "finite elements". This process is called meshing. These finite elements can take a number of shapes, but generally triangular shapes are used for 2-D analysis and tetrahedron for 3-D analysis. The potential, which is unknown throughout the region, is approximated in each of these elements in terms of the potential at their vertices. For each node in the grid, the finite element method is used to set up an equation for the potential as a function of those elements for the surrounding nodes [173].

In this work, COMSOL Multiphysics ® version 4.3b was used to compute the electrical profiles of textured polymeric insulators. The simulation is performed in three consecutive stages namely, pre-processing, solving and post-processing stages. Elements of the physical problem such as geometrical structure, material properties, boundary conditions and meshing criteria are presented as inputs in the pre-processing stage. The mathematical model, normally expressed as differential equations that describe the physical problem, is executed in the solving stage. Finally, in the post-processing stage, the package allows users to generate a suitable plot of the desired post-process variables or parameters [174]. The flowchart in Figure 5.1 shows the general FEM procedures for the simulation works contained in this chapter.

5.3. Modelling of textured silicone rubber insulator

To quantify the effect of textured silicone rubber surface under clean and different polluted conditions on the electric field and potential distribution, 3D models of different textured surfaces were designed by the Computer Aided Design (AutoCAD) software package. These samples were imported into COMSOL Multiphysics for computation purposes. Figure 5.2 shows an example of textured insulator modelling. The modelled samples are rectangular with dimensions 120 mm x 50 mm with the thickness of 6 mm. The electrodes have been drawn according to IEC 60587 test standard (Inclined plan tracking test) [19]. Figure 5.3 shows the dimensions of the high voltage and ground electrode. The design of the textured insulators samples is achieved using a pattern, consisting of an array of contiguous or overlapping protuberances. Three different types of texture with different patterns of hemispherical protuberances were adopted: "A", "B" and "C" as shown in Figure 5.4 where "A" is a contiguous hexagonal pattern; "B" is a hexagonal intersection of overlapping protuberances and "C" is an intersecting square arrangement. A conventional smooth sample "S" is also taken for comparison.
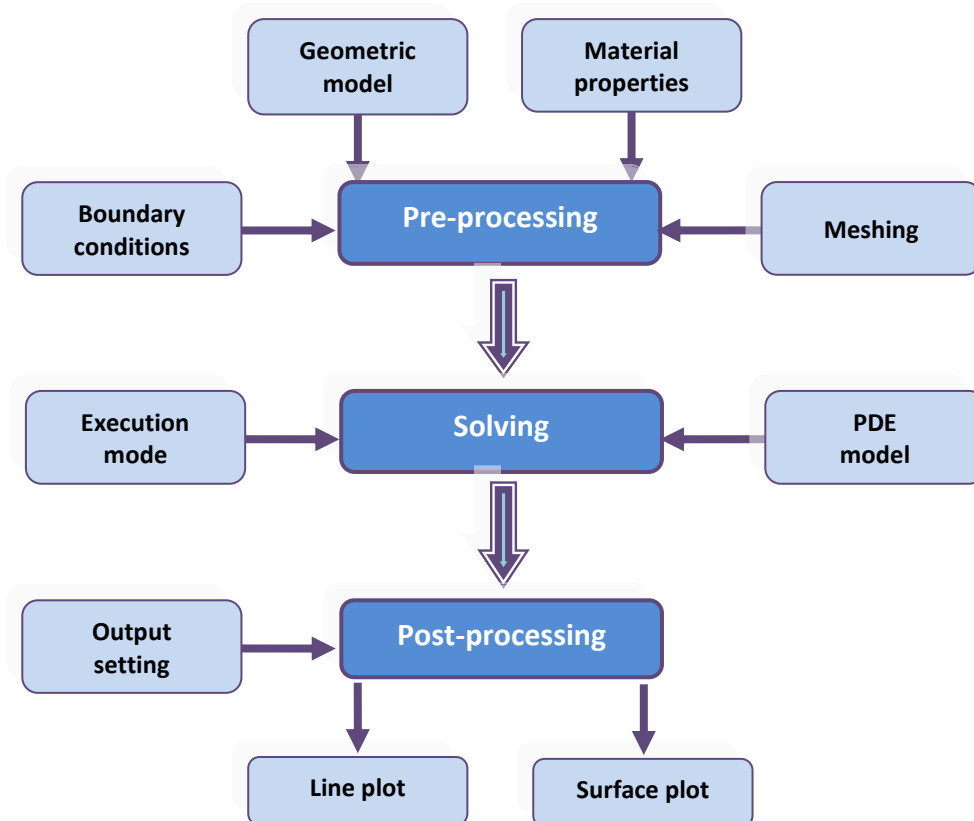
Figure 5.1 General procedures for FEM simulations [174]
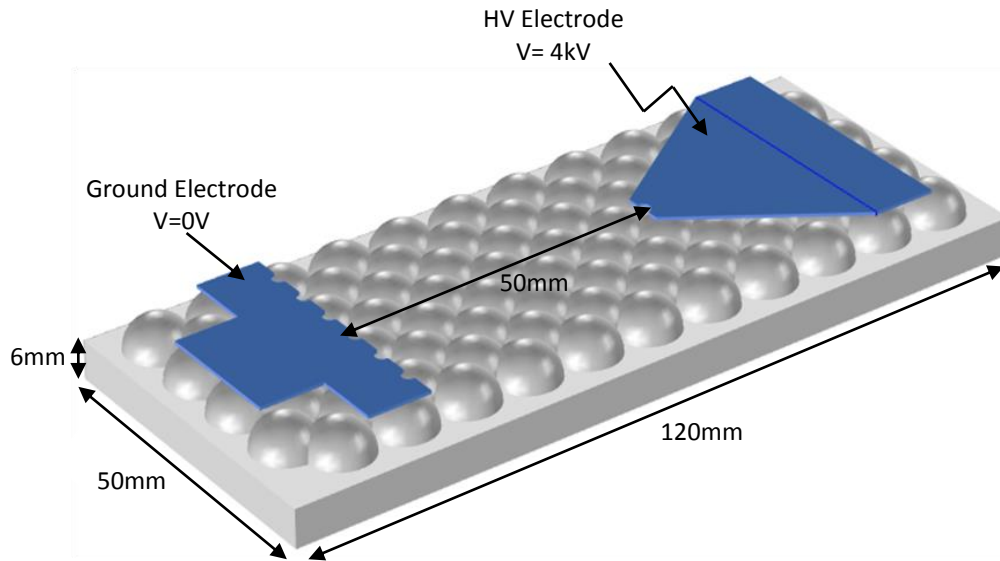
Figure 5.2 Textured silicone rubber sample.
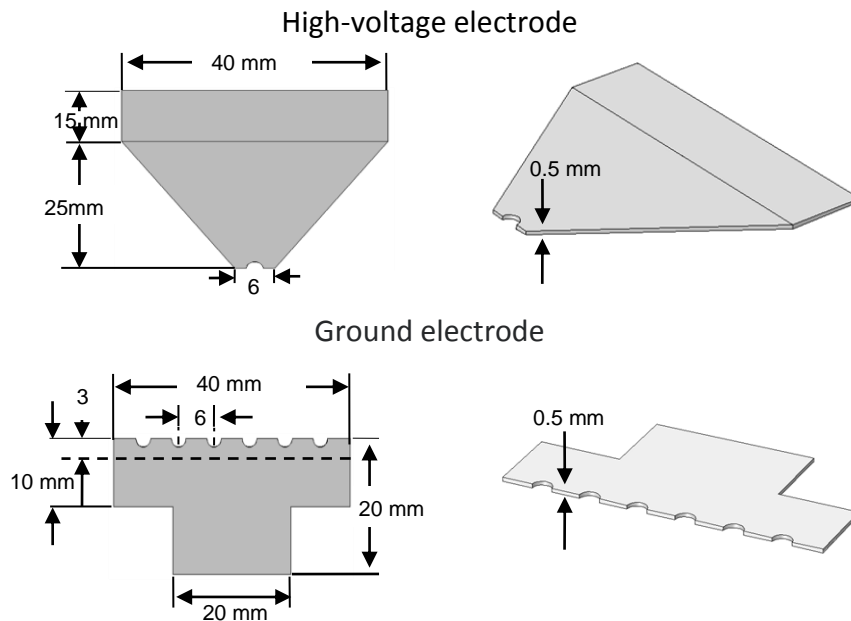
Figure 5.3 Used electrodes

5.4. Analytical study

To illustrate and to compare the effect of different textured patterns on the sample geometry, an analytical investigation has been performed. In addition to the textured patterns, a range of diameters of the hemispherical protuberances was used: 4, 6, 8 and 10 mm.

Figure 5.5 shows the different diameters of hemispherical protuberances of the "A", "B" and "C" sample.
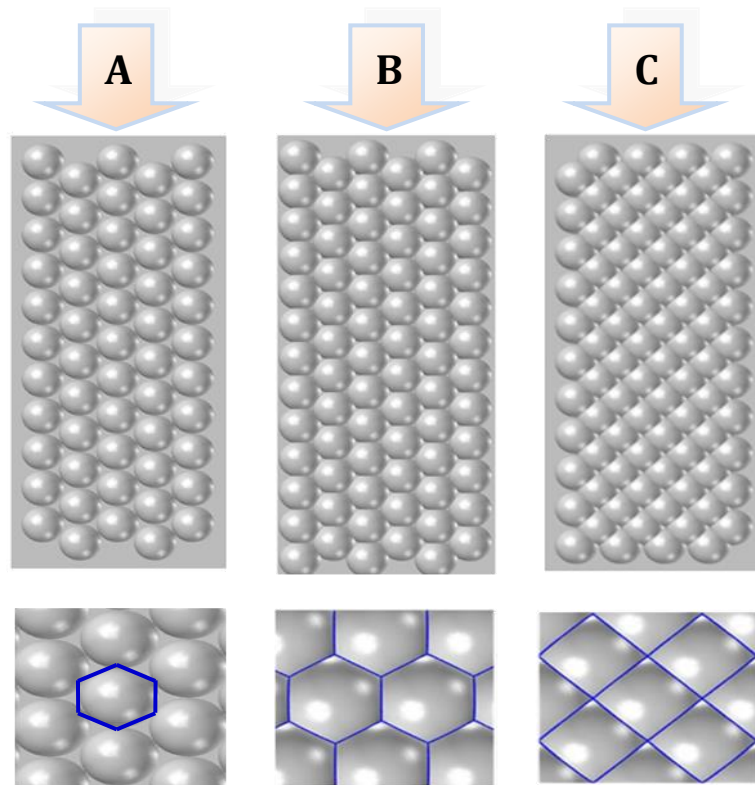
Figure 5.4 Textured silicone rubber samples: "A" Contiguous hexagonal,
"B" Intersecting hexagonal and "C" intersecting square
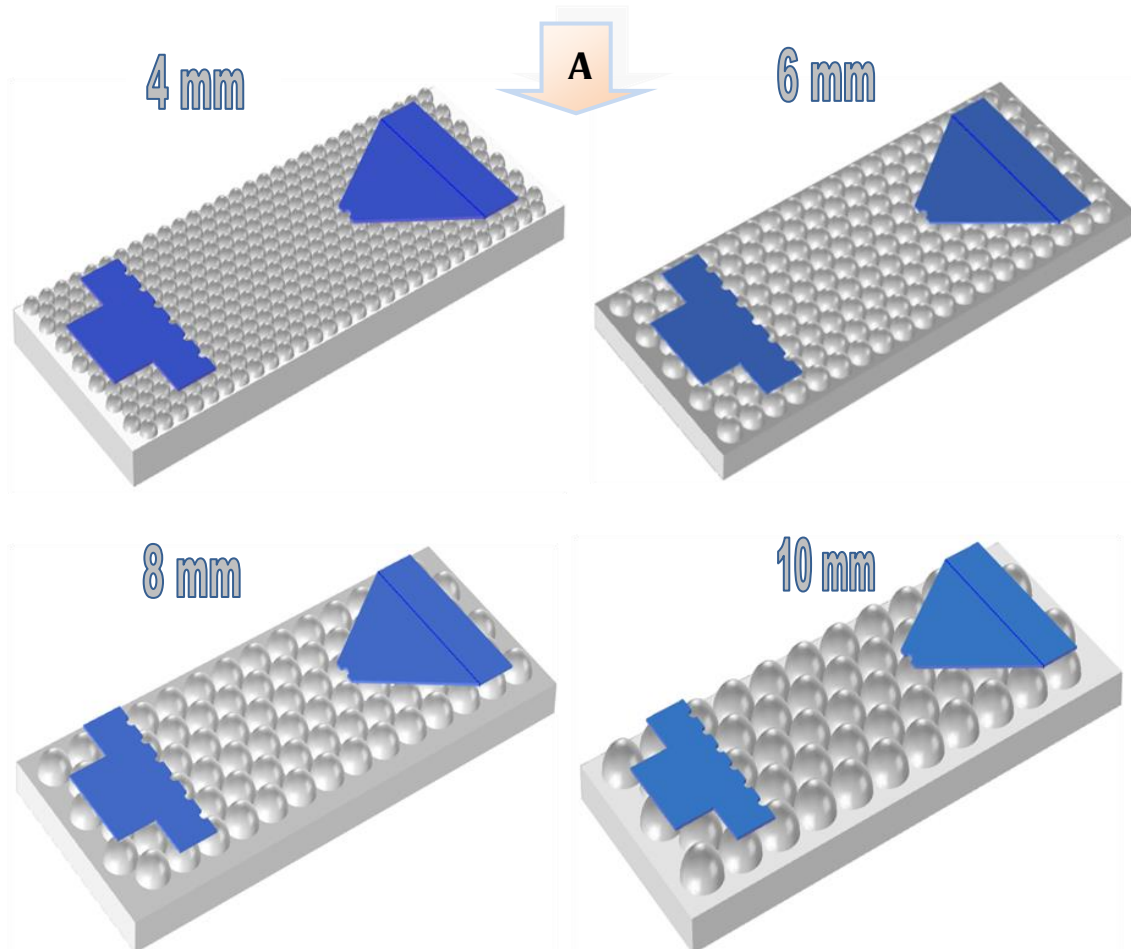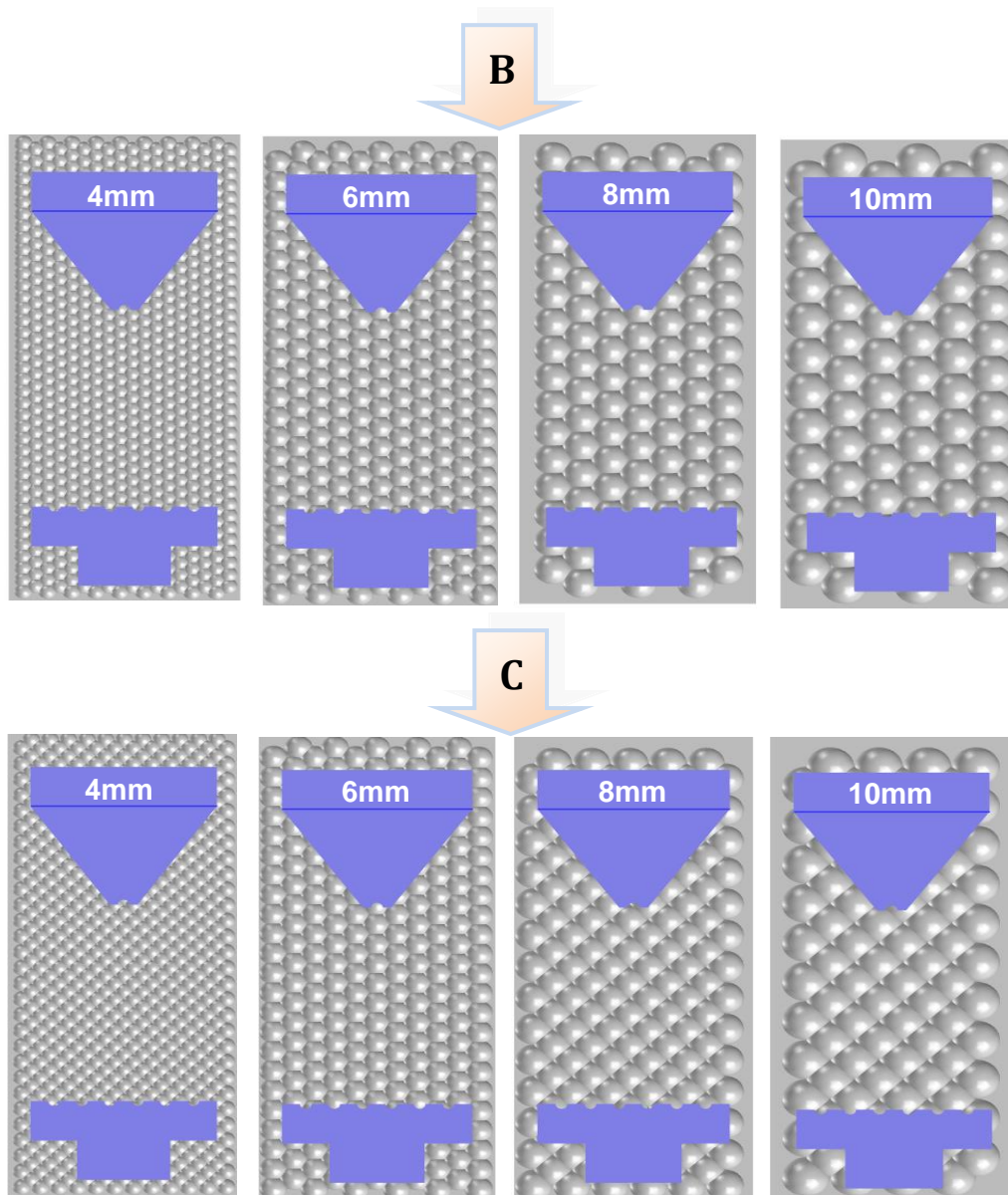
Figure 5.5 Different diameters of hemispherical protuberances of the sample "A" contiguous hexagonal, sample "B" hexagonal intersection of overlapping protuberances and sample "C" intersecting square arrangement

Figure 5.6 (a) shows a close approximation of each protuberance "A", "B" and "C" used in this investigation. Each shape results in a different variation of the surface area.

Table 5.1 shows a summary of the calculated physical quantities (area and edge of the protuberance, the surface and volume of the sample) for different diameters. As can be observed the surface area of the protuberance "C" is lower than "A" and "B". This can explain why the total surface area of "A" and "B" samples is higher than "C".

We can also notice that the presence of protuberances increases the sample surface area compared with the smooth surface.

Figure (5.6 b) shows the edge of each protuberance in blue. We found in Table (5.1) the value of the edge increases with increasing the radius of the protuberance.

(a)

(b)
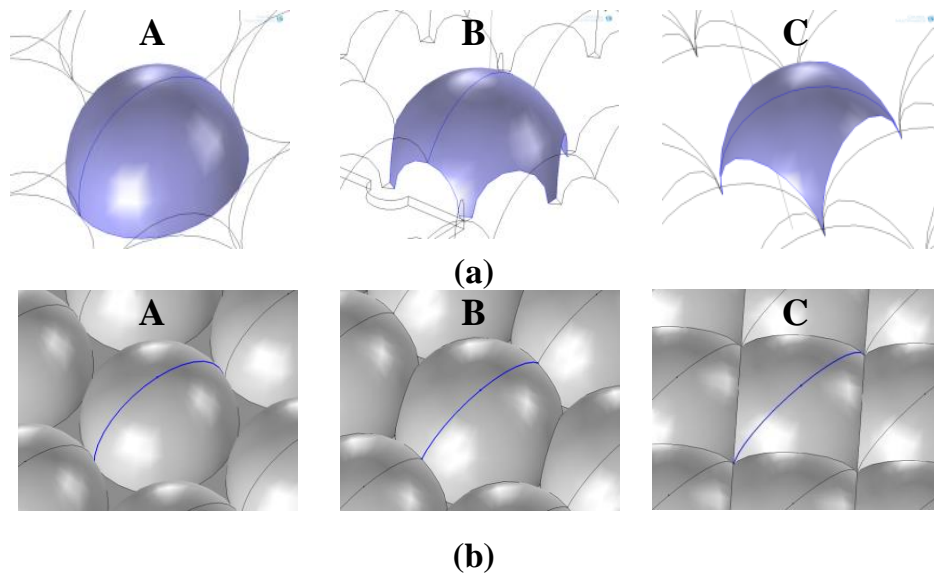
Figure 5.6 Surface protuberances: (a) Area of Protuberance, (b) Edge of
protuberance for textures "A", "B" and "C"

The "A" and "C" configurations have a higher value of edge compared with "B" configuration.

Textured patterns improve the performance of the insulating structure in service by:

a) A substantial increase in the longitudinal creepage distance which could reduce the electric field stress,

b) An increase of surface area which can reduce the leakage current density, and

c) Having paths of preferential contamination and conduction, this can lead to several parallel current paths.

The sample mass (m) can be calculated using the following equation:

$$\rho' = \frac{m}{v} \tag{5.1}$$

Where:

v: is the sample volume calculated by COMSOL (see Table 5.1)

ρ': is the density of the material equal to 1.13 g /cm^3 [126].

The obtained results are shown in Figure 5.7. As can be seen, the maximum dispersion affecting the mass of the three textured specimens is within 5 g margin, while the comparison of smooth and textured samples shows a remarkable difference in weight between 10 and 20 g. Moreover, it can be observed that the larger the diameter of protuberances is, bigger the specimen mass will be. Therefore, it should be taken into account during the industrial applications.

Table 5.1 Calculated physical quantities of the used samples

Diameter (mm)	Protuberance Surface (mm²)				Sample area (cm²)			
	A	B	C	S	A	B	C	S
4	25.11	15.77	10.66		110.7	87.9	81.6	
6	56.50	29.86	23.89	----	107.0	83.0	82.5	60
8	100.4	65.70	42.28		107.2	87.5	82.8	
10	157.0	101.4	65.70		103.1	95.1	82.5	
Diameter (mm)	Edge of protuberance (mm²)				Sample Volume (mm³)			
	A	B	C	S	A	B	C	S
4	6.283	4.262	6.283		42740	43730	44570	
6	9.424	5.911	9.424	----	45380	47440	48540	36000
8	12.57	8.523	12.57		48450	49930	51740	
10	15.71	11.2	15.71		50350	54700	54530	
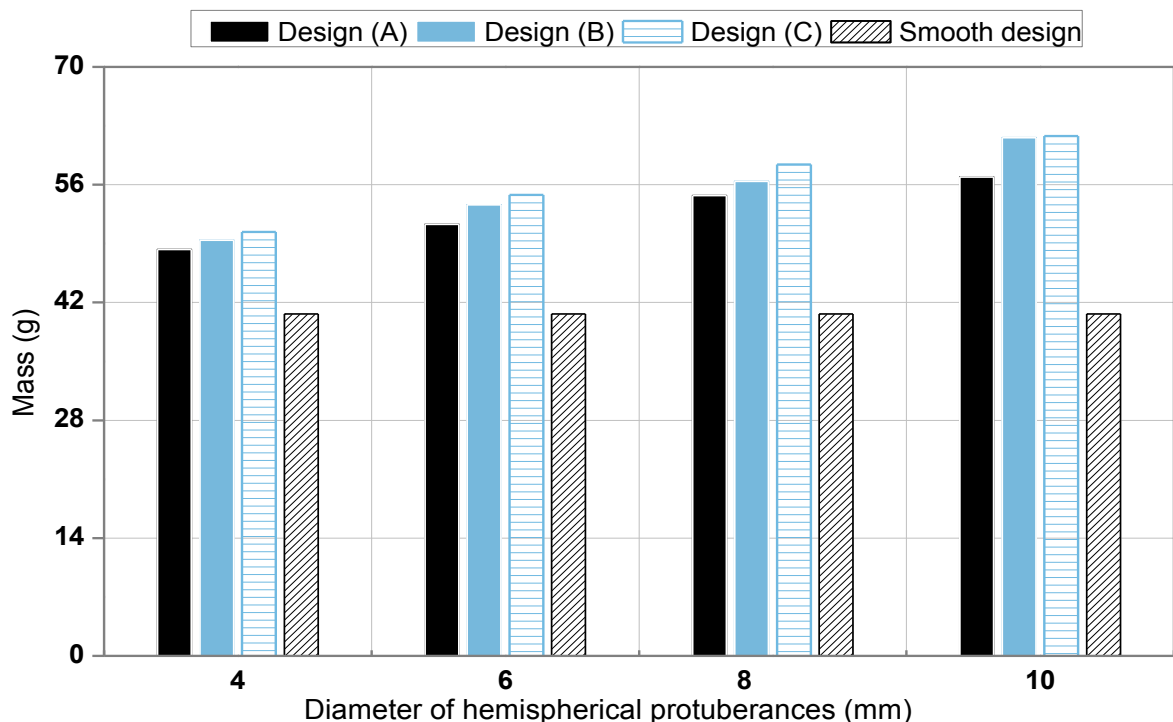
Figure 5.7 Calculated weights for different patterns

5.5. Textured insulator performance under dry conditions

In order to simulate the actual operation conditions, a computation analysis evaluated the performance of textured silicone rubber insulator in dry conditions. The detailed geometric dimensions of three types of textured insulators (A, B and C) with 10 mm diameter of hemispherical protuberances are described in section 3.3.

The process of calculation involves some specific steps which are discussed in the sections that follow.

5.5.1. Material properties

Each region of the model was specified with appropriate material properties as described in Section 5.3. The specimens are made of silicone rubber material type High Temperature Vulcanization (HTV) with an electrical conductivity equal to 10^{-17} S/m and a relative permittivity equal to 3.

The electrical electrodes, with relative permittivity $\varepsilon_r = 1$ and electrical conductivity of 3.774×10^7 S/m is aluminium material. The air region surrounding the insulator was specified with very low conductivity, $\sigma = 1.0 \times 10^{-15}$ S/m.

5.5.2. Boundary Conditions

The top high voltage electrode was energised with a DC voltage of 4 kV. The bottom electrode was connected to the ground at 0V.

A cylinder was added to represent the surrounding air and was simulated large enough to minimise its effect on the distribution of potential near the electrodes and along the sample.

The outer edges of the air background region are assigned with a boundary that assumed zero external current and electromagnetic sources, hence representing a physical system that is in an isolated open space. The tangential electric field is calculated for a surface distance beginning from the HV to the ground electrode.

5.5.3. Meshing

After completing the initial stage with the model structure, as well as specifying material properties and boundary conditions, the entire domain is divided into

non-overlapping triangular elements during the meshing process. The size of the mesh elements can be varied manually on any chosen part of the insulator's surface to enhance the accuracy of the simulation. Fewer mesh elements may reduce the accuracy of the simulation results, while too many elements can lead to high memory consumption and longer processing time.

An optimised mesh will facilitate a faster computation time without reducing the accuracy of the result. Mesh discretisation of textured and conventional (smooth) insulators can be seen in Figure 5.8.

Sample "A"   Sample "B"

Sample "C"   Smooth sample
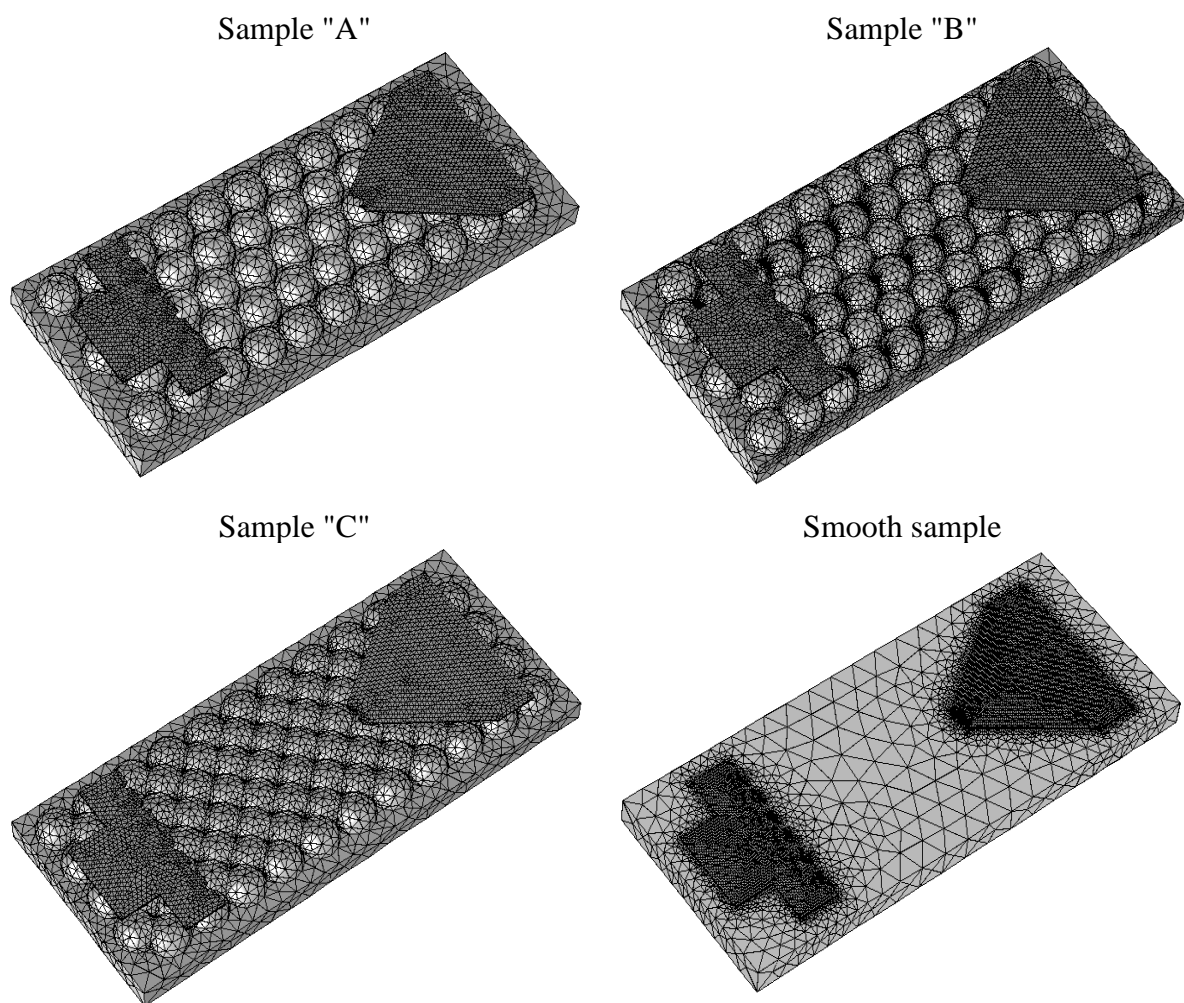
Figure 5.8 Mesh discretisation of four insulators

5.5.4. Solver settings

COMSOL® Multiphysics provides a platform for different modelling and simulation programs, which are linked to selective, advanced, numerical calculations.

It is important to undertake an appropriate physical study before carrying out the simulation process. In order to investigate the electrical field and potential distribution along the textured insulator, the insulator model was simulated in an AC/DC module using Electrostatic and stationary studies.

The electric field distribution is calculated by the minus gradient of electric potential distribution. Due to electrostatic field distribution, the electric field distribution can be written as follows [175]:

$$\vec{E} = -\vec{\nabla} \cdot V \tag{5.2}$$

From Maxwell's equation:

$$\vec{\nabla} \cdot \vec{E} = \frac{\rho}{\varepsilon_0} \tag{5.3}$$

Where:

ρ: is the space charge density.

ε: is the permittivity of the dielectric material.

ε_r: is the relative permittivity of the dielectric material.

ε_0: is the permittivity of vacuum ($\varepsilon_0 = 8.854 \times 10\text{-}12$ F/m).

Poisson's equation is obtained when the expression (5.2) is placed in (5.3).

$$\vec{\nabla} \cdot \vec{\nabla} V = -\frac{\rho}{\varepsilon_0} \tag{5.4}$$

Without space charge, $\rho' = 0$, Poisson's equation becomes Laplace's equation:

$$\vec{\nabla}^2 V = 0 \tag{5.5}$$

Finite element method software was used to find the solution for Laplace's differential equations.

5.5.5. Simulation results for dry case and analysis

This section presents the electric field stress, potential distributions and length between electrodes along all samples under dry conditions. The electric field and potential are calculated for a surface distance beginning from the HV to the ground electrode.

5.5.5.1. Equipotentials and potential distribution

The equipotentials lines along the surface distance of smooth insulator and textured sample "A" are shown in figure 5.9 (a) and 5.9 (b) respectively under dry clean surface conditions. The equipotentials contours were concentrated near the electrodes which represent three material elements (stainless steel, silicone rubber and air). Jordan et al [176, 177] it is confirmed that the location at the triple point is known for high emission of electrons in the presence of a strong electrical field.

The voltage distributions calculated on the distance between the electrodes for the different patterns under dry and clean conditions are compared in Figure 5.10.

(a) Smooth surface   **(b)** Textured surface type **"A"**
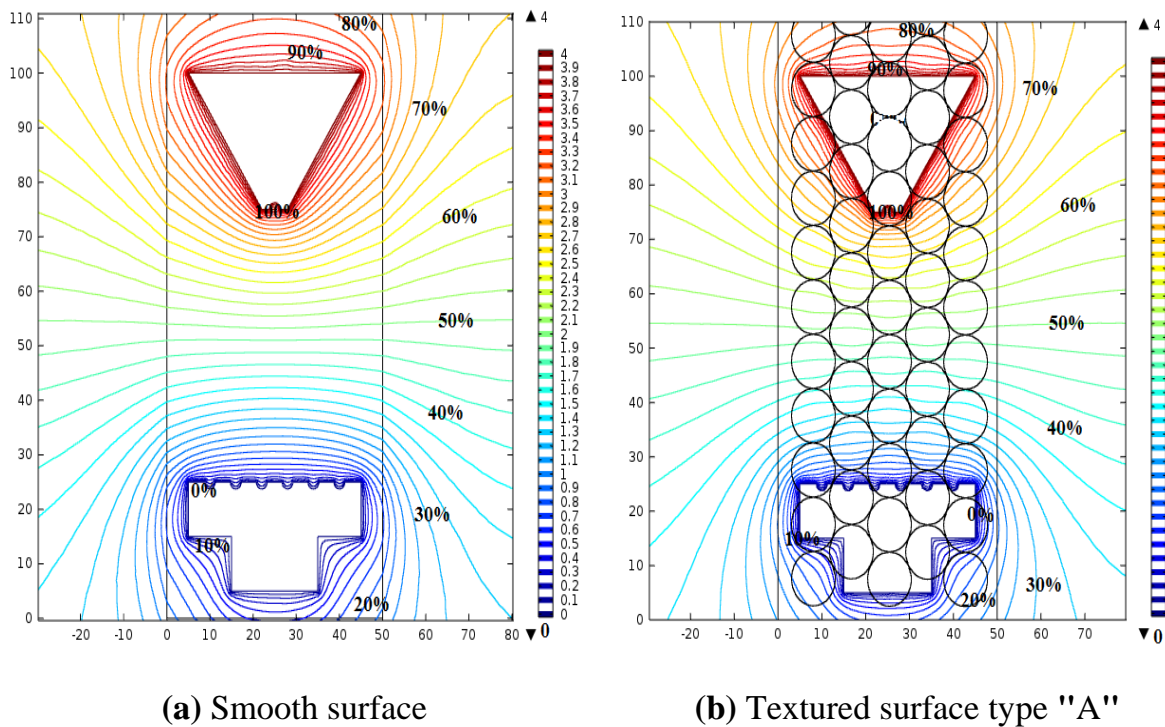
Figure 5.9 Equipotential lines of insulators

The surface potential is distributed in a non-linear way along the distance between electrodes. As expected, it is observed that the potential decreases gradually from the high voltage to the ground end. The major difference between smooth and textured surfaces was that the voltages were calculated at different surface distances, along the protuberances and their profiles.

As can be observed, the textured surfaces increase the surface distance of the insulating sample due to the presence of protuberances. For the "A" and "C" cases, the

potentials follow very similar trends.
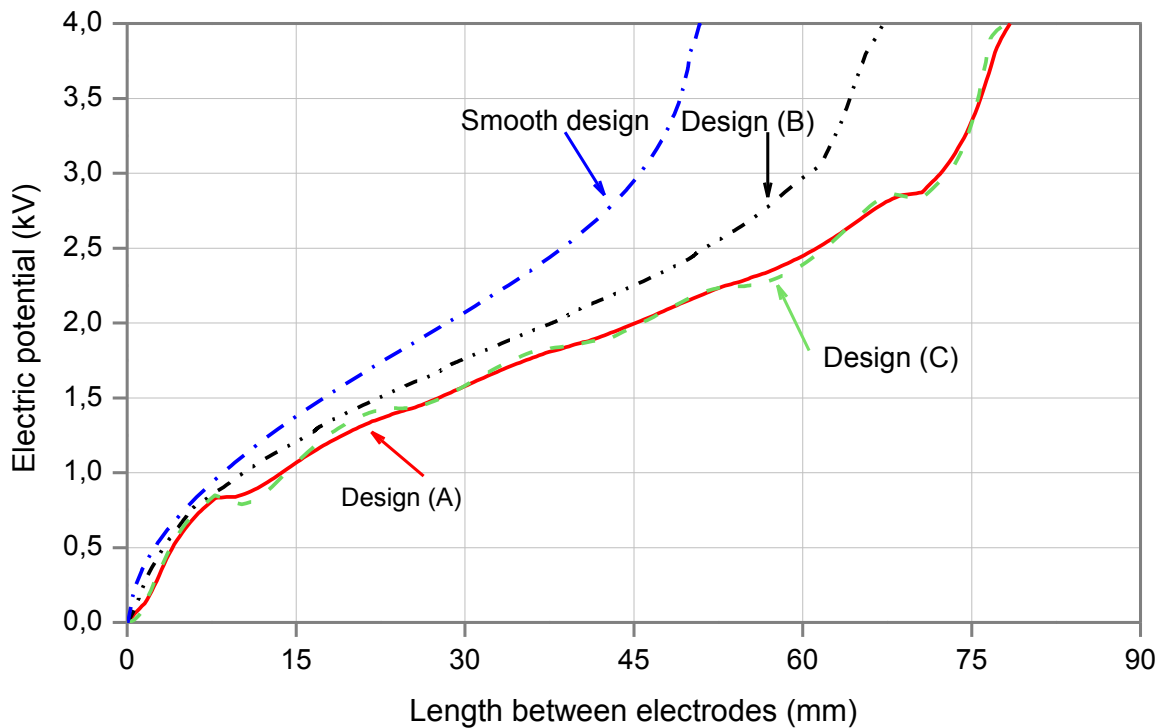
Figure 5.10 Comparison of the potential distribution for different design

5.5.5.2. Electric field distribution

Figure 5.11 shows four plots of the tangential electric field strength with different surface distances depending on the insulator design. Peaks can be seen in the rate of change of the tangential electric field at both the HV electrode and the ground electrode. These peaks confirmed the equipotential results concerning the high field regions in Figure 5.9. This can be explained by the high concentration of the charges near electrodes.

However, away from the electrodes along the surface distance of the insulator, the gradient of the tangential electric field for all patterns was reduced to a lower, more or less constant value. Undulations can be also observed on the tangential electric field profile in the case of textures samples. The increase in tangential electric field strength was correlated to the calculations that were considered over a less surface distance along the samples.
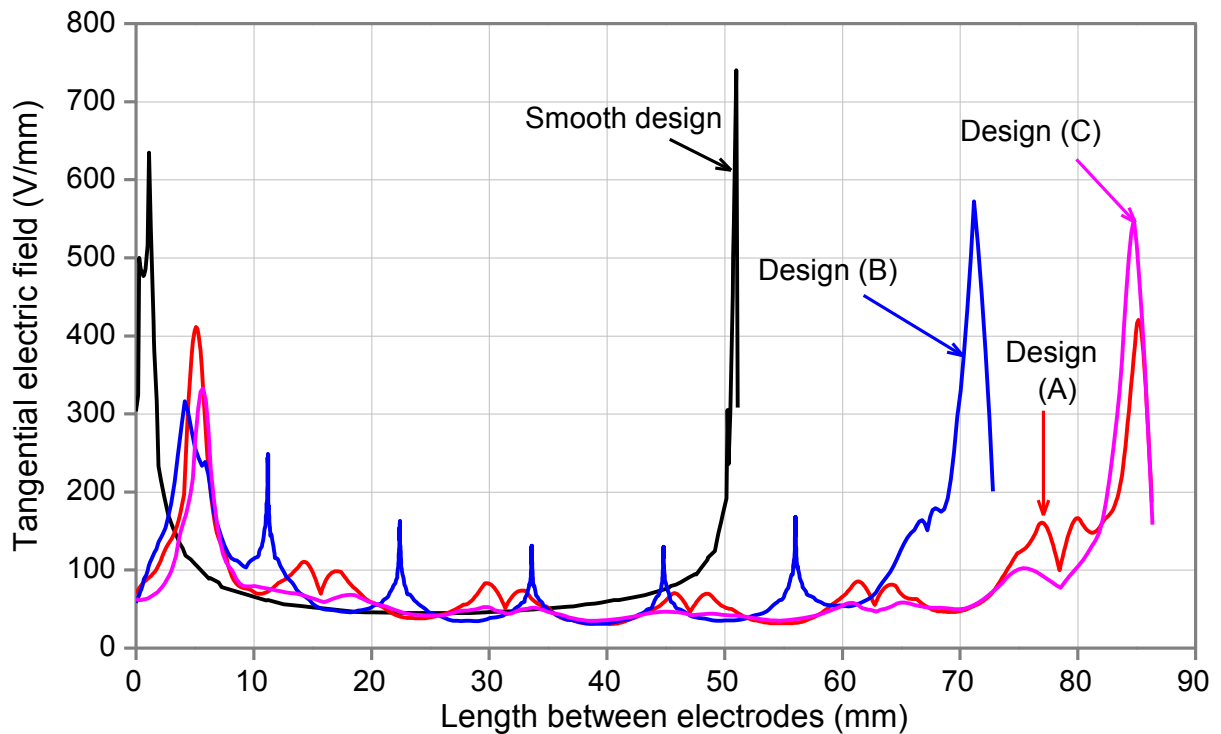
Figure 5.11 Comparison of the electric field strength distribution on the surface of the silicone rubber insulation

As can be observed from figure 5.12, the textured surfaces increase the surface distance of the insulating sample compared with the smooth case without increasing the overall length of the sample. This is because the path along the edge profile of the insulator includes the edge profile along the protuberance's circumferences. In addition, it can be observed that larger the diameter of protuberances is, lengthier the surface distance of the specimen is. Moreover, the "A" and "C" configurations give a surface distance of 85 mm, however configuration "B" gives only a surface distance of 73 mm.

a. **Effect of different diameters of protuberance on the electric field**

Figure 3.13 presents a comparison of electric field distributions for the different diameters. It is clear that the sample of 4 mm shows higher stress that is related to the shortest length between electrodes, which increases the electric field. However, the maximum stress is reduced with the increase of diameter; the sample with 10 mm of diameter shows lower stress.
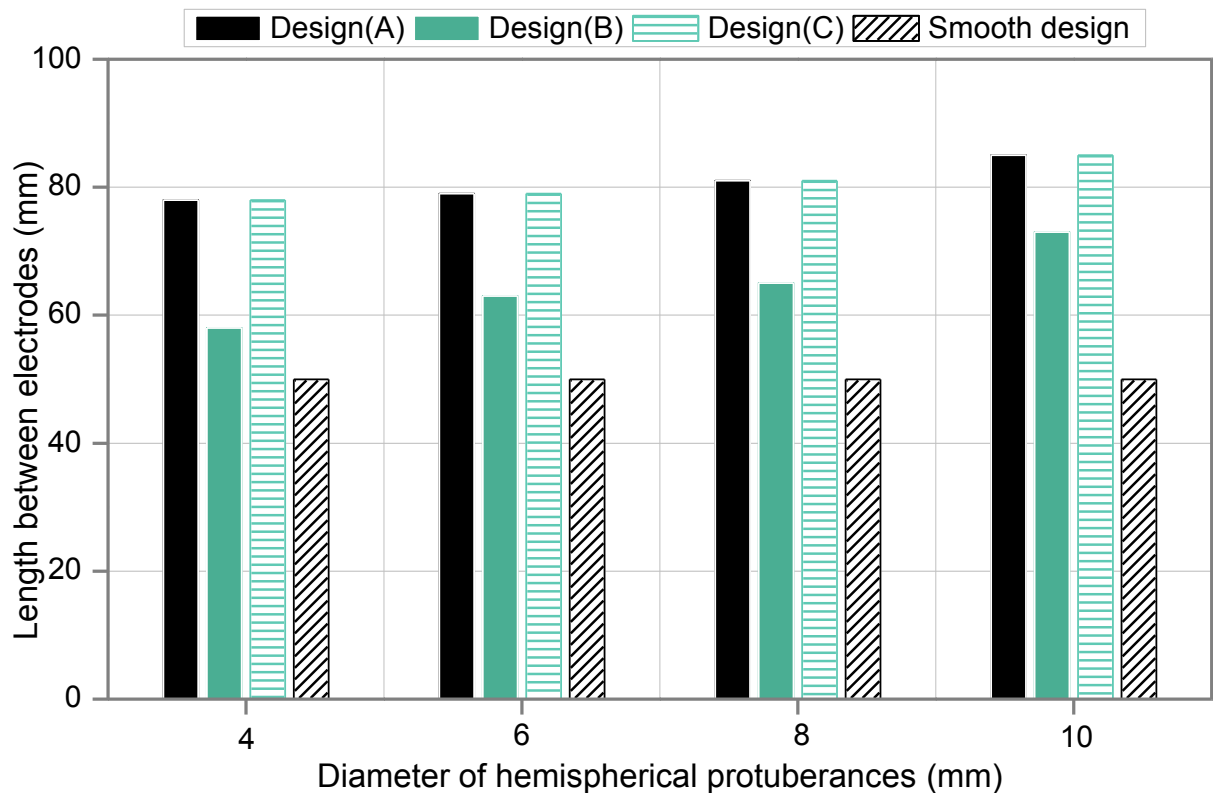
Figure 5.12 Variation of creepage distance for all models and different range of diameters

In Figure 5.14, the maximum E-field strength as a function of the diameter of the protuberance is plotted. In the case of the smooth sample, the plot showed the highest electric field strength was at a location very close to the HV electrode with a value of 740 V/mm at a surface distance of 50 mm. The configuration "B" exhibits the highest value of the tangential electric field for different diameters of protuberances compared to other textured samples. The maximum calculated value was 736V/mm with a diameter of 4mm, showing an increase of about 29 % compared to the diameter of 10 mm (572V/mm). On the other hand, the lowest values of the tangential E-field were obtained for the "A" sample (500V/mm for the 4mm and 420 V/mm for 10mm) showing a substantial decrease of more than 50% compared to the smooth sample. Therefore, it can reduce significantly the risk of the initiation of dry band arcing.
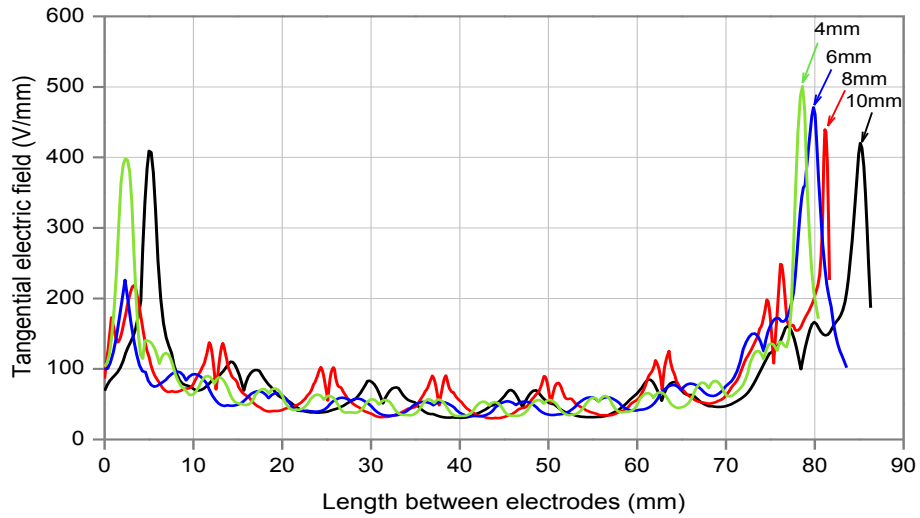
(a) Silicone rubber insulator design **"A"**
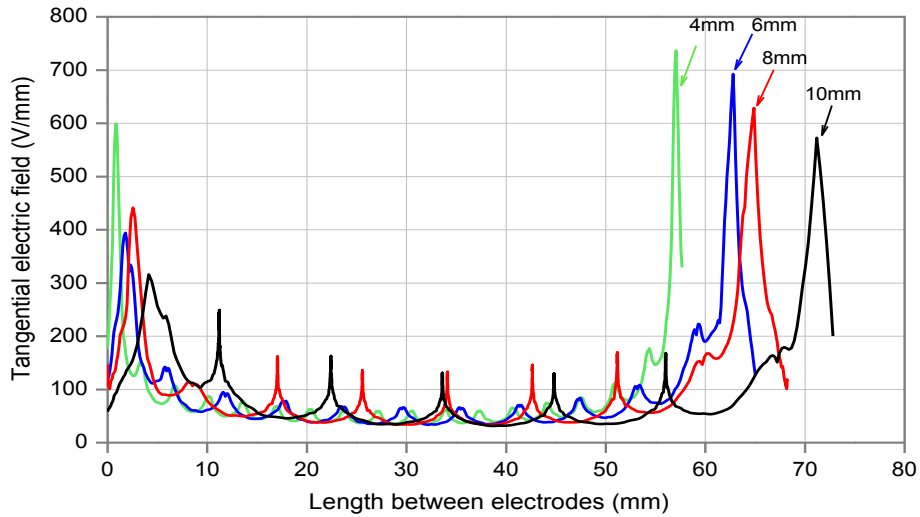
(b) Silicone rubber insulator design **"B"**
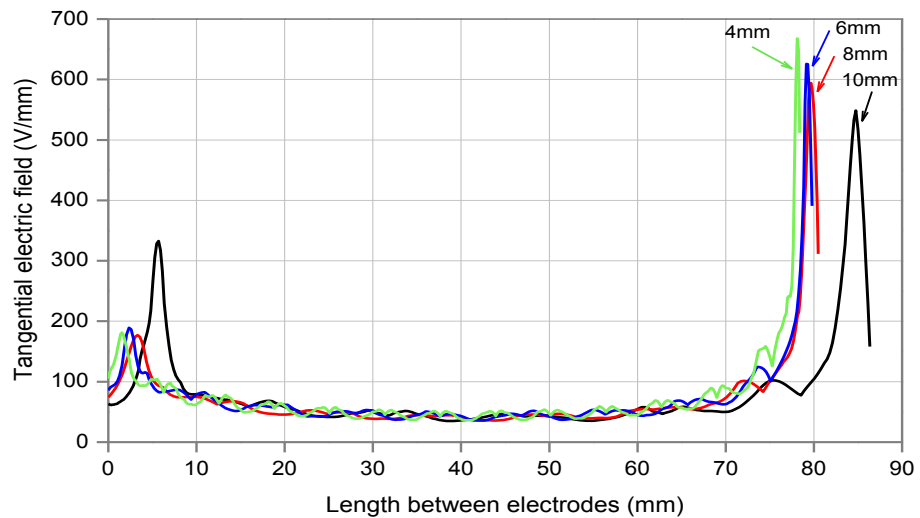
(c) Silicone rubber insulator design **"C"**

Figure 5.13 Electric field distribution along silicone rubber insulators for different
diameter
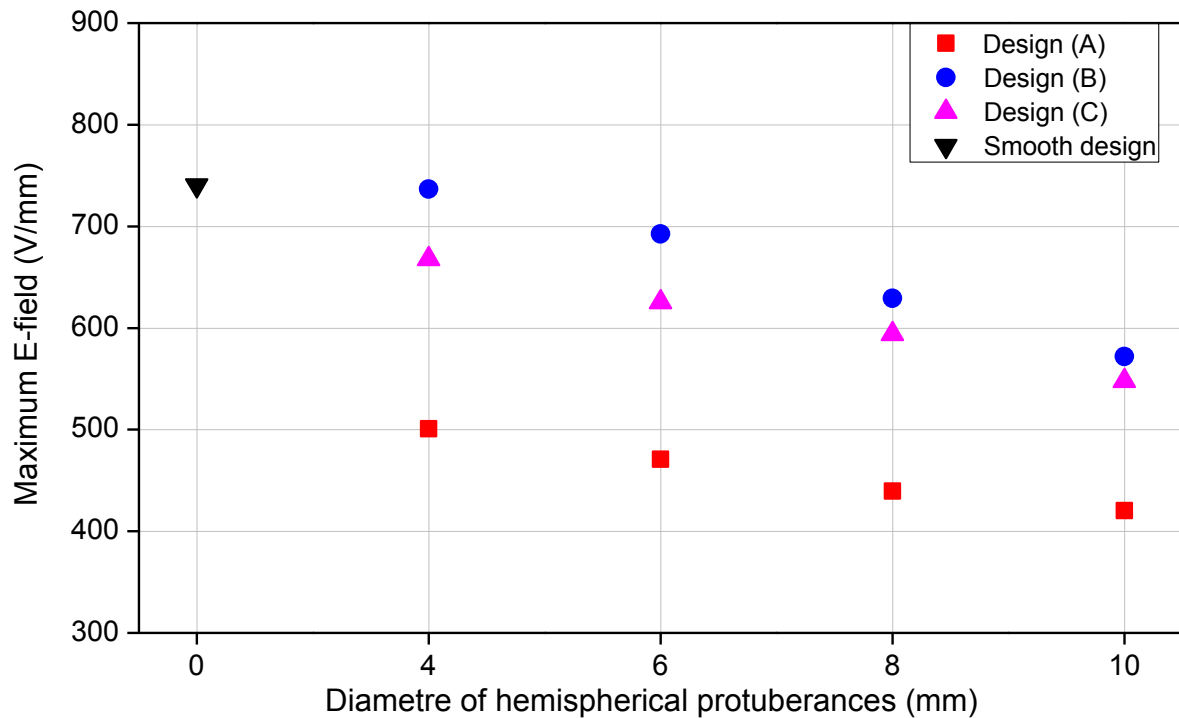
Figure 5.14 Maximum electric field strength for different configuration and different range of diameter

b. Effect of the applied voltage on the maximum electric field

As mentioned in the previous results, the E-field magnitudes are larger close to the HV and ground electrodes. The Maximum values of the E-field influence the presence of corona activity within and on the surface of the dielectric material. This will result in degradation or changes in the surface properties of the polymer. Research by U.S. based EPRI indicated that a maximum limit of the E-field was around 450 V/mm [178, 159].

Figure 5.15 shows the maximum electric field strength variation as a function of the applied voltage for three types of texture with 10 mm diameter of hemispherical protuberances and smooth sample.

Simulations are performed for 6 voltages between 1 and 6 kV. A value of 450 V/mm is considered as the threshold for corona initiation. It is noticed that the maximum E-field values increases linearly with the applied voltage. Furthermore, the electric field values for smooth sample are higher than the critical corona threshold starting with the applied voltage of 2.5 kV. Whereas, for the textured samples, the maximum electric field values exceed the critical corona threshold starting with the applied voltage 3.1,

3.2 and 4.3 kV respectively. These findings have concluded that the textured isolators bear the highest applied voltages.
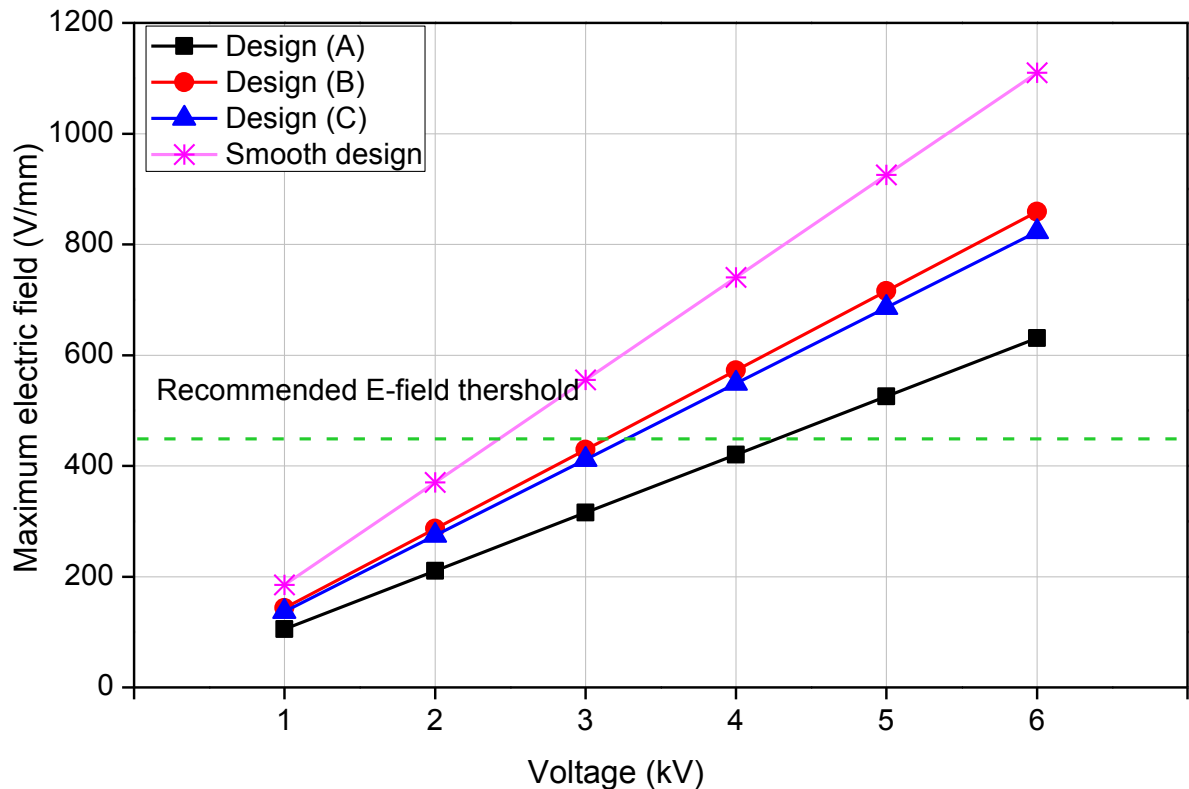
Figure 5.15 Maximum electric field along textured silicone rubber insulators under dry conditions as a function of system voltage

5.6. Textured insulator performance under polluted conditions

It is known that a strong and uncontrolled electrical field on a high voltage insulator is liable to cause damage, such as ageing and partial discharge. This is due to exposure of insulators to several climatic conditions such as atmospheric contaminations. These contaminants are accumulated on the surface of insulators uniformly or partially when moisture level reaches certain values, it forms a conductive layer on the insulator surface which results in the decrease of the surface resistivity and thereby enabling leakage current to flow across the insulators. And then, discharges activity will start and affect the performance of the insulator surface in different ways. Therefore, it is very essential to analyse the effect of the contaminations on the surface of the textured silicone insulators.

5.6.1. Distribution of pollution on textured silicone rubber insulation

The accumulation of pollutants on the surface of insulators process strictly depends on several factors such as shape of insulators, speed and direction of wind, rain, fog, the type and the amount of pollution. The aim of this part is to investigate the effect of the geometry chosen for the texture on the distribution and the accumulation of pollution on silicone rubber surfaces.

A one mm pollution layer has been deposited along the sample surfaces. The pollution distribution shape on the three types of textured silicone rubber surface "A", "B" and "C" is shown in (Figure 5.16). The studied diameters of the hemispherical protuberances range from 4 to10 mm.
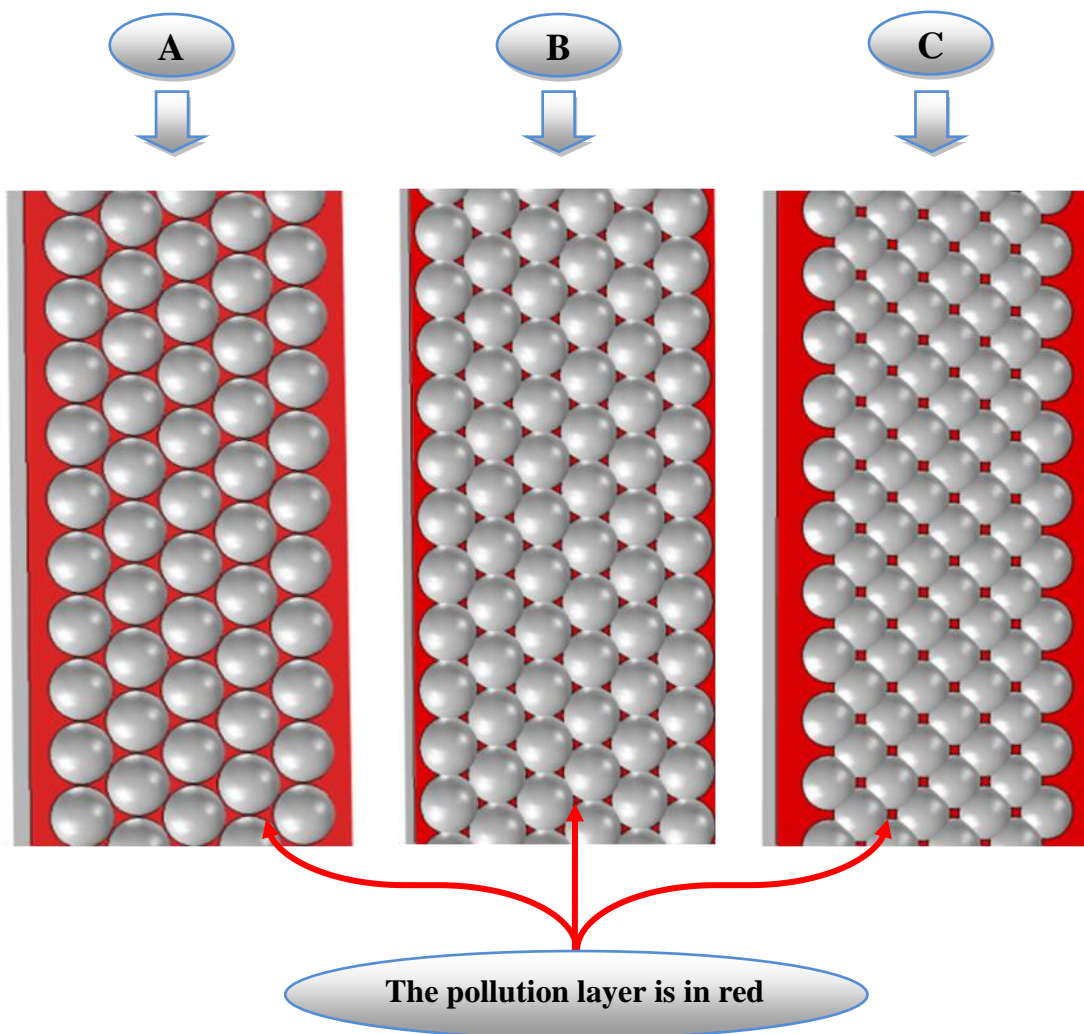
Figure 5.16 Pollution distribution shape on the textured surfaces

Results of calculations on various surfaces considering the accumulated pollution volume are illustrated in Figure 5.17. The increase of the diameter of protuberances reduces their total number on the surface, in the same time, the depth and the spaces of the gaps are higher, which leads to increase the accumulated pollution volume. It can be also noted that the effectiveness of texture "C" is clearly observed. It reduces the pollution deposition on the insulator surface compared to patterns "A" and "B" due to their particular form, thereby improves the pollution performance of polymeric insulators. The increase of the accumulation of pollution on the insulator surface will reduce the length of the creepage distance which can increase the field stress and then the flashover occurs and material degradation will be significant.
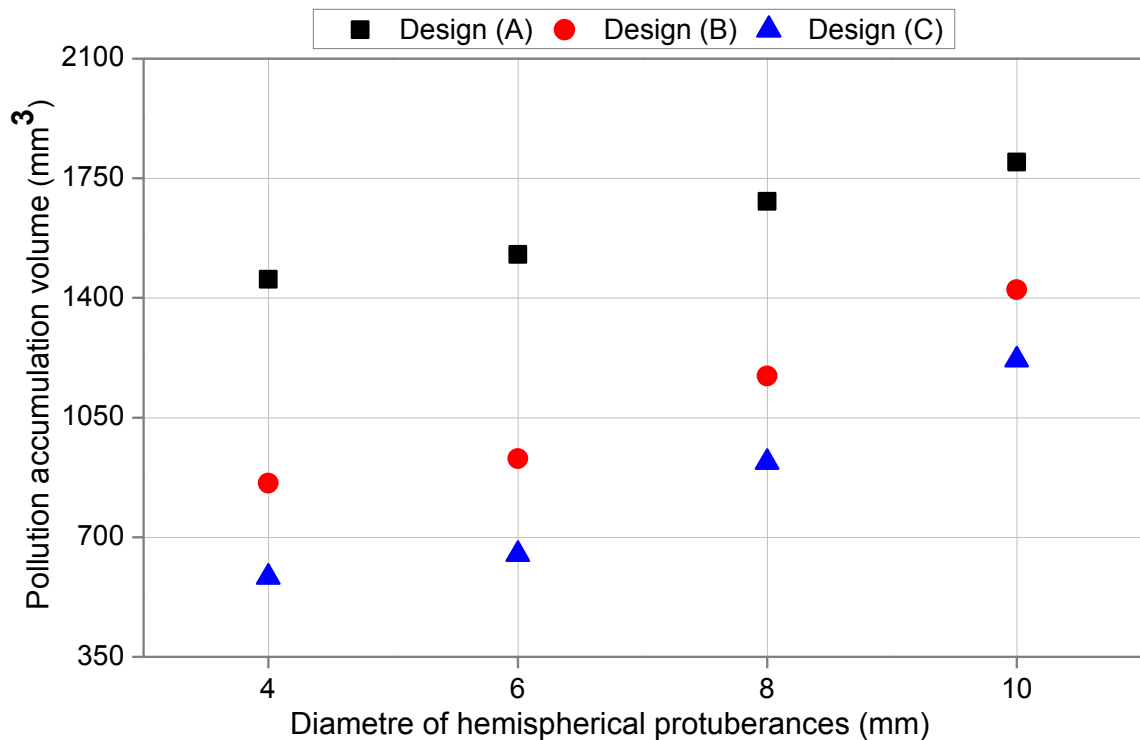
Figure 5.17 Accumulated pollution volumes

5.6.2. Textured insulator performance under uniform pollution distribution

This section studies the effect of uniform pollution layer on the tangential electric field and potential distribution along the textured silicone rubber patterns. The results for the smooth sample are again added for comparison purposes. The process of calculation involves some specific steps which are discussed in the sections that follow:

5.6.2.1. Modelling insulators geometry

For the work done in this section, the same models of insulators (textured and smooth) were adopted for the clean condition with the surface being covered by a thin pollution layer.

The pollution layer was assumed homogeneous and uniformly distributed along the distance between the electrodes electric of the insulators, at thickness 1 mm. The schematic of a textured silicone rubber "A" with 10 mm of the diameter of hemispherical protuberances under polluted conditions is shown in Figure 5.18.
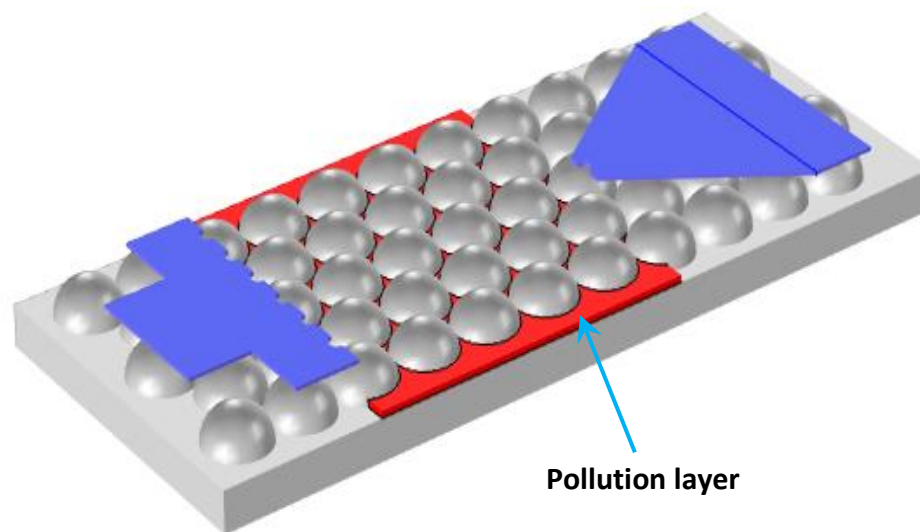
Pollution layer

Figure 5.18 Schematic of a textured silicone rubber "A" with 10 mm of the diameter of hemispherical protuberances under polluted conditions

5.6.2.2. Material Properties

It is axiomatic that the pollution layer deposited on insulator surface under dry conditions is risk-free, with a negligible capacitive current due to high surface resistance. However, the resistance drops significantly when the pollution layer becomes wet on exposure to humid atmospheres such as fog, dew and moisture, where the layer becomes a conductor.

The relative permittivity for the pollution layer was set 80, considering water as the dominant substance when the pollution layer is completely wet and saturated with

moisture. The conductivity of the pollution layer was set to 6×10^{-7} S/m, a value adopted from the laboratory measurements reported in [178].

The electrical properties of the textured, smooth samples and electrodes electric are the same as that for dry case.

5.6.2.3. Solver settings

The conductance of the clean insulator is very small, the electric field is capacitive distribution and axisymmetric, which can be solved with the electrostatic field method [180]. But for the polluted insulators, the existence of the leakage current on the surface results in the capacitive and resistive electric field distribution. While; it found that the E-field along the polluted insulators is not a static field in the complete sense. Therefore, accurate results cannot be obtained by the Electrostatic solving method [24]. It is necessary to use another module to determine the distribution of the E-field and electric potential on the insulating surface during the passage of the current. Asenjo et al [180, 181] which is the first to suggest a method of solving the E-field distribution of a polluted insulator in the complex domain. The method is based on a Quasi-static approximation.

The insulator model was simulated in an "AC/DC" module using a quasi-static electric current solver. The equations used in quasi-static electric current solver are Eqs.5.6; 5.7; 5.8 respectively. J_e value in the solution of the problem is set to zero since there no external current source is present. As the finite triangle elements are merged, an equation system for the solution of the problem is obtained. The potential and electric field are obtained by solving the equation system.

$$\vec{\nabla} \cdot \vec{J} = -\frac{\partial \rho}{\partial t} \tag{5.6}$$

$$\vec{J} = \sigma \vec{E} + \vec{J}_e \tag{5.7}$$

$$\vec{E} = -\vec{\nabla} \cdot V \tag{5.8}$$

Where:

J: current density (A/m^2);

ρ: space charge density;

E: electric field intensity (V/m);

J_e: external current density (A/m^2);

σ: electric conductivity (S/m);

V: applied voltage (V).

5.6.2.4. Simulation results and analysis

The electric field is plotted along a line through the junction of the pollution layer - air- insulating material along the length of the insulator.

The tangential electric field is calculated as in Figure 5.19 along the surface distance under uniform pollution condition. It is clearly seen that the peak magnitude of the tangential electric field for the smooth surface insulator was higher; 1048 V/mm at a surface distance of 50 mm.

The maximum calculated value for case "A" is 799 V/mm at a surface distance of 75 mm, for case "B" is 635 V/mm at a surface distance of 66 mm, and the tangential electric field strength along the design "C" reaches a lower peak with a value of 624 V/mm at a surface distance of 75 mm. When compared to the smooth surface, there was a 67% reduction in the stress on the surface of the insulator which will reduce the discharge activity across the surface near electrodes. It can be also observed that the tangential electric field strength for sample "A" is bigger than for "B" and "C" samples. This is to be expected due to the positive relationship of the electric field with the pollution accumulation on the insulator surface. These findings confirmed the previously obtained results concerning the accumulated pollution volume (Figure 5.17).

However, away from the electrodes along the surface distance of the insulator, the electrical field values for patterns "A", "B" and "C" are unstable. The high and low values are related to the concentration of the pollution layer. The calculated values are high when the pollution layer is close to the HV electrode, the peak value for the sample "A" is 694 V/mm, for sample "B" is 447 V/mm, and the electric field strength for the sample "C" reaches a lower peak with a value of 308 V/mm. Then these peak values begin to decrease in the case of the pollution layer is concentrating in the middle of the samples and rise again when the pollution layer being close to the ground electrode but with lower values, where the peak values of the electric field

strength for the sample "A" is 327V/mm, 218 V/mm for the sample "B" and
175 V/mm for the sample "C".
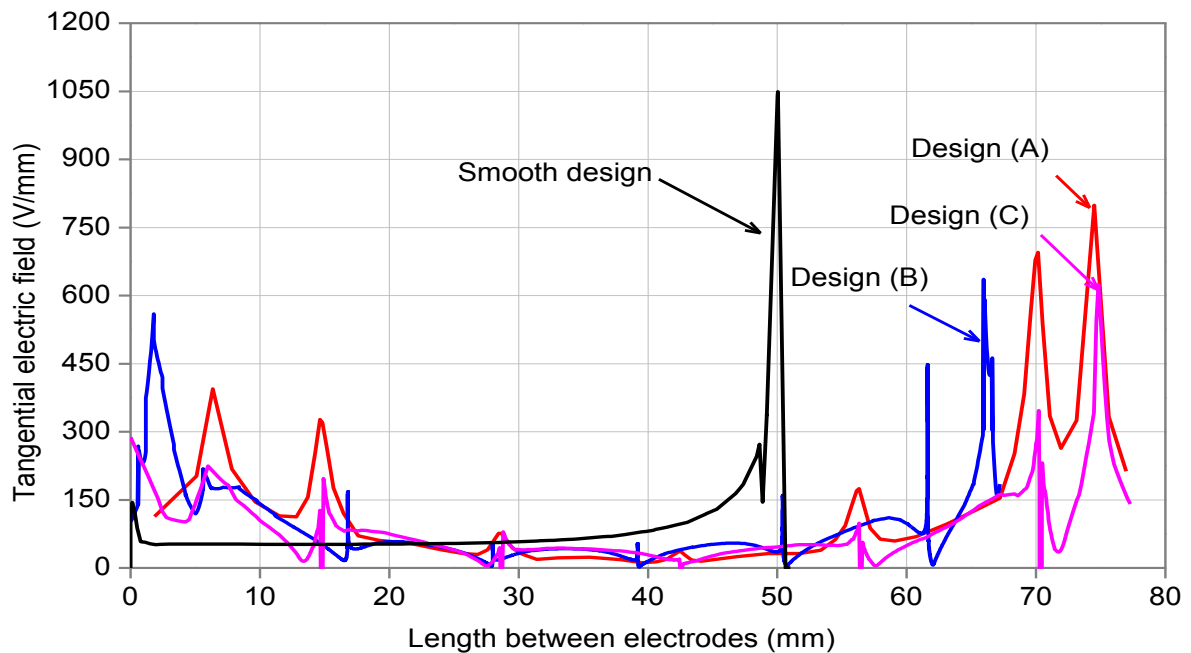
Figure 5.19 Tangential electric field distributions along the surface for different
patterns

The results shown in Figure 5.20 illustrated a comparison of the potential
distribution along the central axis for the different patterns. It is observed that the
potential decreases gradually from the high voltage to the ground end. Moreover, the
potential distribution on the smooth surface is more concentrated than the other
configuration which is related to the reduction of the surface distance between the HV
and the ground electrodes.

Figures 5.21, 5.22, 5.23 and 5.24 compares the electric field strength distribution
along the surface of the "A", "B", "C" and "smooth" samples under dry and clean
condition with that of uniform polluted case.

It is clearly shown that the magnitude of the E-field when the surface is uniformly
polluted has a higher magnitude compared with the case when it is clean and dry. The
presence of the pollution layer enhances the electric field strength on the cases "B" and
"C" by a factor of about 1.11 and 1.14 respectively.
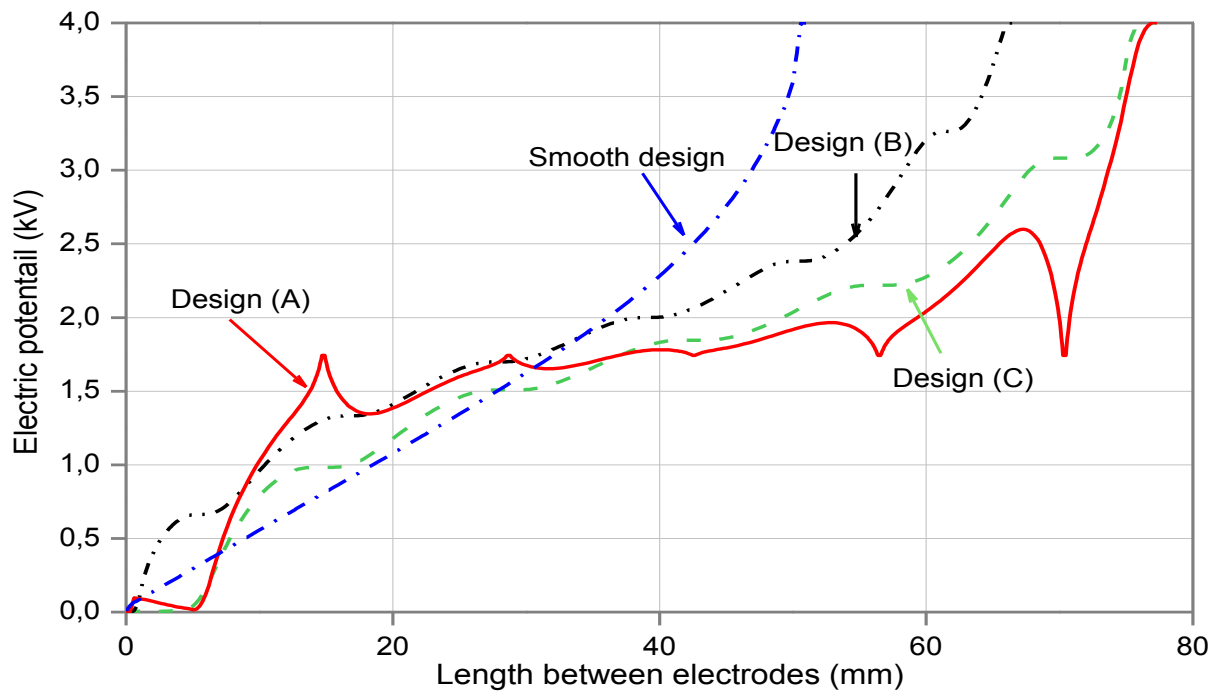
Figure 5.20 Electric potential along the surface for different patterns

The surface distances of the different patterns under clean and uniformly polluted condition are given in Table 5.2. It is clear that the existence of the pollution layer does not change the surface distance of the smooth sample, but rather decreases the overall length of the textured samples because the electric field was calculated along the line passing over the pollution layer and the insulation surface. We note that the percentage of decreasing in length was 15% for the sample "A" and "C" and 10% for "B". The greater the thickness of the contamination layer, the more likely it will result in the coverage of surfaces protuberances, and thus reduce the total length between electrodes compared to the clean surfaces.

Table 5.2 Calculated lengths between electrodes (mm)

Sample	Conditions		
	Dry and Clean	**Uniform pollution**	**Percentage of change**
A	86.34	75.00	15.0%
B	72.79	66.00	10.0%
C	86.34	75.00	15.0%
S	50.00	50.00	0.00%
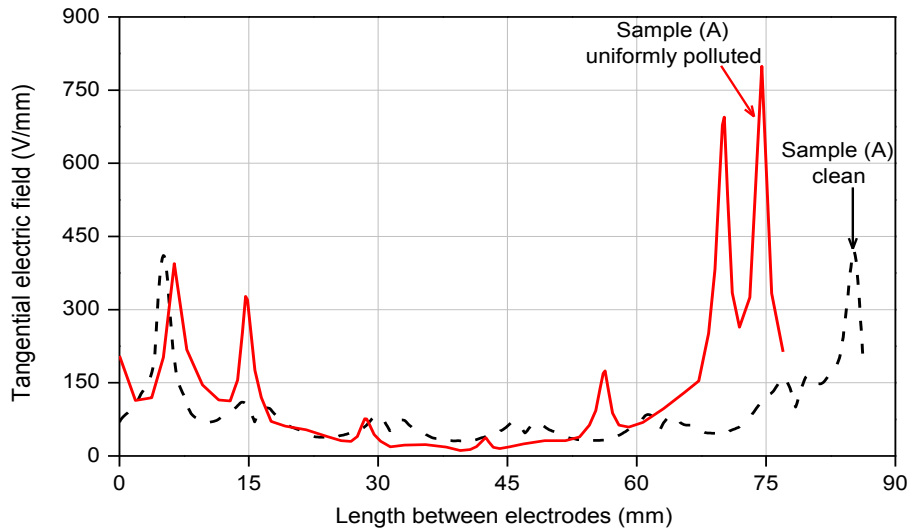
Figure 5.21 Electric field strength distribution along the sample "A" under
clean and uniformly polluted surface condition
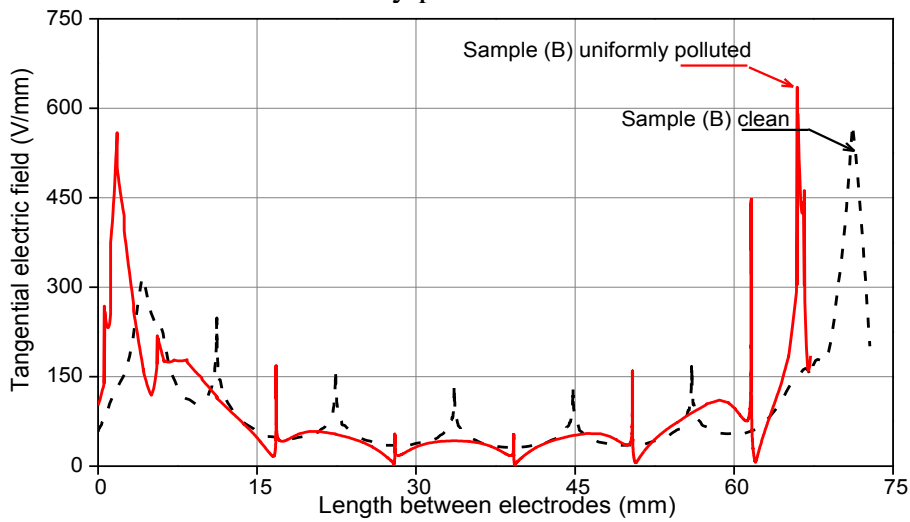
Figure 5.22 Electric field strength distribution along the sample "B" under
clean and uniformly polluted surface condition
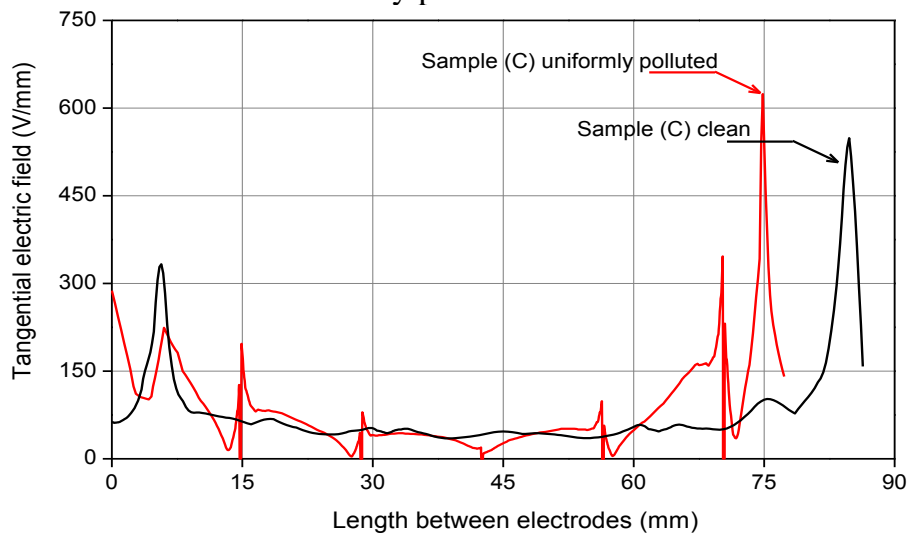
Figure 5.23 Electric field strength distribution along the sample "C" under
clean and uniformly polluted surface condition
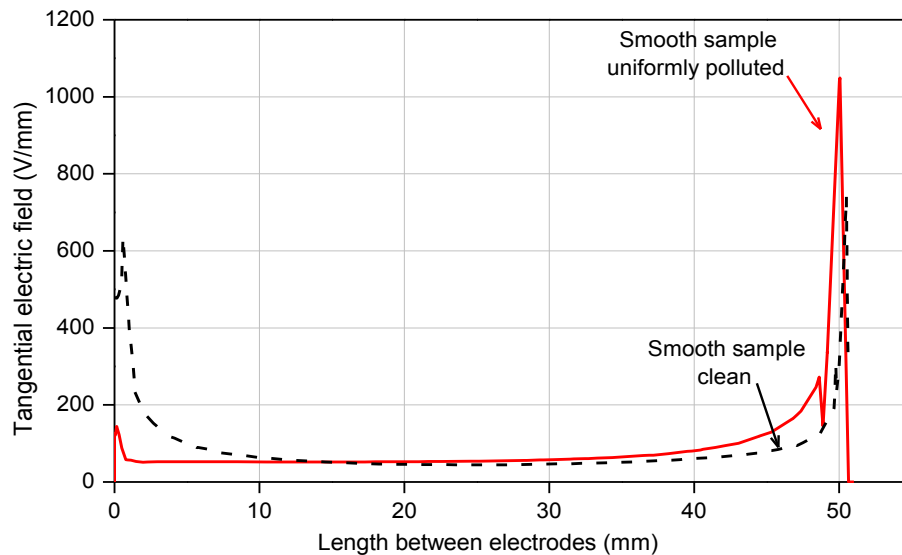
Figure 5.24 Electric field strength distribution along the smooth sample under
clean and uniformly polluted surface condition

5.6.3. Textured insulator performance under non-uniform pollution condition

The distribution of the pollution layer on the surface of the insulators depends on several factors such as the shape of the insulators, their position in operation, weather conditions, and the electrostatic attraction of the polluting particles in the presence of the electric field. As a result, the distribution of pollution along the insulators is far from uniform. For this purpose, the main objective of this part is to study the impact of the accumulation of non-uniform pollution on the electric field.

In this study, three parameters of the pollution layer are taken into account, such as thickness, width and location. The electric field is analyzed using the finite element method (FEM) combined with the design of experiments methodology (DOE) to evaluate the contribution of the factors studied and their interaction on the total variation of the studied responses. To carry out this modeling, we chose a textured insulator type "A" with a hemispherical protuberance diameter of 10 mm.

5.6.3.1. Introduction to design of experiments method (DOE)

In general, the design of experiments method will seek to identify and establish the links between 2 types of variables:

- *The Responses:* physical variable studied;

- *The Factors:* physical variables that can be modified by the experimenter, supposed to influence the variations in response.

More specifically, it also aims to understand the relationships between the response and the factors, as well as the factors between them.

The DOE is a set of complementary techniques (mathematics and statistics) that help its user to determine the experiments to be carried out as well as to understand and exploit the results obtained.

In the following, we will discuss the methodology to implement to use them. This methodology is structured in four steps (see Figure 5.25).

5.6.3.2. Definition of factors and levels

To quantify the effect of non-uniform pollution layer on the E-field, three levels for each parameter are chosen. Three configurations of non-uniform pollution distribution were studied (Figure 5.26), the first is a polluted band near the HV electrode, the second is located near the ground electrode and the third is situated in the middle of the sample, three widths of pollution layer (10, 25 and 40 mm) and three thickness (0.6, 1 and 1.4 mm). The parameters studied and their levels of variation are presented in Table 5.3.

The electric field is calculated using finite (MEF) simulation. The conductivity $(6 \times 10^{-7}$ S/m) and permittivity (80) of the pollution layer are maintained constant throughout the simulation. The applied voltage is equal to 4kV.

Table 5.3 Values of parameters at various levels

Parameters	Levels			
Thickness, (mm)	T (x_1)	0.6	1	1.4
Width, (mm)	W (x_2)	10	25	40
Location	L (x_3)	ground	middle	HV
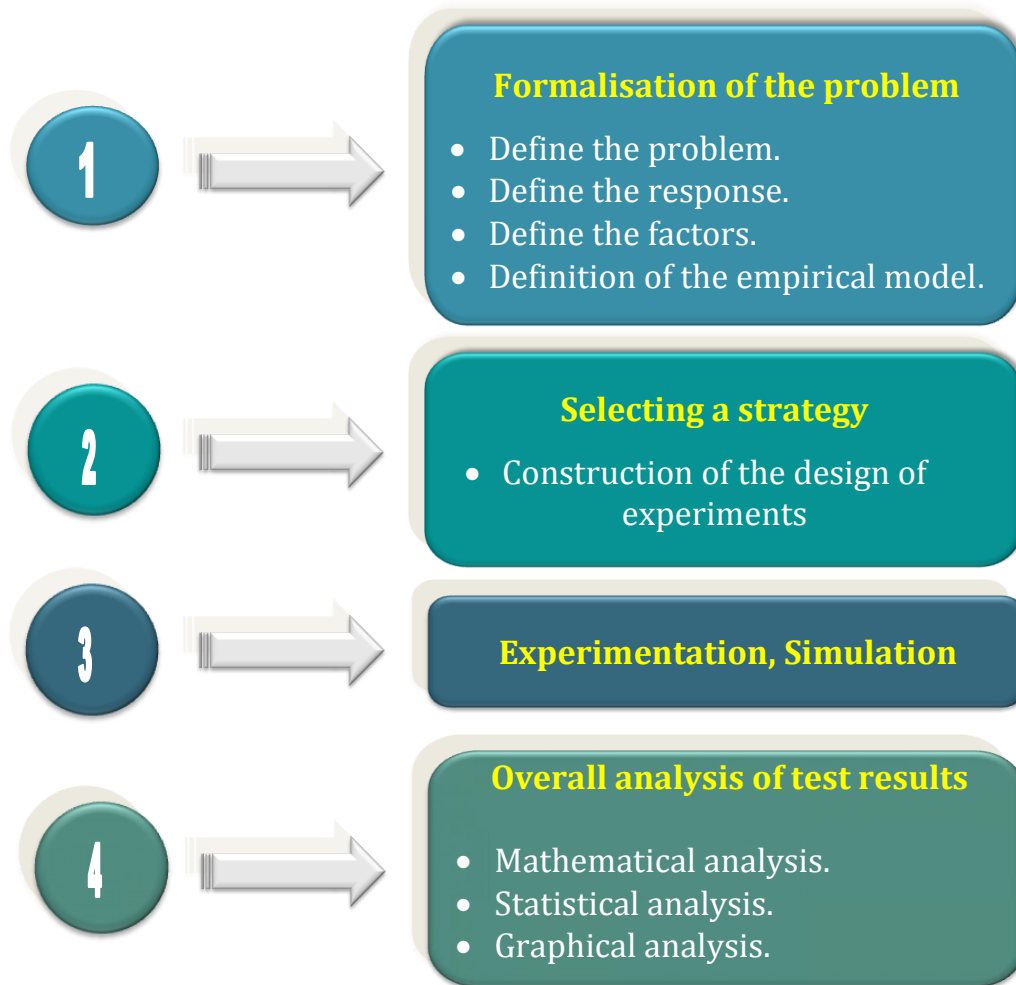
Figure 5.25 Design of experiment process

5.6.3.3. Definition of the Empirical model

This step allows, once the influential factors are identified, to find the equation that best describes the variations of the studied phenomenon (Y) according to these factors. Any response can be written in the following form:

$$Y = f(x_1, x_2, \ldots\ldots, x_k) + \varepsilon \qquad (5.9)$$

Response   Factors   Erreur

Usually, a quadratic model is used which correctly defines the response variations. The general form of the quadratic model is as follows:
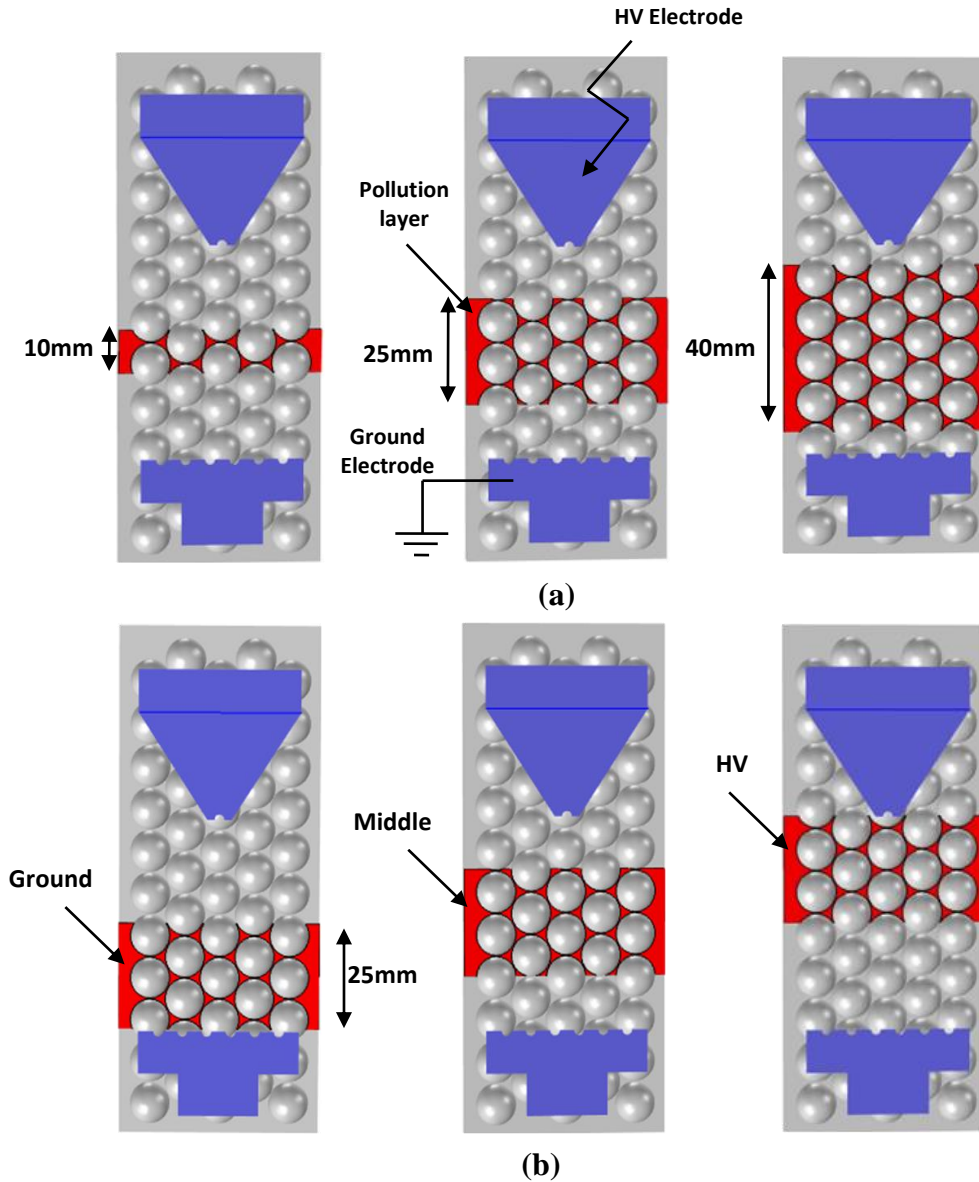
Figure 5.26 Configuration of non-uniform pollution distribution: (a) Non-uniform
pollution layer of 10, 25, 40 mm in middle of textured model, (b) Location of the
pollution band

$$Y = b_0 + \sum_{j=1}^{k} b_j x_j + \sum_{\substack{u,j=1 \\ u \neq j}}^{k} b_{uj} x_u x_j + \sum_{j=1}^{k} b_{jj} x_j^2 \qquad (5.10)$$

Where:

Y: The desired response (the electric field);

b_0: The constant term of the equation;

b_j: The linear term;

b_{uj}: The interaction term;

b_{jj}: The squared term;

x_j: The variables that correspond to the factors studied (thickness, width and Location of the pollution layer).

The mathematical model of the electric field under non-uniform pollution is written in this case as follows:

$$E_{max}(V/mm) = b_0 + b_1 T + b_2 W + b_3 L + b_{12} TW + b_{13} TL + b_{23} WL + b_{11} T^2 + b_{22} W^2 + b_{33} L^2 \quad (5.11)$$

This equation will be verified a posteriori through statistical analysis, in order to verify that the quadratic model of the electric field under non-uniform pollution gives a usable interpretation of the real phenomenon. This verification will be presented in the section (5.6.3.6).

5.6.3.4. Construction of the experimental design

Our model has 3 factors at 3 levels and therefore requires choosing a design of experiments of Taguchi L27.

The notation L27 indicates the following:

- L (Number of tests) = L (Levels) ^{factors}.
- Number of tests = (number of levels for each factor) $^{number\ of\ factors}$ = 3^3 = 27.

The Taguchi design and simulation results obtained are presented in Table (5.4).

The analysis of these results will enable the desired model coefficients to be calculated and, above all, the factors that do not have a significant influence on the calculated response and which can, therefore, be removed from our study will be identified.

5.6.3.5. Mathematical analysis of test results

The mathematical analysis is based on the estimation of the coefficients of equation (5.11), by using the least squares method. The results of the calculations are given in Table 5.5.

Table 5.4 Taguchi design L (3^3) and simulation results of maximum E-field

Test no	Studied parameters			Response
	Thickness T (x_1), mm	Width W (x_2), mm	Location L (x_3)	Maximum E-field, V/mm
1	0.6	10	Ground	471.715
2	0.6	10	Middle	459.404
3	0.6	10	HV	495.058
4	0.6	25	Ground	533.283
5	0.6	25	Middle	521.289
6	0.6	25	HV	562.694
7	0.6	40	Ground	609.945
8	0.6	40	Middle	603.639
9	0.6	40	HV	619.821
10	1	10	Ground	628.254
11	1	10	Middle	607.724
12	1	10	HV	635.082
13	1	25	Ground	683.078
14	1	25	Middle	659.167
15	1	25	HV	692.776
16	1	40	Ground	711.282
17	1	40	Middle	701.915
18	1	40	HV	755.358
19	1.4	10	Ground	720.294
20	1.4	10	Middle	688.951
21	1.4	10	HV	769.319
22	1.4	25	Ground	782.508
23	1.4	25	Middle	747.133
24	1.4	25	HV	797.219
25	1.4	40	Ground	845.392
26	1.4	40	Middle	818.802
27	1.4	40	HV	868.560

Table 5.5 Values of the model coefficients

Coefficients		Values
Constant term	b_0	162.2
Linear terms	b_1	481.3
	b_2	4.01
	b_3	6.9
Interaction terms	b_{12}	-0,737
	b_{13}	5.06
	b_{23}	-0.012
Squared terms	b_{11}	-81.3
	b_{22}	0.0129
	b_{33}	31.42

5.6.3.6. Statistical analysis of the model

The statistical analysis of the model is the main step in the analysis of the results. An analysis of variance (ANOVA) was performed on the simulation results to identify statistically significant or influential factors on the observed response (electric field). The analysis of variance is presented in Table 5.6.

To determine whether the association between the response (E_{max}-field) and each term (T, W and L) in the model is statistically significant, the P-value of the term was compared to the significance level (denoted alpha or α =0.05). A significance level of 0.05 indicates a 5% risk of concluding that a difference exists when there is no actual difference. When the P-value is less than or equal to the significance level ($P \leq \alpha$), we conclude that there is a statistically significant association between the maximum E-field and the term.

Table 5.6 ANOVA for maximum E-field

Term	DF	Seq SS	Adj SS	Adj MS	F	P-value	Conclusion
T	1	259519	8321	8321.1	51.64	0.000	Inf
W	1	62294	1493	1492.8	9.26	0.007	Inf
L	1	2453	59	59.0	0.37	0.553	N-Inf
T*T	1	1016	1016	1016.1	6.31	0.022	Inf
W*W	1	51	51	50.5	0.31	0.583	N-Inf
L*L	1	5924	5924	5923.9	36.76	0.000	Inf
T*W	1	234	234	234.4	1.45	0.244	N-Inf
T*L	1	49	49	49.1	0.30	0.588	N-Inf
W*L	1	0	0	0.4	0.00	0.963	N-Inf
Erreur	17	2739	2739	161.1			
Total	26	334281					

Where:

T: The pollution layer thickness;

W: The pollution layer width;

L: The location of layer;

DF: The degrees of freedom;

seq SS: The sequential sum of squares;

adj SS: The adjusted sum of squares;

MS: The mean squares;

F: The standard «F» statistic;

P-value: The probability of testing the significance of null hypothesis;

Inf: mean the term is influent; N-Inf: means the term is non-influent.

In the case of non-significance (the value of P > α), we conclude that the terms do not present any statistically significant association with the response. It is preferable to reduce the model and repeat the analysis of variance, removing a not significant term one by one until only statically significant terms remain. From Table 5.7, removing these elements of the model we only find influential elements. Model reduction lets us simplify a model and increase the precision of predictions. A high value of «F» with a low value of «P» means that the term is highly significant.

Table 5.7 Verification of ANOVA on the maximum E-field

Source	DF	Seq SS	Adj SS	Adj MS	F	P-value	Conclusion
T	1	259519	8118	8118.4	55.46	0.000	inf
W	1	62294	62294	62294.3	425.59	0.000	inf
L	1	2453	2453	2453.2	16.76	0.001	inf
T*T	1	1016	1016	1016.1	6.94	0.015	inf
L*L	1	5924	5924	5923.9	40.47	0.000	inf
Erreur	21	3074	3074	146.4			
Total	26	334281					

The final mathematical model of the maximum electric field is written as follow:

$$E_{max}(V/mm) = 174.4 + 462.9T + 3.922W + 11.67L - 81.3T^2 + 31.42L^2 \qquad (5.12)$$

The determination coefficient $R^2\ adj$ indicates the percentage variation in the response explained by the model. The descriptive quality associated with this model is indicated in equation (5.13).

$$R^2(adj) = 98.9\% \qquad (5.13)$$

The value of $R^2\ adj$ is close to 100%, and therefore indicates the good descriptive quality of the model.

5.6.3.7. Normality test

The Anderson-Darling statistic measures how well the data follow a particular distribution.

The hypotheses for the Anderson-Darling test are:

- Null hypothesis (H$_0$): The data follow a specified distribution.

- Alternative Hypothesis (H$_1$): The data do not follow a specified distribution.

To determine whether the data follow the normal distribution, we compare the P-value to the significance level. Usually, a significance level (denoted as alpha or $\alpha = 0.05$).

✓ If the P-value is less than or equal to the significance level (P $\leq$ α), the decision is to reject the null hypothesis (H$_0$) and conclude that the data do not follow a normal distribution.

✓ If the P-value is larger than the significance level, the decision is not to reject the null hypothesis and conclude that the data follow a normal distribution.

The probability plot was used to assess how well the electric field data follow a normal distribution (Figure 5.27).

The electric field values follow the fitted distribution line closely. The normal distribution appears to be a good fit to the data because the data to follow closely the straight line.

The Anderson-Darling test performed on these results gives a P-value equal to 0.936, which is greater than the significance level of 0.05. The null hypothesis indicates that the data follow a normal distribution.

The confidence intervals on a probability plot show the 95% confidence bounds for the individual percentiles of the distribution. These intervals form the outer solid lines on the plot and can be used to assess the precision of the individual percentile estimates. The confidence intervals should not be used to assess the distribution fit.

5.6.3.1. Pareto diagram

It is possible to determine which terms contribute the most to the variability in the electric field from the following relationship:

$$\text{CRT} = \frac{\text{SeqSS}}{\text{SeqSS totale}} \qquad (5.13)$$

Where:

CRT: The contribution of the term to the variation in the response ($E_{\max}$-field).

SeqSS: The sequential sum of squares associated for a term.

SeqSS total: The total sum of squares.
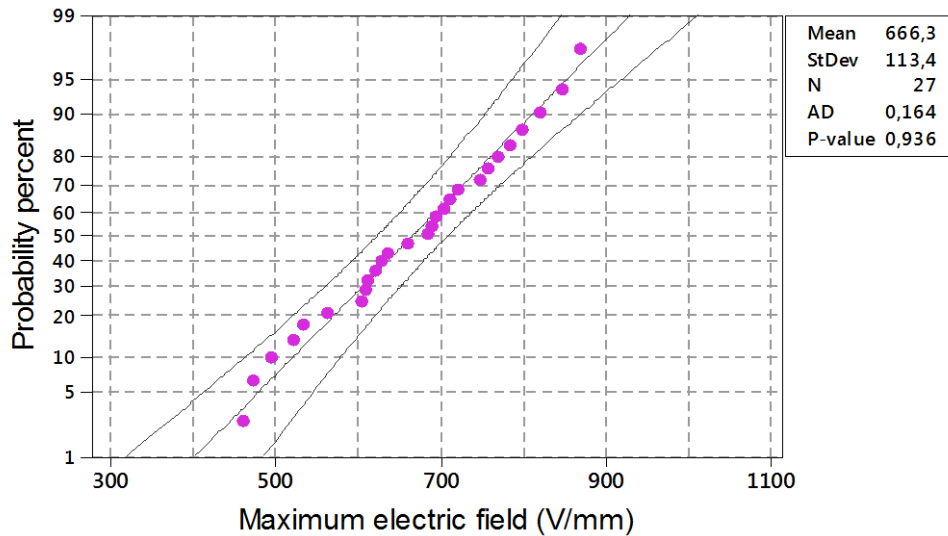
Figure 5.27 Normality plots with 95% confidence intervals of the electric field

The parameters contributions are more marked on the Pareto diagram Figure 5.28. It is shown that the effect of the thickness *(T)* and the width *(W)* of the pollution layer are important and contributes them both to explain about 96.28% of the variations in the maximum electric field. On the other hand, the influence of the pollution layer location *(L)* is 0.73% in the total variation, which does not represent a remarkable contribution to the electric field. The interactions *T*W, T*L* and *W*L* they have no effect on the total variation of the electric field.
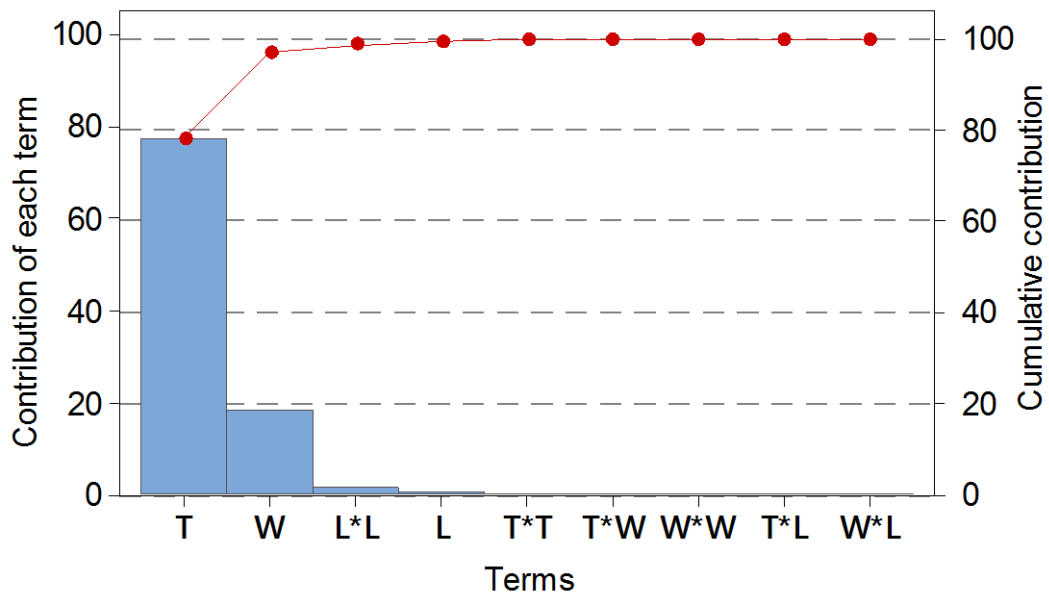
Figure 5.28 Pareto diagram for electric field

5.6.3.2. Graphs of average effects of the factors and interactions

The effects of the factors *T*, *W* and *L* on the maximum E-field are represented graphically in Figure 5.29 It can be observed that the thickness is the most influencing factor on the maximum E-field and when the pollution layer thickness increased the electric field stress is increased despite the contaminant does not change.

This observation leads to the conclusion that the electric field intensity increases with the increase in the pollution severity. Also, an increase in the maximum electric field on the surface with an increase in pollution layer width was observed. As the pollution layer width increases, the voltage required to establish a partial arc along the pollution layer decreases resulting in an increase in the maximum electric field and a decrease in the pollution layer resistance. Therefore, it is noticed that there is a small difference observed in the maximum E-field due to the pollution position. The electric field is higher when the pollution layer is located near the HV ends than ground ends and the middle position. The presence of the conductive layer in the middle location reduces slightly the electric field stress comparatively to both near HV and ground. This due to the presence of two dry bands near the electrodes, which leads to decrease the maximum electric field applied on each one of them.

The influence of the variation of each factor on the effect of the other factors is represented graphically by the interaction plot (Figure 5.30). This plot display means for the levels of one factor on the x-axis and a separate line for each level of another factor. In this interaction plot for the maximum E-field, the lines are parallel, this indicates that no interaction occurs between (*T*W*; *T*L* and *W*L*).
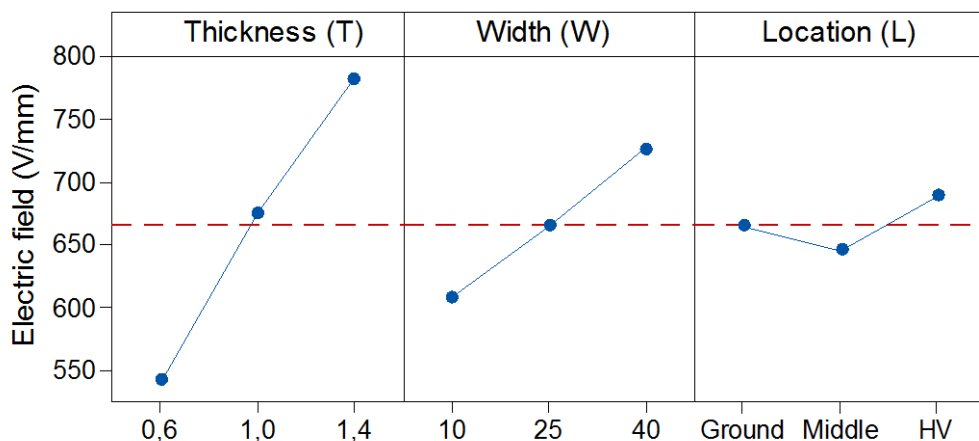
Figure 5.29 Effects of the factors *T*, *W* and *L* on the maximum electric field
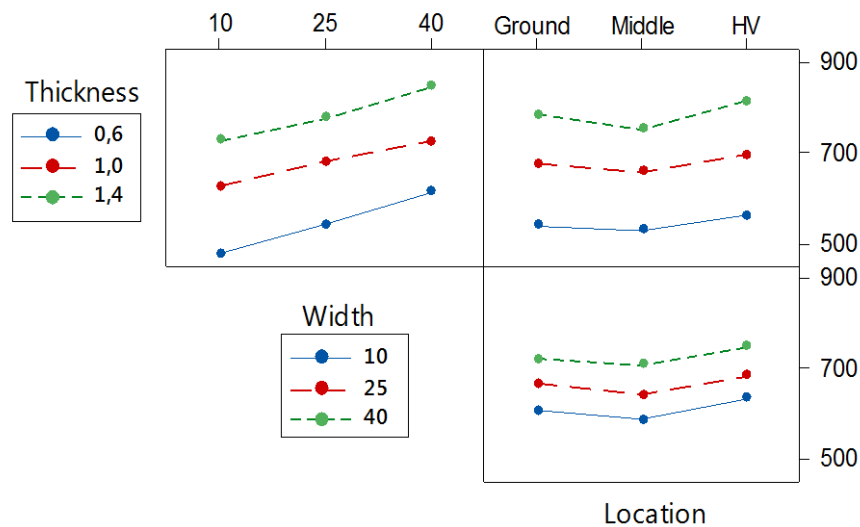
Figure 5.30 Graph of interaction between *T*, W and L on the maximum E-field

5.7. Conclusion

The present work describes the simulation of electric field distribution on a textured insulator surface using the COMSOL Multiphysics finite element analysis to assess whether the expected improvement can be achieved for textured insulators prototypes.

According to the results of simulation and analysis, it can be concluded that the electric field distribution along insulator is obviously influenced by the insulator geometry. All samples with textured surface show a better behaviour of the electric field distribution than the traditional non-textured surface.

The diameter of the hemispherical protuberances has an important effect on the potential distribution as well as on the maximum electrical field. The bigger the diameter is, the lower the maximum electric field strength is which improve the performance of the insulation.

Under the pollution conditions, the performance of the intersecting square "C" was superior to that of the other textured insulators. Moreover, the contiguous hexagonal pattern "A" is the most prone to accumulate pollution leading to an increase in the electric field.

In the case of non-uniform pollution distribution, the length and thickness of the pollution layer are the dominant factors that influence the maximum E-field.

Chapter 06

GENERAL CONCLUSIONS AND FUTURE WORKS

6.1. General conclusions

The main objectives of this thesis are to understand the performance of traditional and textured SiR insulators under different environmental conditions. The performance of the insulators was investigated through extensive experimental investigation, alongside numerical analysis techniques. The research work findings were summarized within the previous chapters and this section will synthesize them to answer at least these research questions:

1) Do the textured insulators really have a better performance compared to the traditional insulators?

2) What is the main difference between the behaviour of textured silicone rubber insulators at DC and AC voltage?

3) Among the various textured surfaces, who have better ability and efficiency to resist erosion and reduce the electric field strength on the surface?

4) Which parameters can affect the E-field strength of textured silicone rubber insulating surfaces in the presence of the pollution layer?

For experimental work, the performance of SiR insulators was investigated using the inclined plane test. The IEC-60587 inclined plane test is an extremely important method for the evaluation of the anti-erosion and anti-tracking performance of insulating materials. Both AC and positive DC tests on rectangular silicone rubber samples with smooth and textured surfaces were performed. The findings of this work can be summarised as follows:

• The results of the IPT showed that the textured insulator design has a superior electrical performance in comparison with the conventional design under AC and positive DC voltage.

- The dynamics of the discharges for textured samples at the DC test were significantly different than the AC test. For the AC test, the discharge activity started near the HV electrode that is a series of small streamer discharges and moving in the direction of the polluted flow to reaching the ground electrode. Also, the discharges activity at the AC test was highly mobile, frequent and unable to settle at any point on the area near the ground electrode. Whereas the discharges activities at the DC test was more intense and not as mobile resulting in greater loss of material due to erosion.

- From the textured designs, the intersecting square design showed the best performance as the loss of material due to erosion was minimal compared with the intersecting hexagonal design.

- The application of the DC voltage resulted in great erosion in both textured materials (intersecting hexagonal and square), which exceeded the erosion observed during the AC voltage.

- In DC tests, an eroded mass in the HV electrode was observed, whereas the ground electrodes show an increase in mass because of the formation of a solid brown layer on its surface. On the contrary, during the AC test, the HV electrodes lost a very little mass, while we did not observe any change in the ground electrode.

- Traditional SiR samples tend to show a high-brightness point that is concentrated at a certain region near the ground electrode, resulting in severe erosion and material loss. The temperature of the bright points much exceeds the pyrolytic temperature of silicone rubber materials which leads to the intense erosion.

For numerical analysis, the finite element analysis and solver software package, COMSOL Multiphysics®, was used to calculate the tangential electric field strength and voltage distribution along the textured and non-textured insulators surface under dry and clean conditions and then under various wet polluted conditions. In the case of non-uniform pollution distribution, we have combined the finite element with the design of experiment method to investigate and describe the behaviour of textured silicone rubber insulators. Various conclusions drawn from this research work are:

- The electric field was at a maximum peak at the HV electrode with a secondary peak at the ground electrode.

- The results showed also that the electric field strength on the all textured surfaces was lower than that of the traditional non-textured surface.

- The electric field calculations along composite insulators under dry conditions showed that the maximum electric field value depends on the system voltage. The field magnitude is greater for systems at higher voltages. The maximum field value was found to occur at the triple point (stainless steel, silicone rubber and air).

- The diameter of the hemispherical protuberances has an important effect on the potential distribution as well as on the maximum electrical field. The bigger the diameter is, the lower the maximum electric field strength is, which improve the performance of the insulation.

- Under the pollution conditions, the performance of the intersecting square "C" was superior to that of the other textured insulators. Moreover, the contiguous hexagonal pattern "A" is the most prone to accumulate pollution leading to increasing the electric field.

- In the case of non-uniform pollution distribution, the length and thickness of the pollution layer are the dominant factors that influence the maximum E-field.

6.2. Future works

This thesis is concerned with the investigation of the performance of high voltage textured silicone rubber insulation material was tested in laboratory investigations under AC and DC excitations. These are followed by extensive computational modelling and simulation studies to evaluate the E-field distribution along textured SiR insulators for DC voltage. Based on the work carried out in this study, there is still a need for further investigations to assess the performance of these textured insulators. The following areas are proposed for future research:

- In this work, the distribution of the electric field along the textured insulators under DC voltage was investigated using COMSOL Multiphysics programme. Therefore, a comprehensive study is proposed to investigate the performance of the insulators under AC voltage in the same way as the previous study and compare them.

- The effect of the other factors of the pollution on the behaviour of textured

insulators can be investigated using the experimental design method. For example, study the effect of the conductivity of the pollution layer on the electric field strength.

- The Silicone rubber performance was proven superior to other polymers for external insulation. However, it is important to prove the ability of the textured insulators to resist erosion under DC using other insulating materials, such as ethylene propylene diene monomer (EPDM).

- The study of the degradation and aging of textured insulators resulting from exposure to various harsh environmental factors in the DC voltage is an important research area that can help evaluate the performance of these insulators in the long-term. For example, it is suggested to study the effect of ultraviolet radiation, the effect of low temperature as ice and the effect of high temperature.

REFERENCES

[1]   J. S. T. Looms, "Insulators for High Voltages", London, United Kingdom: Peter Peregrinus Ltd, 1988, pp. 2-12.

[2]   A. P. Mishra, R. S. Gorur and S. Venkataraman, "Evaluation of Porcelain and Toughened Glass Suspension Insulators Removed from Service," *IEEE Transactions on Dielectrics and Electrical Insulation*, vol. 15, no. 2, pp. 467-475, April 2008.

[3]   R. Abd-Rahman, A. Haddad, N. Harid and H. Griffiths, "Stress control on polymeric outdoor insulators using Zinc oxide microvaristor composites," *IEEE Transactions on Dielectrics and Electrical Insulation*, vol. 19, no. 2, pp. 705-713, April 2012.

[4]   R. Hackam, "Outdoor HV composite polymeric insulators", *IEEE Transactions on Dielectrics and Electrical Insulation,* vol. 6, no. 5, pp. 557–585, October 1999.

[5]   J. Mackevich and M. Shah, "Polymer outdoor insulating materials. Part I: Comparison of porcelain and polymer electrical insulation," *IEEE Electrical Insulation Magazine*, vol. 13, no. 3, pp. 5-12, May-June 1997.

[6]   A. Rahisham., "Investigations of Zno microvaristor for stress control on polymeric outdoor insulators", PhD Thesis, School of Engineering, Cardiff University, Royaume-Uni, 2012.

[7]   V. M. Moreno and R. S. Gorur, "Accelerated corona discharge performance of polymer compounds used in high voltage outdoor insulators," *1999 Annual Report Conference on Electrical Insulation and Dielectric Phenomena (Cat. No.99CH36319)*, Austin, TX, USA, pp. 731-734, 1999.

[8]   J. Montesinos, R. S. Gorur, B. Mobasher and D. Kingsbury, "Mechanism of brittle fracture in nonceramic insulators, "IEEE Transactions on Dielectrics and Electrical Insulation, vol. 9, no. 2, pp. 236-243, April 2002.

[9]   D. A. Swift. "Insulators for outdoor applications" in Advances in High Voltage Engineering, A. Haddad and D. Warne, Eds. London, United Kingdom: The Institution of Engineering and Technology, pp. 257-307, 2004.

[10]   A. El-Arbaty, E. Nasser, A. El-Sakry, "Selection of insulators suitable for operation in contaminated environments with reference to desert conditions"., International Conference Large High Voltage Electric Systems, Paris, France, pp. 1–12, 1980.

[11]   IEC 60815:1986, "Guide to selection of insulators in respect of polluted conditions", 1986.

[12]   R. S. Gorur, E.A. Cherney, J.T. Burnham, "Outdoor insulators", Ravi S. Gorur, Inc., USA, 1999.

[13]   A. H. El-hag, S. H. Jayaram and E. A. Cherney, "Effect of insulator profile on aging

performance of silicone rubber insulators in salt-fog," IEEE Transactions on Dielectrics and Electrical Insulation, vol. 14, no. 2, pp. 352-359, April 2007.

[14] A. H. El-hag, S.H. Jayaram, E.A. Cherney, "Calculation of leakage current density of silicone rubber insulators under accelerated aging conditions", Journal of electrostatics, vol. 67, no. 1, pp.48-53, Feb 2009.

[15] A. Haddad and R.T. Waters, "Insulating Structures", UK Patent GB2406225B, 2006.

[16] A. Haddad, K. Chrzan, H. Griffiths and R.T. Waters, "A new approach to anti-fog design for polymeric insulators", International Symposium on High Voltage (ISH), Ljubljana, Slovenia, paper T4-446, 2007.

[17] A. Haddad, H. Griffiths and R. T. Waters, "Principles of Anti-Fog Design for Polymeric Insulators," 2007 IEEE International Conference on Solid Dielectrics, Winchester, pp. 302-305, 2007.

[18] A. Haddad, R. Waters, H. Griffiths, K. Chrzan, N. Harid, P. Sarkar, and P. Charalampidis, "A new approach to anti-fog design for polymeric insulators," IEEE Transactions on Dielectrics and Electrical Insulation, vol. 17, no. 2, pp. 343-350, April 2010.

[19] IEC 60587:2007, "Electrical insulating materials used under severe ambient conditions. Test methods for evaluating resistance to tracking and erosion", 2007.

[20] P. Sarkar, A. Haddad, R. T. Waters, H. Griffiths, N. Harid and P. Charalampidis, "Inclined-plane tests of textured silicone rubber Samples," *2010 International Conference on High Voltage Engineering and Application*, New Orleans, LA, pp. 532-535, 2010.

[21] R. T. Waters, A. Haddad, H. Griffiths, N. Harid, P. Charalampidis and P. Sarkar, "Dry-band discharges on polluted silicone rubber insulation: control and characterization," *IEEE Transactions on Dielectrics and Electrical Insulation*, vol. 18, no. 6, pp. 1995-2003, December 2011.

[22] S. Ilhan, A. Ozdemir, S. H. Jayaram and E. A. Cherney, "Numerical and experimental investigation of the effects of pollution on glass suspension-type insulators," *IEEE Transactions on Dielectrics and Electrical Insulation*, vol. 22, no. 5, pp. 2987-2994, Oct 2015.

[23] D. Fahmi, L. A. Novario, I. M. Y. Negara and R. Wahyudi, "Comparative analysis of electric field distribution on glass and ceramic insulator using finite element method," *2016 International Seminar on Intelligent Technology and Its Applications (ISITIA)*, Lombok, pp. 515-520, 2016.

[24] W. Sima, Q. Yang, C. Sun and F. Guo, "Potential and electric-field calculation along an ice-covered composite insulator with finite-element method," *IEE Proceedings - Generation, Transmission and Distribution*, vol. 153, no. 3, pp. 343-349, May 2006.

[25] A. H. El-hag, S. H. Jayaram and E. A. Cherney, "Effect of insulator profile on aging performance of silicone rubber insulators in salt-fog," in *IEEE Transactions on*

Dielectrics and Electrical Insulation, vol. 14, no. 2, pp. 352-359, April 2007.

[26]   J. F. Hall, "History and bibliography of polymeric insulators for outdoor applications," *IEEE Transactions on Power Delivery*, vol. 8, no. 1, pp. 376-385, Jan. 1993.

[27]   J. Mackevich and S. Simmons, "Polymer outdoor insulating materials. II. Material considerations," *IEEE Electrical Insulation Magazine*, vol. 13, no. 4, pp. 10-16, July-Aug. 1997.

[28]   E. A. Cherney, "Non-Ceramic insulators-a simple design that requires careful analysis," *IEEE Electrical Insulation Magazine*, vol. 12, no. 3, pp. 7-15, May-June 1996.

[29]   T. Zhao and R. A. Bernstorf, "Ageing tests of polymeric housing materials for non-ceramic insulators," *IEEE Electrical Insulation Magazine*, vol. 14, no. 2, pp. 26-33, March-April 1998.

[30]   R. S. Gorur, G. G. Karady, A. Jagota, M. Shah and A. M. Yates, "Aging in silicone rubber used for outdoor insulation," *IEEE Transactions on Power Delivery*, vol. 7, no. 2, pp. 525-538, April 1992.

[31]   D. A. Swift, A. Haddad, and D. Warne, "Insulators for outdoor applications," Advances in high voltage engineering, ISBN 0852961588, 2004.

[32]   R. S. Gorur, E. A. Cherney and J. T. Burnham, "Outdoor Insulators". Phoenix, Arizona, USA: Ravi S. Gorur Inc., 1999.

[33]   R. S. Gorur, E. A. Cherney, R. Hackam and T. Orbeck, "The electrical performance of polymeric insulating materials under accelerated aging in a fog chamber," *IEEE Transactions on Power Delivery*, vol. 3, no. 3, pp. 1157-1164, July 1988.

[34]   L. H. Meyer, E. A. Cherney and S. H. Jayaram, "The role of inorganic fillers in silicone rubber for outdoor insulation alumina tri-hydrate or silica," *IEEE Electrical Insulation Magazine*, vol. 20, no. 4, pp. 13-21, July-Aug. 2004.

[35]   T. Kikuchi, S. Nishimura, M. Nagao, K. Izumi, Y. Kubota, and M. Sakata, "Survey on the use of non-ceramic composite insulators, "*IEEE Transactions on Dielectrics and Electrical Insulation*, vol. 6, no. 5, pp. 548–556, Nov. 1999.

[36]   E. Da Silva, "Reliability of composite insulators," in Technical meeting on Optimisation of Overhead Line Infrastructure, Supergen - AMPerES, Manchester, UK, 2008.

[37]   J. T. Burnham and R. J. Waidelich, "Gunshot damage to ceramic and nonceramic insulators," *IEEE Transactions on Power Delivery*, vol. 12, no. 4, pp. 1651-1656, Oct. 1997.

[38]   J. T. Burnham, P. S. Givens and T. M. Grisham, "High strength polymer post insulators enable economical transmission lines with low environmental impact," *Proceedings of IEEE/PES Transmission and Distribution Conference*,

Chicago, USA, pp. 494-503, 1994.

[39]   R. S. Gorur *et al.*, "Sudden flashover of nonceramic insulators in artificial contamination tests," *IEEE Transactions on Dielectrics and Electrical Insulation*, vol. 4, no. 1, pp. 79-87, Feb. 1997.

[40]   S. M. Gubanski, "Properties of silicone rubber housings and coatings," *IEEE Transactions on Electrical Insulation*, vol. 27, no. 2, pp. 374-382, April 1992.

[41]   J. M. Seifert and D. Stefanini, "High Pollution Resistant Composite Insulators," International Conference on High Voltage Engineering and Application (ICHVE), Chongqing, China, pp. 32-35, 2008.

[42]   J. W. Chang and R. S. Gorur, "Surface recovery of silicone rubber used for HV outdoor insulation," *IEEE Transactions on Dielectrics and Electrical Insulation*, vol. 1, no. 6, pp. 1039-1046, Dec. 1994.

[43]   D. A. Swift, C. Spellman and A. Haddad, "Hydrophobicity transfer from silicone rubber to adhering pollutants and its effect on insulator performance," *IEEE Transactions on Dielectrics and Electrical Insulation*, vol. 13, no. 4, pp. 820-829, Aug. 2006.

[44]   K. Kunde, R. Hennings, M. Kuhl, A. Schütz, H. Jansses, and U. Stietzal, "New experience with composite insulators ", in Proc. Cigre Session 1998, Paper No 15-206, 1998.

[45]   S. M. Gubanski, A. Dernfalk, J. Andersson and H. Hillborg, "Diagnostic Methods for Outdoor Polymeric Insulators," *IEEE Transactions on Dielectrics and Electrical Insulation*, vol. 14, no. 5, pp. 1065-1080, Oct. 2007.

[46]   C. Tourreil, "Failure rates of high voltage line insulators," Insulator news and market report, vol. May/Jun, 2000.

[47]   Y. Yuan and T. Lee. "Contact angle and wetting properties," Springer Series in Surface Sciences, vol. 51, pp. 1-27, 2013.

[48]   D.K. Bhana, D.A. Swift, "An investigation into the Temporary Loss of Hydrophobicity of Some Polymeric Insulators and Coatings", Proceedings of the 4th International Conference on Properties and Applications of Dielectric Materials, Brisbane, paper 5208, 1994.

[49]   Wacker Chemie, "Silicones pour applications haute et moyenne" Available: **http://www.yumpu.com/fr/document/view/16039531/silicones-pour-applications-haute-et-moyenne-wacker-chemie** (Accessed on 2013) .

[50]   J. S. T. Looms. "Insulators for High Voltages", London, United Kingdom: Peter Peregrinus Ltd, pp. 2-12, 1988.

[51]   IEC 60120:1984, "Dimensions of ball and socket couplings of string insulator units", 1984.

[52]   IEC 61466-1:1997, "Composite string insulator units for overhead lines with a nominal voltage greater than 1000 V – Part 1: standard strength classes and end fittings", 1997.

[53]   S. M. Gubanski and A. E. Vlastos, "Wettability of naturally aged silicon and EPDM composite insulators," *IEEE Transactions on Power Delivery*, vol. 5, no. 3, pp. 1527-1535, July 1990.

[54]   Y. Zhu, M. Otsubo, C. Honda, and S. Tanaka, "Loss and recovery in hydrophobicity of silicone rubber exposed to corona discharge," Polym. Degrad. Stab., vol. 91, no. 7, pp. 1448–1454, juillet 2006.

[55]   J. Kim and M. K. Chaudhury, "Corona-discharge-induced hydrophobicity loss and recovery of silicones," *in 1999 Annual Report Conference on Electrical Insulation and Dielectric Phenomena*, vol. 2, pp. 703–706, 1999.

[56]   C. A. Spellman, H. M. Young, A. Haddad, A. R. Rowlands, and R. T. Waters, "Survey of polymeric insulator ageing factors," *Proceedings of the Eleventh International Symposium on High Voltage Engineering, Conf. Pub*, vol.164, no. 467, pp. 160-163, 1999.

[57]   S. Amin and M. Amin, "Natural aging of SiR insulators in Pakistan," *in International Conference on Emerging Technologies (ICET)*, pp. 114-117, 2009.

[58]   J.S.T. Looms, "Insulators for high voltages", IEE Power Engineering Series, vol. 7, Peter. Peregrinus Ltd., ISBN 9780863411168, 1988.

[59]   P.J. Lambeth, "Effect of pollution on high-voltage outdoor insulators", Proceedings of the Institution of Electrical Engineers, Vol. 118, no. 9R, pp. 1107-1130, 1971.

[60]   T. Tanaka, "Aging of polymeric and composite insulating materials. Aspects of interfacial performance in aging," *IEEE Transactions on Dielectrics and Electrical Insulation*, vol. 9, no. 5, pp. 704-716, Oct. 2002.

[61]   V. K. Agarwal, "Aging of multi stressed polymeric insulators," *IEEE Transactions on Electrical Insulation*, vol. 24, no. 5, pp. 741-764, Oct. 1989.

[62]   G. G. Karady, "Flashover mechanism of non-ceramic insulators", *IEEE Transactions on Dielectrics and Electrical Insulation*, Vol. 6, no. 5, pp.718–723, 1999.

[63]   W. T. Starr, "Polymeric outdoor insulation," in *IEEE Transactions on Electrical Insulation*, vol. 25, no. 1, pp. 125-136, Feb. 1990.

[64]   G. G. Karady, M. Shah and R. L. Brown, "Flashover mechanism of silicone rubber insulators used for outdoor insulation-I," in *IEEE Transactions on Power Delivery*, vol. 10, no. 4, pp. 1965-1971, Oct. 1995.

[65]   R. S. Gorur, J. Montesinos, L. Varadadesikan, S. Simmons and M. Shah, "A laboratory test for tracking and erosion resistance of HV outdoor insulation," *IEEE Transactions on Dielectrics and Electrical Insulation*, vol. 4, no. 6, pp. 767-774, Dec. 1997.

[66] B. Venkatesulu and M. J. Thomas, "Studies on the Tracking and Erosion Resistance of RTV Silicone Rubber Nanocomposite," 2008 Annual Report Conference on Electrical Insulation and Dielectric Phenomena, Quebec, QC, pp. 204-207, 2008.

[67] R. G. Houlgate and D. A. Swift, "Composite rod insulators for AC power lines: electrical performance of various designs at a coastal testing station," *IEEE Transactions on Power Delivery*, vol. 5, no. 4, pp. 1944-1955, Oct. 1990.

[68] J. Reynders, I. Jandrell, and S. Reynders, " Review of aging and recovery of silicone rubber insulation for outdoor use, *" IEEE Transactions on Dielectrics and Electrical Insulation,* vol. 6, no. 5, pp. 620-631, 1999.

[69] S. H. Kim, E. A. Cherney, R. Hackam and K. G. Rutherford, "Chemical changes at the surface of RTV silicone rubber coatings on insulators during dry-band arcing," IEEE Transactions on Dielectrics and Electrical Insulation, vol. 1, no. 1, pp. 106-123, Feb 1994.

[70] Y. Zhu, M. Otsubo, and C. Honda, "Behavior of water droplet on electrically stressed polymeric coating surface, " Surface and Coatings Technology, vol. 201, no. 9–11, pp. 5541–5546, Feb. 2007.

[71] R. S. Gorur, J. W. Chang and O. G. Amburgey, "Surface hydrophobicity of polymers used for outdoor insulation," IEEE Transactions on Power Delivery, vol. 5, no. 4, pp. 1923-1933, Oct. 1990.

[72] A. de la O, R. S. Gorur and J. T. Burnham, "Electrical performance of non-ceramic insulators in artificial contamination tests. Role of resting time," IEEE Transactions on Dielectrics and Electrical Insulation, vol. 3, no. 6, pp. 827-835, Dec. 1996.

[73] H. Hillborg, and U. W. Gedde, "Hydrophobicity changes in silicone rubbers", *IEEE Transactions on Dielectrics and Electrical Insulation*, vol.6, no.5, pp. 703-717, Nov.1999.

[74] R. J. Hill, "Laboratory analysis of naturally aged silicone rubber polymer insulators from contaminated environments, 138 to 145 kV," *Proceedings of IEEE/PES Transmission and Distribution Conference,* Chicago, IL, USA, pp. 488-493, 1994.

[75] H. Janssen, A. Herden, H. C. Kärner, "The loss and recovery of hydrophobicity on silicone rubber surfaces", 10th International Symposium on High Voltage Engineering, Montreal, Canada, 1997.

[76] J. Kindersberger, M. Kuhl, "Effect of hydrophobicity on insulator performance"; 6th ISH, New Orleans, paper 12.01, 1989.

[77] A. E. Vlastos and E. Sherif, "Experience from insulators with RTV silicon rubber sheds and shed coatings, in *IEEE Transactions on Power Delivery*, vol. 5, no. 4, pp. 2030-2038, Oct. 1990.

[78] A. Phillips and T. Shaw, "Field Guide - Visual Inspection of NCI, Revision 1 (1008739)," EPRI, Palo Alto, CA, USA, 2004.

[79] "STRI - Guide 5, 2005, Guide for Visual Identification of Deterioration & Damages on Suspension Composite Insulators," STRI, Ludvika, Sweden. 2005.

[80] J. Burnham, "Guideline for Visual Identification of Damaged Polymer Insulators, http://ewh.ieee.org/soc/pes/iwg/NCIEvaluation/POLYMERDAMAGEGUIDELINE.doc." vol. 2009, 1998.

[81] A. Phillips, "Review for the State of the Art and Application of Polymer Materials / Insulation used in Distribution Class (12 - 46 kV class) Substation," EPRI, 2003.

[82] "STRI - Guide 3, 2005, Composite Insulator Status Program: Field Inspection of Composite Line Insulators," STRI, Ludvika, Sweden. 2005.

[83] A. Phillips, "Application of Polymer Insulators (NCI): Workshop Presentations (1002660)." EPRI, Palo Alto, CA, USA, 2003.

[84] IEEE, "Guide for Application of Composite Line Post Insulators," IEEE Std 1572-2004, pp.1-16, 2004.

[85] IEEE, "Energized Line Working with Polymer Insulators for Voltages 60kV and above," in 11th International Conference on Transmission & Distribution Construction, Operation and Live-Line Maintenance, (ESMO), New Mexico, USA, 2006.

[86] IEC 60815-1:2008, "Selection and dimensioning of high-voltage insulators intended for use in polluted conditions, Part 1definitions, information and general principles", 2008.

[87] IEC 60507:1993, "Artificial pollution tests on high-voltage insulators to be used on a.c. systems", May 1993.

[88] ASTM D2303, "Standard test method for liquid contaminant, inclined plane tracking and Erosion of Insulating Materials", 1997 (Reapproved 2004).

[89] IEC 62217: 2006, "Polymeric insulators for indoor and outdoor use with a nominal voltage > 1000V- General definitions, test methods and acceptance criteria", 2006.

[90] IEC 60507:2013, "Artificial pollution tests on high-voltage ceramic and glass insulators to be used on a.c. systems", 3rd edition, 2013.

[91] S. H. Kim and R. Hackam, "Effects of saline-water flow rate and air speed on leakage current in RTV coatings," *IEEE Transactions on Power Delivery*, vol. 10, no. 4, pp. 1956-1964, Oct. 1995.

[92] A. H. El-Hag, A. N. Jahromi and M. S. Pasand "Prediction of leakage current of non-ceramic insulators in early aging period", *Electric Power Systems Research,* vol. 78, pp.1686-1692, 2008.

[93] G. Alice., "Tracking wheel test for dc polymeric insulators", Master Thesis, Electrical Energy Engineering, University of Padua, Italy, 2011.

[94]   A. Krivda *et al.*, "Inclined-plane tracking and erosion test according to the IEC 60587 Standard," in *IEEE Electrical Insulation Magazine*, vol. 25, no. 6, pp. 14-22, Dec 2009.

[95]   R. Porzel and M. Muhr, "Technical diagnostics, non-destructive state-estimation instead of damaging voltage test", 10th International Conference on HV Engineering, pp. 405-408, Montreal, Canada, 1997.

[96]   CIGRE Working Group 22.03, "Worldwide service experience with HV composite insulators", Electra, vol. 130, pp. 67-77, 1990.

[97]   CIGRE Working Group 22.03, Review of "in service diagnostic testing" of composite insulators", Electra, vol. 169, pp. 105-119, Dec, 1996.

[98]   A. N. Jahromi, A. H. El-Hag, S. H. Jayaram, E. A. Cherney, M. Sanaye-Pasand and H. Mohseni, "A neural network-based method for leakage current prediction of polymeric insulators," *IEEE Transactions on Power Delivery*, vol. 21, no. 1, pp. 506-507, Jan. 2006.

[99]   N. Anami, Y. Zhu, S. Hashimoto, M. Otsubo, C. Honda, O. Takenouchi, and Y. Hashimoto, "Evaluation of dry band arc on the polymeric insulator using differential technique and distortion factor of leakage current," in Electrical Insulation and Dielectric Phenomena, pp. 414-417, 2003.

[100]   S. Chandrasekar, C. Kalaivanan, A. Cavallini and G. C. Montanari, "Investigations on leakage current and phase angle characteristics of porcelain and polymeric insulator under contaminated conditions," *IEEE Transactions on Dielectrics and Electrical Insulation*, vol. 16, no. 2, pp. 574-583, April 2009.

[101]   M. Amin, S. Amin, and M. Ali, "Monitoring of Leakage Current for Composite Insulators and Electrical Devices," *Reviews on advanced materials science,* vol. 21, pp. 75- 89, Sep 2009.

[102]   M. Fernando, and S. Gubanski, "Leakage current on non-ceramic insulators and materials," *IEEE transaction on dielectrics and electrical insulation*, vol. 6, no. 5, pp. 660-667, 1999.

[103]   M. Fernando, and S. Gubanski, "Leakage current patterns on contaminated polymeric surfaces," *IEEE transaction on dielectrics and electrical insulation*, vol. 6, no. 5, pp. 688-694, 1999.

[104]   J. Kim, W. Song, J. Lee, Y. Park, H. Cho, Y. Yoo, K. Yang, "Leakage Current Monitoring and Outdoor Degradation of Silicone Rubber," IEEE Transactions on Dielectric and Electrical Insulation, vol. 8, no. 6, pp. 1108-1115, Dec. 2001.

[105]   A. H. El-Hag, S. H. Jayaram and E. A. Cherney, "Fundamental and low frequency harmonic components of leakage current as a diagnostic tool to study aging of RTV and HTV silicone rubber in salt-fog," *IEEE Transactions on Dielectrics and Electrical Insulation*, vol. 10, no. 1, pp. 128-136, Feb. 2003.

[106] S. Kumagai, B. Marungsri, H. Shinokubo, R. Matsuoka and N. Yoshimura, "Comparison of leakage current and aging of silicone rubbers and porcelain in both field and salt-fog tests," *IEEE Transactions on Dielectrics and Electrical Insulation*, vol. 13, no. 6, pp. 1286-1302, Dec. 2006.

[107] Y. C. Chen, C. R. Li, X. Liang, and S. Wang, "The influence of water and pollution on diagnosing defective composite insulator by electric field mapping", in Proc. 11th Int. Symp. on HV Eng., vol.4, London, UK, pp. 345-348, 1999.

[108] STRI GUIDE: "Hydrophobicity Classification Guide," Guide 1, 92/1, 1992.

[109] IEC TS 62073:2003, "Guidance on the measurement of wettability of insulator surfaces", 2003.

[110] M. Berg, R. Thottappillil and V. Scuka, "Hydrophobicity estimation of HV polymeric insulating materials. Development of a digital image processing method," *IEEE Transactions on Dielectrics and Electrical Insulation*, vol. 8, no. 6, pp. 1098-1107, Dec. 2001.

[111] T. Tokoro, Y. Omoto and M. Kosaki, "Image analysis of hydrophobicity of polymer insulators using PVM," *2001 Annual Report Conference on Electrical Insulation and Dielectric Phenomena (Cat. No.01CH37225)*, Kitchener, Ontario, Canada, pp. 581-584, 2001.

[112] K. Hidaka, "Electric field and voltage measurement by using electro-optic sensor," *in Eleventh International Symposium on High Voltage Engineering*, London, UK, pp.1-14, vol.2, Aug. 1999.

[113] S. J. Huang and D. C. Erickson, "The potential use of optical sensors for the measurement of electric field distribution," *IEEE Transactions on Power Delivery*, vol. 4, no. 3, pp. 1579-1585, July. 1989.

[114] K. Hidaka, "Progress in Japan of space charge field measurement in gaseous dielectrics using a Pockels sensor," *IEEE Electrical Insulation Magazine*, vol. 12, no. 1, pp. 17-28, Jan.-Feb. 1996.

[115] R. Zeng, Y. Zhang, W. Chen and B. Zhang, "Measurement of electric field distribution along composite insulators by integrated optical electric field sensor," *IEEE Transactions on Dielectrics and Electrical Insulation*, vol. 15, no. 1, pp. 302-310, Feb. 2008.

[116] H. Daochun, R. Jiangjun, C. Yong, H. Feng, Y. Shifeng, and L. Shoubao, "Calculation and measurement of potential and electric field distribution along 1000 kV AC transmission line composite insulator," in Proceedings of International Conference on Electrical Machines and Systems (ICEMS), pp. 428-433, 2008.

[117] U. Schümann, F. Barcikowski, M. Schreiber, H. C. Kärner, and J. M. Seifert, "FEM Calculation and Measurement of the Electrical Field Distribution of HV Composite Insulator Arrangements," in CIGRE Proceedings, Session 33, No. 404, Paris, 2002.

[118]   M. Abdel-Salam and E. K. Stanek, "Optimizing Field Stress on High-Voltage Insulators," IEEE Transactions on Electrical Insulation, vol. EI-22, no. 1, pp. 47-56, Feb. 1987.

[119]   G. Gerdin, V. Lakdawala and P. Basappa, "Computation of ac and dc electric field around a wet polluted insulator," Annual Report Conference on Electrical Insulation and Dielectric Phenomena, Mexico, pp. 176-179, 2002.

[120]   S. Chakravorti and P. K. Mukherjee, "Power frequency and impulse field calculation around a HV insulator with uniform or non-uniform surface pollution," IEEE Transactions on Electrical Insulation, vol. 28, no. 1, pp. 43-53, Feb. 1993.

[121]   S. M. A. Dhalaan and M. A. Elhirbawy, "Simulation of voltage distribution calculation methods over a string of suspension insulators," IEEE PES Transmission and Distribution Conference and Exposition, USA, vol.3, pp. 909-914, 2003.

[122]   P. B. Zhou, "Numerical Analysis of Electromagnetic Fields", Spinger-Verlag, Berlin, 1993.

[123]   M. Albano, P. Charalampidis, R. T. Waters, H. Griffiths and A. Haddad, "Silicone rubber insulators for polluted environments part 2: textured insulators," *IEEE Transactions on Dielectrics and Electrical Insulation*, vol. 21, no. 2, pp. 749-757, April 2014.

[124]   A. Haddad, K. Chrzan, H. Griffiths and R.T. Waters, "A new approach to anti-fog design for polymeric insulators", International Symposium on High Voltage (ISH), Ljubljana, Slovenia, paper T4-446, 2007.

[125]   A. Haddad, H. Griffiths and R. T. Waters, "Principles of Anti-Fog Design for Polymeric Insulators," *2007 IEEE International Conference on Solid Dielectrics*, Winchester, pp. 302-305, 2007.

[126]   A. Nekeb, A. Haddad, N. Harid, H. Griffiths and R. Waters, "Effects of UV irradiation on textured silicone rubber material," *2012 47th International Universities Power Engineering Conference (UPEC)*, London, pp. 1-5, 2012.

[127]   P. Charalampidis, A. Haddad, R. T. Waters, H. Griffiths, N. Harid and P. Sarkar, "Five-electrode inclined-plane tests of textured silicone rubber samples," 45th International Universities Power Engineering Conference UPEC2010, Cardiff, Wales, pp. 1-5, 2010.

[128]   R. S. Gorus, E. A. Cherney and R. Hackam, "The AC and DC performance of polymeric insulating materials under accelerated aging in a fog chamber," IEEE Transactions on Power Delivery, vol. 3, no. 4, pp. 1892-1902, Oct. 1988.

[129]   Z. Guan, Y. Chen, X. Liang and R. Zhang, "Issues on DC Inclined- Plane Tracking and Erosion Test of Composite Insulators Sheds Protective Materials", Insulators and Surge Arresters, vol. 161, no. 1, pp. 17-22, 1998.

[130] V. M. Moreno and R. S. Gorur, "AC and DC performance of polymeric housing materials for HV outdoor insulators," IEEE Transactions on Dielectrics and Electrical Insulation, vol. 6, no. 3, pp. 342-350, June 1999.

[131] T. G. Gustavsson, S. M. Gubanski, H. Hillborg, S. Karlsson and U. W. Gedde, "Aging of silicone rubber under ac or dc voltages in a coastal environment," IEEE Transactions on Dielectrics and Electrical Insulation, vol. 8, no. 6, pp. 1029-1039, Dec. 2001.

[132] J. V. Vas, B. Venkatesulu and M. J. Thomas, "Tracking and erosion of silicone rubber nanocomposites under DC voltages of both polarities," *IEEE Transactions on Dielectrics and Electrical Insulation*, vol. 19, no. 1, pp. 91-98, February 2012.

[133] V. Rajini and K. Udayakumar, "Degradation of Silicone Rubber under AC or DC Voltages in Radiation Environment," *IEEE Transactions on Dielectrics and Electrical Insulation*, vol. 16, no. 3, pp. 834-841, June 2009.

[134] G. Heger, H. J. Vermeulen, J. P. Holtzhausen and W. L. Vosloo, "A comparative study of insulator materials exposed to high voltage AC and DC surface discharges," *IEEE Transactions on Dielectrics and Electrical Insulation*, vol. 17, no. 2, pp. 513-520, April 2010.

[135] J. Heo, H. Cho and L. Soon, "A comparison of AC and DC surface discharges characteristics for silicone rubber," 2012 IEEE International Conference on Condition Monitoring and Diagnosis, Bali, pp. 629-632, 2012.

[136] R. Sarathi, S. Chandrasekar and N. Yoshimura, "Investigation of tracking phenomena in outdoor polymeric insulation material under DC voltages using wavelets," *IEEE Transactions on Power Delivery*, vol. 21, no. 1, pp. 515-517, Jan. 2006.

[137] N. Mahatho, I. R. Jandrell, T. Govender, "Ageing of silicone rubber insulators under high voltage direct current: results of inclined plane testing and material analysis, " 18th International Symposium on High Voltage Engineering (ISH), Seoul, Korea, pp. 1190–1196, August 2013.

[138] R. A. Ghunem, "Using the inclined-plane test to evaluate the resistance of outdoor polymer insulating materials to electrical tracking and erosion," *IEEE Electrical Insulation Magazine*, vol. 31, no. 5, pp. 16-22, Sept-Oct. 2015.

[139] G. P. Bruce, S. M. Rowland and A. Krivda, "DC inclined-plane testing of silicone rubber formulations," 2008 Annual Report Conference on Electrical Insulation and Dielectric Phenomena, Quebec, QC, pp. 196-199, 2008.

[140] G. P. Bruce, S. M. Rowland and A. Krivda, "Performance of silicone rubber in DC inclined plane tracking tests," IEEE Transactions on Dielectrics and Electrical Insulation, vol. 17, no. 2, pp. 521-532, April 2010.

[141] S. M. Rowland, G. P. Bruce, Y. Liu, A. Krivda and L. E. Schmidt, "Use of image analysis in DC inclined plane tracking tests of nano and micro composites," *IEEE Transactions on Dielectrics and Electrical Insulation*, vol. 18, no. 2, pp. 365-374,

April 2011.

[142]   R. A. Ghunem, S. H. Jayaram and E. A. Cherney, "Comparative inclined plane tests on silicone and EPDM elastomers under DC," *2013 IEEE Electrical Insulation Conference (EIC)*, Ottawa, ON, pp. 356-359, 2013.

[143]   R. A. Ghunem, S. H. Jayaram and E. A. Cherney, "Erosion of silicone rubber composites in the AC and DC inclined plane tests," in *IEEE Transactions on Dielectrics and Electrical Insulation*, vol. 20, no. 1, pp. 229-236, February 2013.

[144]   A. Nekeb, A. Haddad, N. Harid, H. Griffiths, R. Waters, "Effects of UV irradiation on textured silicone rubber material, " Universities Power Engineering Conference (UPEC), 2012 47th International, 4-7 Sept. 2012.

[145]   ISO 4892-2:2006, "Plastics - Methods of exposure to laboratory light sources, " Part 2: Xenon-arc lamps.

[146]   H. Daochun, R. Jiangjun, C. Yong Chen, H. Feng, Y. Shifeng and L. Shoubao, "Calculation and measurement of potential and electric field distribution along 1000 kV AC transmission line composite insulator," *2008 International Conference on Electrical Machines and Systems*, Wuhan, pp. 428-433, 2008.

[147]   D. I. Kovalev, "Calculation of electric fields in electrical high-voltage equipment", *Journal of Russian Electrical Engineering*, vol. 86, no. 10, pp. 579–582, December 2015.

[148]   "Electric field modeling of NCI and grading ring design and application," TR 113-977, EPRI. Palo Alto, CA, Dec. 1999.

[149]   R. S. Gorur, S. Sundhara Rajan and O. G. Amburgey, "Contamination performance of polymeric insulating materials used for outdoor insulation applications," *IEEE Transactions on Electrical Insulation*, vol. 24, no. 4, pp. 713-716, Aug. 1989.

[150]   J. Xu, W. Su, Y. Teng and X. Lin, "Finite element analysis of electric field of outdoor insulators under pollution un-uniform distribution," 2011 1st International Conference on Electric Power Equipment - Switching Technology, Xi'an, pp. 462-465, 2011.

[151]   C. Yong, H. Feng, D. Yizheng, G. bo and Z. qiao-gen, "Study on Withstand Voltage Characteristics and Surface Electrical Field Distribution along Polluted Insulators," 2008 International Conference on High Voltage Engineering and Application, Chongqing, pp. 60-62, 2008.

[152]   B. Marungsri, W. Onchantuek, A. Oonsivilai and T. Kulworawanichpong, "Analysis of electric field and potential distributions along surface of silicone rubber insulators under various contamination conditions using finite element method". World Academy of Science, Engineering and Technology 53, Vol. 3, no. 5, pp. 1353-1363, 2009.

[153]   H. El-Kishky and R. S. Gorur, "Electric field computation on an insulating surface with discrete water droplets,*" IEEE Transactions on Dielectrics and Electrical Insulation*, vol. 3, no. 3, pp. 450-456, June 1996.

[154]   Z. Guan, L. Wang, B. Yang, X. Liang and Z. Li, "Electric field analysis of water drop corona," *IEEE Transactions on Power Delivery*, vol. 20, no. 2, pp. 964-969, April 2005.

[155]   S. Feier-Iova. "The Behavior of Water Droplet on Insulating Surfaces Stressed by Electric Field". Ph.D. Thesis, TU Darmstadt, 2009.

[156]   Y. Zhu, S. Yamashita, N. Anami, M. Otsubo, C. Honda and Y. Hashimoto, "Corona discharge phenomenon and behavior of water droplets on the surface of polymer in the AC electric field," *Proceedings of the 7th International Conference on Properties and Applications of Dielectric Materials (Cat. No.03CH37417)*, Nagoya, Japan, vol.2, pp. 638-641, 2003.

[157]   Weiguo Que and S. A. Sebo, "Typical cases of electric field and voltage distribution calculations along polymer insulators under various wet surface conditions," Annual Report Conference on Electrical Insulation and Dielectric Phenomena, Cancun, Quintana Roo, Mexico, pp. 840-843, 2002.

[158]   S. Chakravorti, and H. Steinbigler, "Boundary-Element Studies on Insulator Shape and Electric Field around HV Insulators with or without Pollution, "*IEEE Transactions on Dielectrics and Electrical Insulation*, Vol. 7, No. 2, pp. 169-176, April 2000.

[159]   A. J. Phillips, et al., "Electric Fields on AC Composite Transmission Line Insulators," IEEE Transactions on Power Delivery, vol. 23, no. 2, pp. 823-830, April 2008.

[160]   B. M'hamdi, M. Teguar and A. Mekhaldi, "Optimal design of corona ring on HV composite insulator using PSO approach with dynamic population size," *IEEE Transactions on Dielectrics and Electrical Insulation*, vol. 23, no. 2, pp. 1048-1057, April 2016.

[161]   T. Doshi, R. S. Gorur and J. Hunt, "Electric field computation of composite line insulators up to 1200 kV AC," *IEEE Transactions on Dielectrics and Electrical Insulation*, vol. 18, no. 3, pp. 861-867, June 2011.

[162]   H. M. Schneider, J. F. Hall, G. Karady and J. Renowden, "Non-ceramic Insulators for Transmission Lines", *IEEE Transactions on Power Delivery*, Vol. 4, no. 4, pp. 2214-2221, Oct. 1989.

[163]   X. Liang, S. Wang, J. Fan and Z. Guan, "Development of Composite Insulators in China", *IEEE Transactions on Power Delivery*, Vol. 6, no. 5, pp. 586-594, Nov. 1999.

[164]   T. Zago., "Performance of textured insulators for overhead lines and substations under polluted conditions", Master Thesis, Electrical Energy Engineering, University of Padua, Italy, 2017.

[165]   P. Charalampidis., "Characterisation of textured insulators for overhead lines and substations", PhD Thesis, School of Engineering, Cardiff University, 2012, Royaume-Uni.

[166] L. H. Meyer, S. H. Jayaram and E. A. Cherney, "Correlation of damage, dry band arcing energy, and temperature in inclined plane testing of silicone rubber for outdoor insulation," *IEEE Transactions on Dielectrics and Electrical Insulation*, vol. 11, no. 3, pp. 424-432, June 2004.

[167] H. Gleizer, A. L. Tan and J. H. Mason, "Electrolytic corrosion as an adjunct to DC tracking and erosion on insulators," *1988 Fifth International Conference on Dielectric Materials, Measurements and Applications*, Canterbury, UK, pp. 135-138, 1988.

[168] P. B. Zhou, "Numerical Analysis of Electromagnetic Fields," Berlin: Spinger Verlag, 1993.

[169] K. J. Bathe. "Finite Element Procedures," New Jersey: Prentice Hall, 1996.

[170] J. Goupy, "Plan d'expériences pour surface de réponse," 3éme édition, Dunod, Paris, 1999.

[171] J. Goupy, "La méthode des plans d'expériences – Optimisation du choix des essais et de l'interprétation des résultats", Ed. Dunod, 1996.

[172] D. C. Montgomery, "Design and analysis of experiments", 6éme edition, Wiley, New York, 2004.

[173] C. Zienkiewicz, R.L. Taylor, "The finite element method", vol. 1 (Mc Graw-Hill, London 1989).

[174] Introduction to COMSOL Multiphysics [Online]. Available: **https://cdn.comsol.com/doc/5.5/IntroductionToCOMSOLMultiphysics.pdf** (Accessed on 2013).

[175] S. Sangkhasaad, "High Voltage Engineering," Thailand, 3rd edition, Printed in Bangkok, Thailand, pp. 121-123, March 2006.

[176] N. M. Jordan et al, "Electron Emission near a Triple Point," *2008 IEEE International Power Modulators and High-Voltage Conference*, Las Vegas, NV, pp. 311-311, 2008.

[177] N. M. Jordan., "Laser Fabrication of high-K dielectrics for High Current Cathodes", PhD thesis, Department of Nuclear Engineering and Radiological Sciences, Ann Arbor, United States, University of Michigan, 2008.

[178] EPRI, Palo Alto, CA., "Application guide for transmission line NCI", pp.111-566, 1998.

[179] D. L. Williams, A. Haddad, A. R. Rowlands, H. M. Young, and R. T. Waters, "Formation and characterization of dry bands in clean fog on polluted insulators", IEEE Transactions on Dielectrics and Electrical Insulation, vol.6, no. 5, pp.724-731, 1999.

[178] E. S. Asenjo, N. O. Morales and A. E. Valdenegro, "Solution of low frequency complex fields in polluted insulators by means of the finite element method," *IEEE Transactions on Dielectrics and Electrical Insulation*, vol. 4, no. 1, pp. 10-16, Feb.

1997.

[180]   S. E. Asenjo and O. N. Morales, "Low Frequency Complex Fields in Polluted Insulators," *IEEE Transactions on Electrical Insulation*, vol. EI-17, no. 3, pp. 262-268, June 1982.